Electronic Band Structure and Magnetism of NiAs-type Transition-Metal Pnictides

Masato MORIFUJI

January 1990

Abstract

NiAs-type transition-metal pnictides have attracted much interest due to their various magnetic ordering and structural transformation. In this thesis the magnetic properties and the structural transformation from the NiAs-type to the MnP-type structure of Fe-, Co- and Ni-arsenides are discussed from the viewpoint of itinerant d electrons on the basis of electronic band structures obtained by a self-consistent augmented plane wave (APW) method.

First, the non-magnetic bands of CoAs, NiAs, FeSb and CoSb with the NiAs-type structure and those of FeAs and CoAs with the MnP-type structure are calculated by using the self-consistent APW method. Energy dispersion curves, density of states and Fermi surface are shown. Furthermore, for NiAs-type CoAs bonding nature between a Co atom and an As atom for each band is examined by calculating bond orders.

Secondly, the structural transformation from the NiAs-type to the MnP-type structure of CoAs and NiAs is studied. A crucial question is why the structural transformation to the MnP-type structure occurs in CoAs but not in NiAs. To answer this question the generalized electronic susceptibility is calculated by evaluating matrix elements of the electron-lattice interaction with use of the crystal potential and the wave functions determined by the APW band calculations. The calculated results indicate that the structural transformation to the MnP-type

structure is likely to occur in CoAs but not in NiAs.

Thirdly, paramagnetic susceptibilities of FeAs, CoAs and NiAs are calculated. In FeAs and CoAs the observed paramagnetic susceptibility shows anomalous temperature dependence. At high temperatures, the inverse paramagnetic susceptibility obeys the Curie-Weiss law. At low temperatures, with decreasing temperature it increases passing through a broad minimum. Such a behavior of the paramagnetic susceptibility is very similar to that observed in a semiconductor FeSi whose paramagnetic susceptibility was well explained by a spin-fluctuation theory. Since the density of states near the Fermi level of FeAs and CoAs reveals a characteristic behavior simlar to that of FeSi, the paramagnetic susceptibilities of FeAs and CoAs are calculated on the basis of the spin-fluctuation theory, by taking account of the characteristic shape of the density of states obtained by the APW band calculation. The calculated result is in agreement qualitatively with the observation.

Finally, the double helical magnetic ordering of FeAs is discussed by using the tight-binding model whose transfer integrals are taken so as to reproduce the band structure obtained by using the APW method. Instability of the paramagnetic phase against formation of a magnetic ordering described by a general wave vector is studied. Furthermore, the total electronic energy of double helical spin density wave (DHSDW) state is calculated as a function of wave vectors. By minimizing the total energy the wave vector and the relative

phase angle of the most stable DHSDW state at 0 K are determined. The obtained magnetic ordering is very close to the observed one. From these studies it has been found that the observed double helical ordering is well understood from the viewpoint of the itinerant electrons.

Acknowledgements

The author would like to express his sincere thanks to Professor K. Motizuki, under whose guidance this work was done, for helpful suggestions and valuable discussions and her help in preparing the manuscript. Without her continuous encouragement, this work would not have been completed. He thanks gratefully to Professor N. Suzuki for helpful suggestions and valuable discussions. He also thanks to Dr. M. Shirai for valuable discussions. He thanks gratefully to Professor A. Yanase for providing him the computer programs for APW band calculations.

CONTENTS

§1. Introduction

Transition-metal pnictides having the NiAs-type or MnP-type structure have been intensively studied due to their interesting physical properties. They show a rich variety in magnetic ordering, depending on their constitutive atoms. Furthermore, some of them show a structural transformation from the NiAs-type to the MnP-type structure. The crystal and magnetic structures of transition-metal arsenids and antimonides are shown in table 1-1.

Among transition-metal arsenides and antimonides, CrAs[1], MnAs[2,3] and CoAs[1] reveal the structural transformation from the NiAs-type to the MnP-type structure with decreasing temperature. The transition temperatures are 1100 K ,398 K and 1250 K, respectively. VAs[1] and FeAs[4] have the MnP-type crystal structure at all temperatures. NiAs[5] and all transition-metal antimonides[5,6] have the NiAs-type structure at all temperatures. Podloucky discussed the crystal structure of transition-metal arsenides by calculating a difference between the band energies in the NiAs-type structure and those in the MnP-type structure, based on a simple tight-binding model taking into account p states at the As sites and d states at the metal sites. He obtained a structural trend which agrees with observations[7]. Katoh and Motizuki developed a microscopic theory of electron-lattice interaction on the basis of the electronic bands obtained by the APW method[8,9]. They studied the instability of the NiAs-type structure of CrAs, MnAs, CrSb and MnSb against formation of

the MnP-type structure and clarified why the structural transformation to the MnP-type structure occurs in CrAs and MnAs but not in CrSb and MnSb. They emphasized that wave number dependence of matrix elements of the electron-lattice interaction plays an important role in the microscopic theory of structural phase transition.

As for magnetic properties, MnAs[2] and MnSb[10] become ferromagnets below T_C= 319 K and 573 K, respectively. CrSb[10] and CoSb[11] become antiferromagnets below T_N= 680 and 40 K, respectively. CrAs[12] and FeAs[4] in the MnP-type phase become double helical magnets with helical axes along the c-axes below T_N=240 K and 77 K, respectively, while $Mn_{1-t}Fe_tAs$[13] and $V_{1-t}Mn_tAs$[14] in Mn-rich composition become helical magnets with helical axes along the a-axes. CoAs[15] and NiAs[16] do not show any magnetic ordering. The paramagnetic susceptibilities of FeAs and CoAs with the MnP-type structure show anomalous temperature dependence. At high temperatures, the inverse paramagnetic susceptibility obeys the Curie-Weiss law. At low temperatures, with decreasing temperature it increases passing through a broad minimum. On the other hand, the paramagnetic susceptibility of NiAs, whose crystal structure is of NiAs-type, is almost temperature-independent. These facts indicate that the temperature dependence of the paramagnetic susceptibility is related to the crystal structure. The effective moment of FeAs estimated from the Curie constant is 3.1 μ_B/Fe, which is much larger than the saturation moment 0.5μ_B/Fe obtained by a neutron

diffraction measurement at 12 K. This fact indicates an itinerant character of the d electrons.

The purpose of this thesis is (1) to understand microscopically the various magnetic properties of MX(M=Fe,Co,Ni; X=As,Sb) in a unified way from the viewpoint of the itinerant d electrons of the transition-metal atoms, and (2) to clarify the origin of the structural transformation from the NiAs-type to the MnP-type structure observed in some of transitiom-metal arsenides.

In order to accomplish our purpose, we first calculate the non-magnetic bands of CoAs, NiAs, FeSb and CoSb with the NiAs-type structure and those of CoAs and FeAs with the MnP-type structure, by using a self-consistent APW method[17]. We also calculate bond orders to clarify bonding nature in these compounds. The results are shown in §2. In §3, we study the structural transformation from the NiAs-type structure to the MnP-type structure by calculating a generalized electronic susceptibility with use of matrix elements of the electron-lattice interaction evaluated based on the rigid muffin-tin approximation. In §4 we study the magnetic properties. In §4.1 we study the anomalous temperature dependence of the paramagnetic susceptibility observed in FeAs and CoAs on the basis of a spin-fluctuation theory by taking account of a characteristic behavior of the density of states of these compounds obtained by the self-consistent APW band calculation. In §4.2 we discuss the double helical magnetic ordering observed in FeAs.

Table 1-1. Crystal and magnetic structures of transition-metal arsenides and antimonides.

arsenides

	TiAs	VAs	CrAs	MnAs	FeAs	CoAs	NiAs
crystal structure	TiP	MnP	NiAs ↔MnP	NiAs ↔MnP	MnP	NiAs ↔MnP	NiAs
magnetism	para	para	double helix	ferro	double helix	para	para

antimonides

	TiSb	VSb	CrSb	MnSb	FeSb	CoSb	NiSb
crystal structure	NiAs	NiAs	NiAs	NiAs	NiAs	NiAs	NiAs
magnetism			anti-ferro	ferro		anti-ferro	dia-mag

§2. Electronic Band structure

2.1 APW band calculation

The unit cell of hexagonal NiAs-type structure (D_{6h}) and its 1st Brillouin zone are shown in Fig.2-1(a) and (b), respectively. The unit cell contains two metal atoms 1 and 2, and two anion atoms 3 and 4, as shown in Fig.2-1(a). Positions of metal atoms are (0,0,0) and (0,0,c/2) and those of anion atoms are (2a/3,a/3,c/4) and (a/3,2a/3,3c/4).

The orthorhombic unit cell of the MnP-type structure and its 1st Brillouin zone are shown in Fig.2-2(a) and (b), respectively. The unit cell of the MnP-type structure is twice as large as that of the NiAs-type structure and contains four metal atoms 1,2,3,4 and four anion atoms 5,6,7,8 as shown in Fig.2-2(a). The a- and b-axes of the orthorhombic MnP-type structure correspond to the c- and b-axes of the hexagonal NiAs-type structure, respectively. The positions of atoms[18] are

metal 1 :[ua , 0 , vc] ,
metal 2 :[(1/2+u)a, 0 , (1/2-v)c] ,
metal 3 :[(1/2-u)a, b/2 ,(1/2+v)c] ,
metal 4 :[(1-u)a , b/2 ,(1-v)c] ,
anion 5 :[u'a ,b/2 , v'c] ,
anion 6 :[(1/2+u')a,b/2 ,(1/2-v')c] ,
anion 7 :[(1/2-u')a, 0 ,(1/2+v')c] ,
anion 8 :[(1-u')a , 0 ,(1-v')c] ,

where $(u,v) = (0.0033, 0.1993)$,

$(u',v') = (0.1992, 0.5773)$ for FeAs

and $(u,v) = (0.0020, 0.2002)$,

$(u',v') = (0.1996, 0.5807)$ for CoAs.

The MnP-type distortion is described as a frozen longitudinal phonon of M_4^- mode at the M point in the Brillouin zone of the NiAs-type structure. The atomic displacements of metal and anion atoms are shown in Fig.2-3. For metal atoms the displacement in the c-plane is much larger than that along the c-axis, and for anion atoms the displacement occurs only along the c-axis.

The APW method is based on the muffin-tin approximation. In this approximation, the crystal is divided into two parts. One consists of spheres placed at each atomic site, which are called muffin-tin spheres. The other is the region outside the muffin-tin spheres. The crystal potential is assumed to be spherical in the muffin-tin spheres and to be constant outside the muffin-tin spheres. The crystal wave functions are expanded in a series of reciprocal lattice vectors as

$$\Psi(\mathbf{k},\mathbf{r}) = \sum_i c_i \chi(\mathbf{k}+\mathbf{G}_i,\mathbf{r}) \ , \tag{2.1}$$

where

$$\chi(\mathbf{k}+\mathbf{G}_i) = \begin{cases} \sum_{\ell=0}^{\infty} \sum_{m=-\ell}^{\ell} A_{\ell m}^{\nu}(\mathbf{k}+\mathbf{G}_i) R_\ell(|\mathbf{r}-\mathbf{R}_\nu|) Y_{\ell m}(\mathbf{r}-\mathbf{R}_\nu) & \text{(inside } \nu\text{th MT sphere)} \\ e^{i(\mathbf{k}+\mathbf{G}_i)\cdot\mathbf{r}} & \text{(outside MT spheres)} \ . \end{cases} \tag{2.2}$$

$\mathbf{k}$ is a wave vector in the 1st Brillouin zone, G_i is a reciprocal lattice vector and $A^{\nu}_{\ell m}$ is a coefficient which is determined by the condition that the wave function is continuous on the muffin-tin sphere. $A^{\nu}_{\ell m}$ is expressed as

$$A^{\nu}_{\ell m}(k_i) = 4\pi e^{ik_i \cdot r_\nu} i^{\ell} Y_{\ell m}(\hat{k}_i) j_{\ell}(|k_i| S_\nu)/R_{\ell}(S_\nu) \qquad (2.3)$$

where $k_i = k + G_i$, $\hat{k}_i = k_i/|k_i|$, j_ℓ is a ℓth order spherical Bessel function, S_ν is a radius of the νth muffin-tin sphere and R_ℓ is a solution of the radial Schrödinger equation in which the relativistic effect except the spin-orbit interaction is included[19]. The potential in the νth muffin-tin sphere is determined by using the charge density as follows:

$$\begin{aligned} V^{\nu}_{\pm}(r) = {} & \frac{8\pi}{r}\int_0^r r'^2 \rho_\nu(r')\,dr' + 8\pi\int_r^{S_\nu} r'\rho_\nu(r')dr' - \frac{2Z_\nu}{r} \\ & + {\sum_{\ell\mu}}' \frac{2(Q_\nu - \rho_0\Omega_\nu)}{|R_\nu - R_{\ell\mu}|} - {\sum_{\ell\mu}}' \frac{2Z_\mu}{|R_\nu - R_{\ell\mu}|} + 8\pi\int_{S_\nu}^{\infty} r'\rho_0 dr' \\ & + V^{xc\ \nu}_{\pm}(r)\ , \end{aligned} \qquad (2.4)$$

where the sign $\pm$ denotes the potential for spin up and spin down states, respectively, Z_ν is the core charge of the νth atom, $\rho_\nu(r)$ is the spherical charge density inside the νth muffin-tin sphere, ρ_0 is the uniform charge density outside the muffin-tin spheres, Ω_ν is the volume of the νth muffin-tin sphere and Q_ν is the total electron number in the νth muffin-tin sphere. $V^{xc\ \nu}_{\pm}(r)$ is the exchange and correlation potential inside the νth muffin-

tin sphere. The first and the second terms denote the Coulomb potential from electrons in the νth muffin-tin sphere. The third term is the potential from the nuclear charge of the νth muffin-tin sphere. The fourth and fifth terms are the Coulomb potential arising from the electron and nuclear charges of the other muffin-tin spheres, respectively. The lattice sum can be calculated by using the method obtained by Evald. The sixth term denotes a contribution from the uniform charge density outside the muffin-tin spheres. For the exchange and correlation potential, $V_{\pm}^{xc}(r)$, the local spin density approximation is used. We have adopted the formula obtained by Gunnarsson and Lundqvist for the exchange and correlation potential[20]. That is given by

$$V_{\pm}^{xc\ \nu}(r) = -\frac{2}{\pi\alpha r_s}\left[\ \beta(r_s) \pm \frac{1}{3}\,\delta(r_s)\zeta_s/(1\pm 0.297\zeta_s)\right] . \qquad (2.5)$$

$$\beta(r_s) = 1 + 0.0545 r_s \ell n(1+11.4/r_s) \qquad (2.6a)$$

$$\delta(r_s) = 1 - 0.036 r_s + 1.36 r_s/(1+10 r_s) \qquad (2.6b)$$

$$r_s = [3\rho_\nu(r)/4\pi]^{1/3} \quad \zeta_s = [\rho_{\nu+}(r) - \rho_{\nu-}(r)]/\rho_\nu(r) \qquad (2.6c)$$

where $\rho_{\nu\pm}(r)$ is the charge density of spin up and down states, respectively. $\rho_\nu(r)$ is the sum of $\rho_{\nu+}(r)$ and $\rho_{\nu-}(r)$ and $\alpha=(4/9\pi)^{1/3}$.

The procedure of the APW band calculation is as follows:

(1) Calculating the atomic wave function and the charge density.

(2) Constructing the muffin-tin potential.

(3) Solving the eigen-equation and obtaining eigen-energies and eigen-vectors.

(4) Constructing new charge density.

The starting charge density is a superposition of the self-consistent charge densities of neutral atoms. The atomic configurations of neutral atoms are Cr:$(3d)^5(4s)^1$, Fe:$(3d)^6(4s)^2$, Co:$(3d)^7(4s)^2$, Ni:$(3d)^8(4s)^2$, As:$(4s)^2(4p)^3$, Sb:$(5s)^2(5p)^3$. Cores are considered to be frozen. Using sampling points such as Γ, A, K, H ,M and L for the NiAs-type compounds and (1/8,1/8,1/8), (1/8,1/8,3/8), (1/8,3/8,1/8), (3/8,1/8,1/8), (3/8/3/8,1/8), (3/8,1/8,3/8), (1/8,3/8,3/8) and (3/8,3/8,3/8) for the MnP-type compounds, the procedure (2),(3),(4) are repeated until a change of the eigen-energies becomes small enough. The accuracy of the eigenvalues is 0.01 Ryd. We have used the criterion that $\ell_{max}=8$ and $|\mathbf{k}+\mathbf{G}|_{max}= 3.0\times(2\pi/a)$. The muffin-tin radii are taken to be half the nearest neighbor metal-anion distance for both metal and anion. The lattice parameters and the muffin-tin radii are shown in table 2-1.

Table 2-1 Lattice constants and muffin-tin radii

CoAs (NiAs-type)	a=3.57 c=5.23	$R_{Co}=R_{As}=1.2204$
NiAs	a=3.60 c=5.01	$R_{Ni}=R_{As}=1.2133$
FeAs	a=5.4404 b=3.3712 c=6.0259	$R_{Fe}=R_{As}=1.1556$
CoAs(MnP-type)	a=5.2852 b=3.4883 c=5.8675	$R_{Co}=R_{As}=1.1805$
FeSb	a=4.06 c=5.13	$R_{Fe}=1.2415$ $R_{Sb}=1.3227$
CoSb	a=3.87 c=5.19	$R_{Co}=R_{Sb}=1.2908$

(Å)

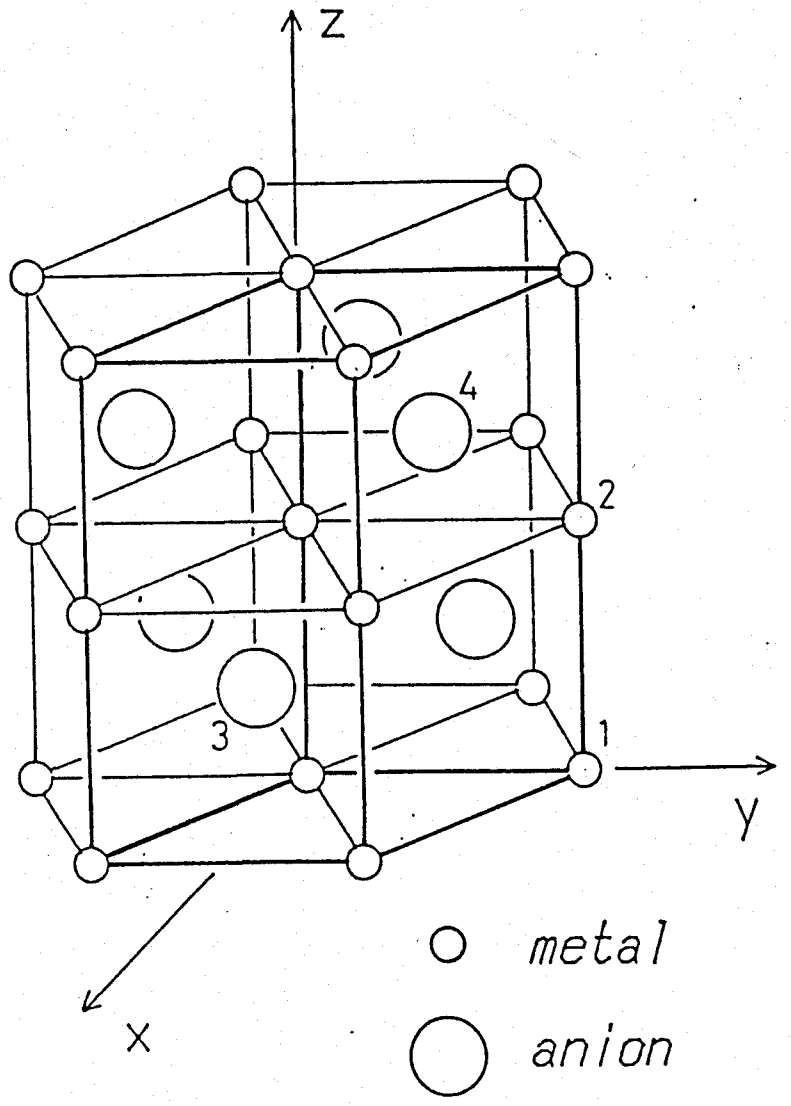

Fig.2-1. (a) The NiAs-type crystal structure.

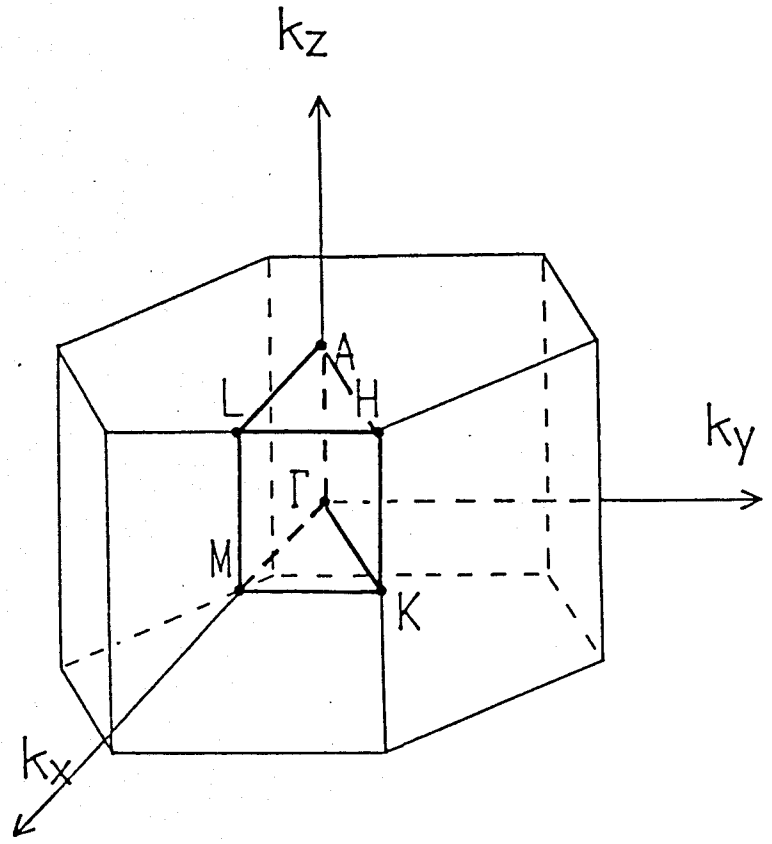

(b) The first Brillouin zone for the hexagonal Bravais lattice with symmetry points.

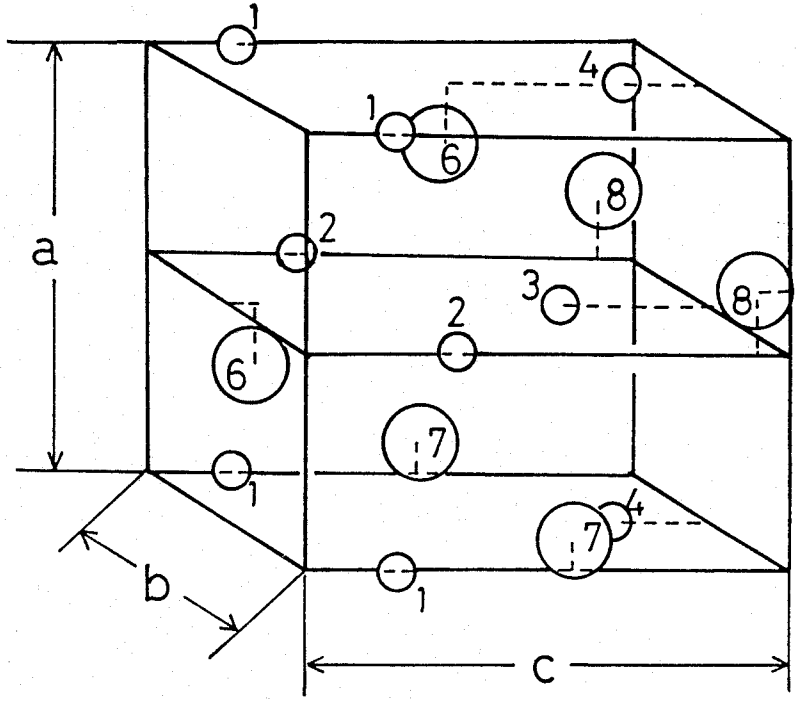

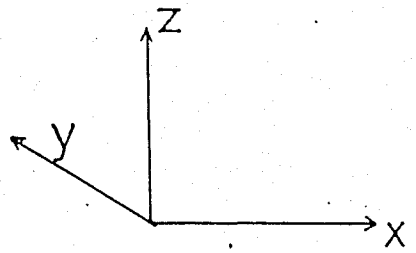

Fig.2-2. (a) The MnP-type crystal structure.

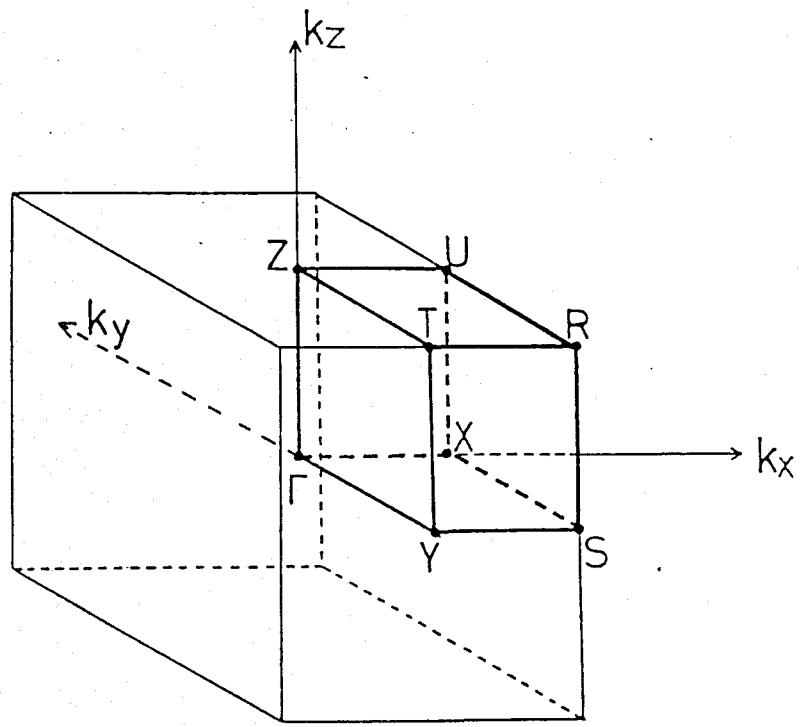

(b) The first Brillouin zone for the orthorhombic lattice with symmetry points.

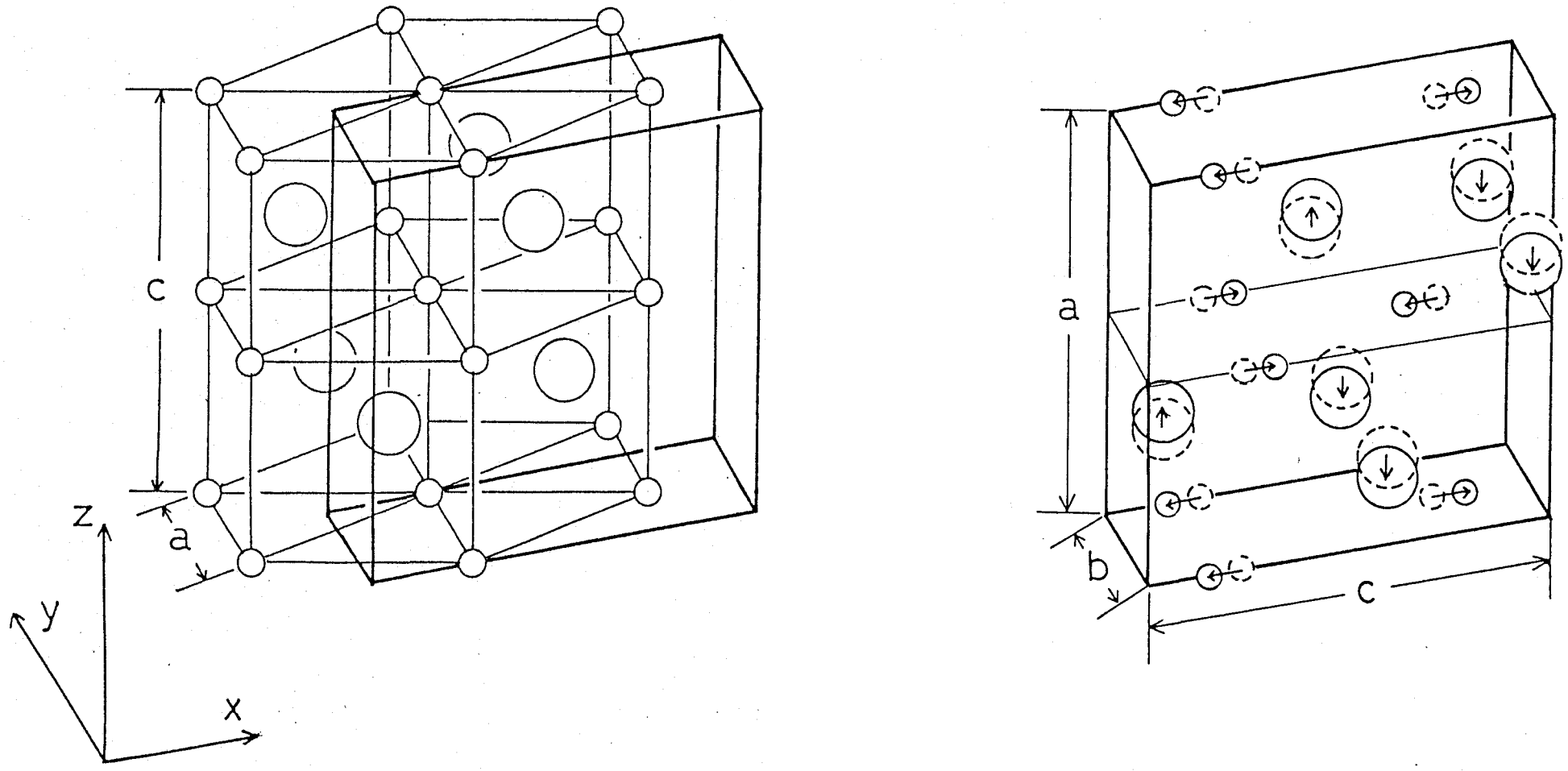

Fig.2-3. Relation between NiAs-type lattice (left) and MnP-type lattice (right).

2.2 Results and discussion

2.2.1 CoAs, NiAs, FeSb and CoSb (NiAs-type structure)

The energy dispersion curves of the non-magnetic bands of NiAs-type CoAs and NiAs along the symmetry lines are shown in Fig.2-4(a) and (b). The lowest two bands consist of s states of As. Sixteen bands above them mainly consist of As-p states and metal-d states. Fermi level is denoted as a small arrow. Density of states are calculated by using the linear interpolation tetrahedron method[21,22] with eigen-energies of 60 points in 1/24 Brillouin zone. The calculated densities of states of CoAs and NiAs are shown in Fig.2-5(a) and (b). The dot and dot-dashed curves denote the contributions from the metal-d states and As-p states inside the muffin-tin sphere, respectively. The density of states at the Fermi level is

$\rho(E_F) = 46$ [states /Ryd unit cell] for CoAs,

$\rho(E_F) = 31$ [states /Ryd unit cell] for NiAs.

These values are much smaller compared with 158 [states/Ryd unit cell] of NiAs-type MnAs and 102 [states /Ryd unit cell] of NiAs-type CrAs[8]. These small values of $\rho(E_F)$ are consistent with the fact that both CoAs and NiAs do not show any magnetic ordering, whereas MnAs becomes a ferromagnet and CrAs becomes a helical magnet. The energy dispersion curves of CoAs and NiAs resemble each other. But the Fermi level of NiAs is higher than that of CoAs because of a difference of the number of valence

electrons.

We have calculated Fermi surface of CoAs and NiAs by using the spline interpolation method. The results are shown in Fig.2-6 and 7. The Fermi surface of CoAs consists of three kinds of hole surface around the ΓA axis, which are shown in Fig.2-6(a), (b) and (c), respectively, and an electron pocket around the H point. The Fermi surface of NiAs consists of two kinds of hole surface shown in Fig.2-7(a) and (b) and an electron surface shown in Fig.2-7(c). From the shape of the Fermi surface we can expect for CoAs a good nesting between two hole surfaces shown in Fig. 2-6(a) and (b) by the wave vector ΓM. In NiAs, however, we cannot expect a good nesting by the wave vector ΓM, because the Fermi surface which corresponds to the hole surface of CoAs shown in Fig.2-6(b) vanishes completely. The MnP-type distortion is described as a frozen longitudinal phonon of M_4^- mode at the M point. Therefore, we can say that the obtained Fermi surface is favorable to causing the lattice distortion from the NiAs-type to the MnP-type in CoAs, but not in NiAs. We will make further discussion about srtuctural phase transition in §3.

The dispersion curves of the non-magnetic band of FeSb and CoSb are shown in Fig.2-8(a) and (b). Gross feature of the band of CoSb is similar to that of CoAs. The calculated densities of states are shown in Fig.2-9 (a) and (b). The density of states at the Fermi level is

$\rho(E_F)$ = 97 [states/Ryd unit cell] for FeSb,

$\rho(E_F)$ = 40 [states/Ryd unit cell] for CoSb.

The Fermi surface of CoSb consists of three kinds of hole surface around the ΓA axis shown in Fig.2-10(a), (b) and (c) and a hole pocket around the H point shown in Fig.2-10(d). These surfaces are very similar to those of CoAs.

2.2.2 FeAs and CoAs (MnP-type structure)

The energy dispersion curves of non-magnetic band of the MnP-type FeAs and CoAs are shown in Fig.2-11(a) and (b), respectively. There are 32 bands which consist of metal-d states and As-p states. The density of states are calculated with eigen-energies of 48 points in 1/8 zone and the results are shown in Fig.2-12(a) and (b). For these compounds the Fermi level is located at a steep dip of the density of states, contrary to the case of MnAs in which the Fermi level is located at a peak of the density of states. The density of states of CoAs and FeAs increases steeply below the Fermi level. Such a characteristic behavior of the density of states of MnP-type CoAs and FeAs will be reflected in the anomalous temperature dependence of the paramagnetic susceptibilities of these compounds. The density of states at the Fermi level is

$\rho(E_F)$ = 72 [states/Ryd unit cell] for FeAs,

$\rho(E_F)$ = 62 [states/Ryd unit cell] for CoAs.

Gross feature of the band of MnP-type CoAs is quite different from that of the NiAs-type CoAs. For MnP-type CoAs, large peaks

in the density of states of the p-d band of NiAs-type CoAs become less sharp. And the density of states above the Fermi level increases and the width of the p-d bands becomes wider than that of NiAs-type CoAs.

The Fermi surface of FeAs consists of four kinds of hole surface. They are shown in Fig.2-13(a), (b), (c) and (d). Two of them are hole pockets around the Z point. The other two surfaces have complicated shapes. From the charactristic shape of the Fermi surface shown in Fig.2-12(c), we may expect a good nesting by a wave vector along the ΓX direction. The observed helical magnetic structure is described by the wave vector which is about $(3/4)\Gamma X$[4]. We suggest a possibility of a spin density wave for the helical magnetism of FeAs.

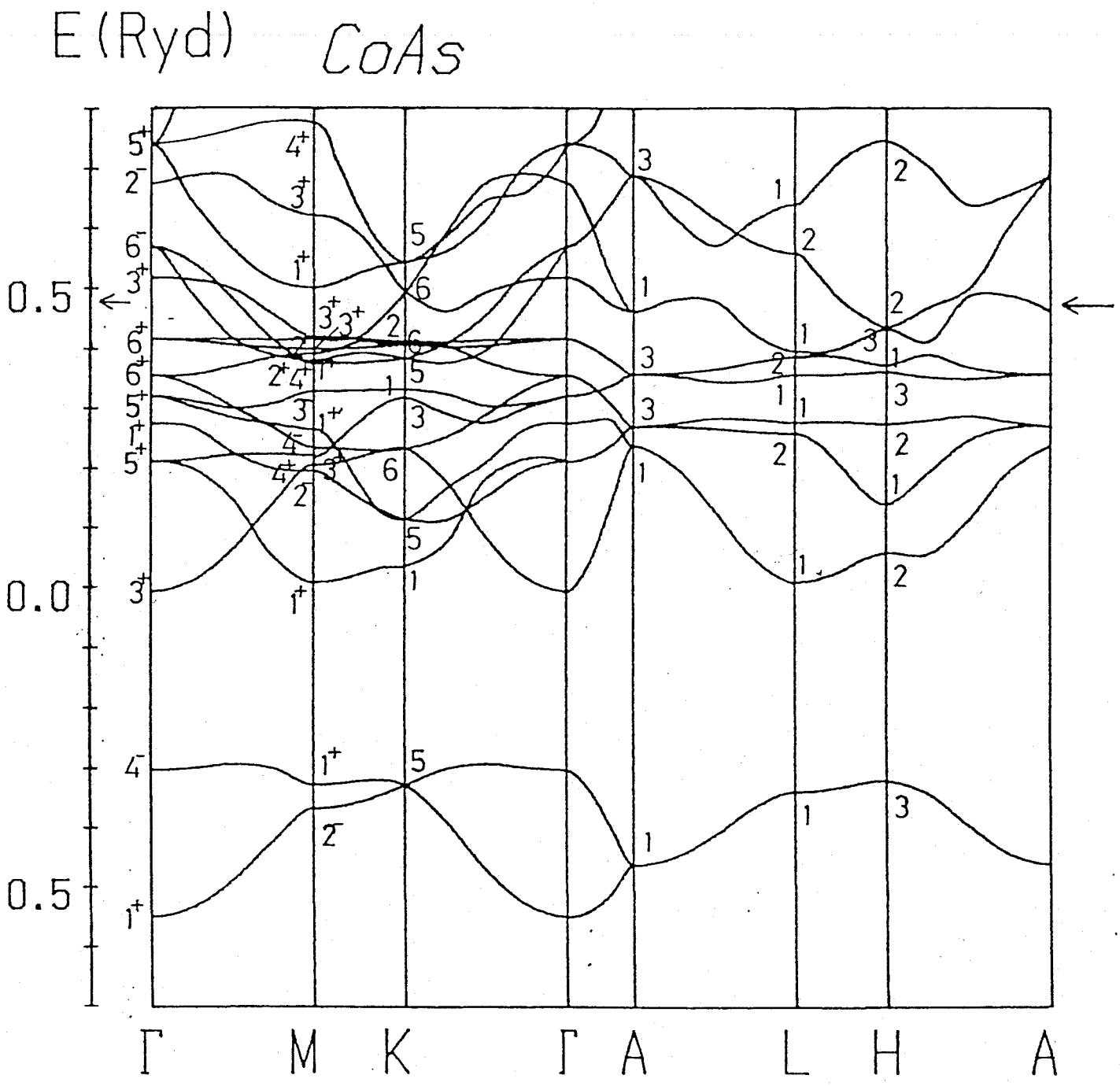

Fig.2-4(a). Dispersion curves of CoAs.

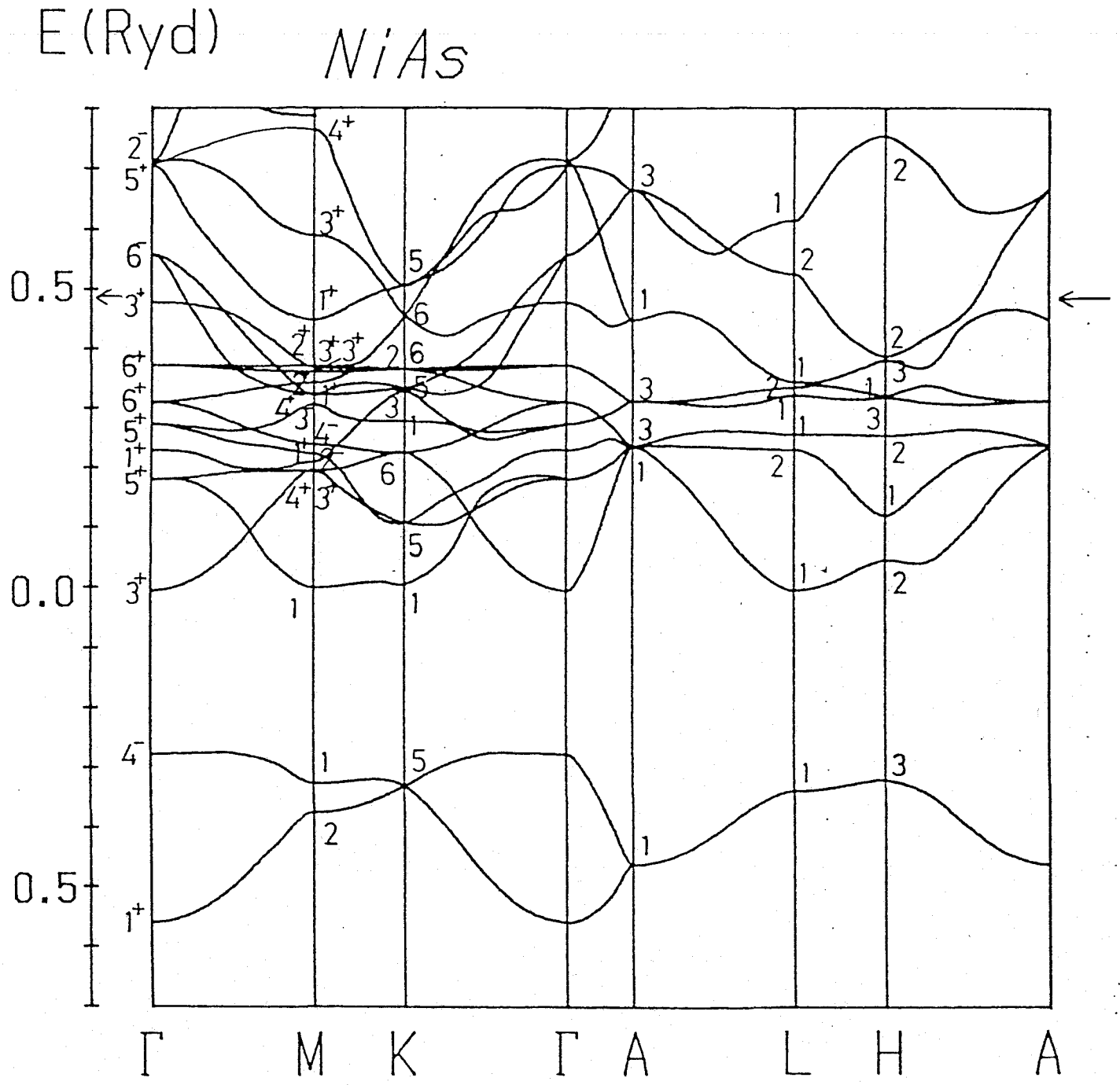

Fig.2-4(b). Dispersion curves of NiAs.

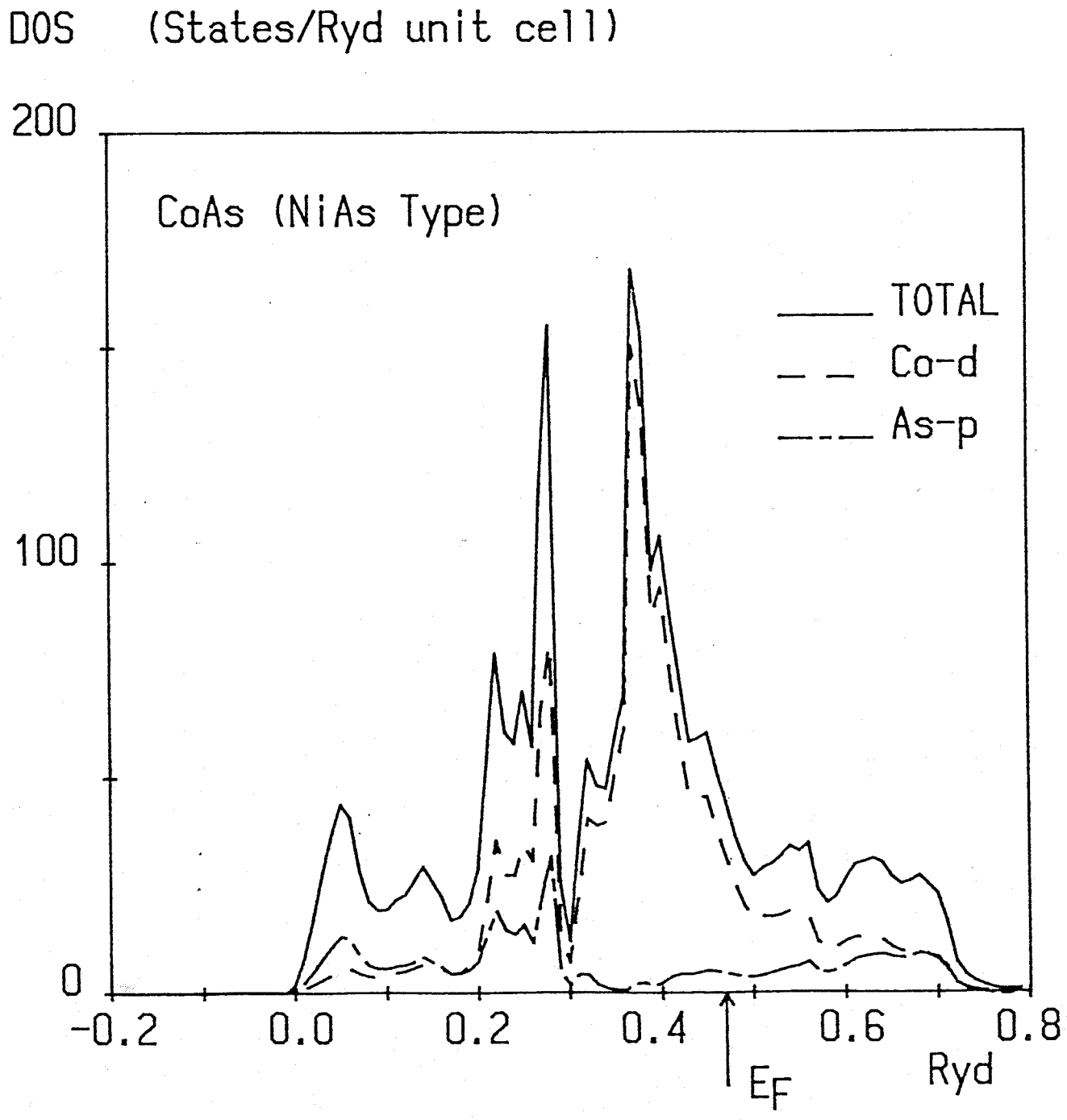

Fig.2-5(a). Density of states of CoAs.

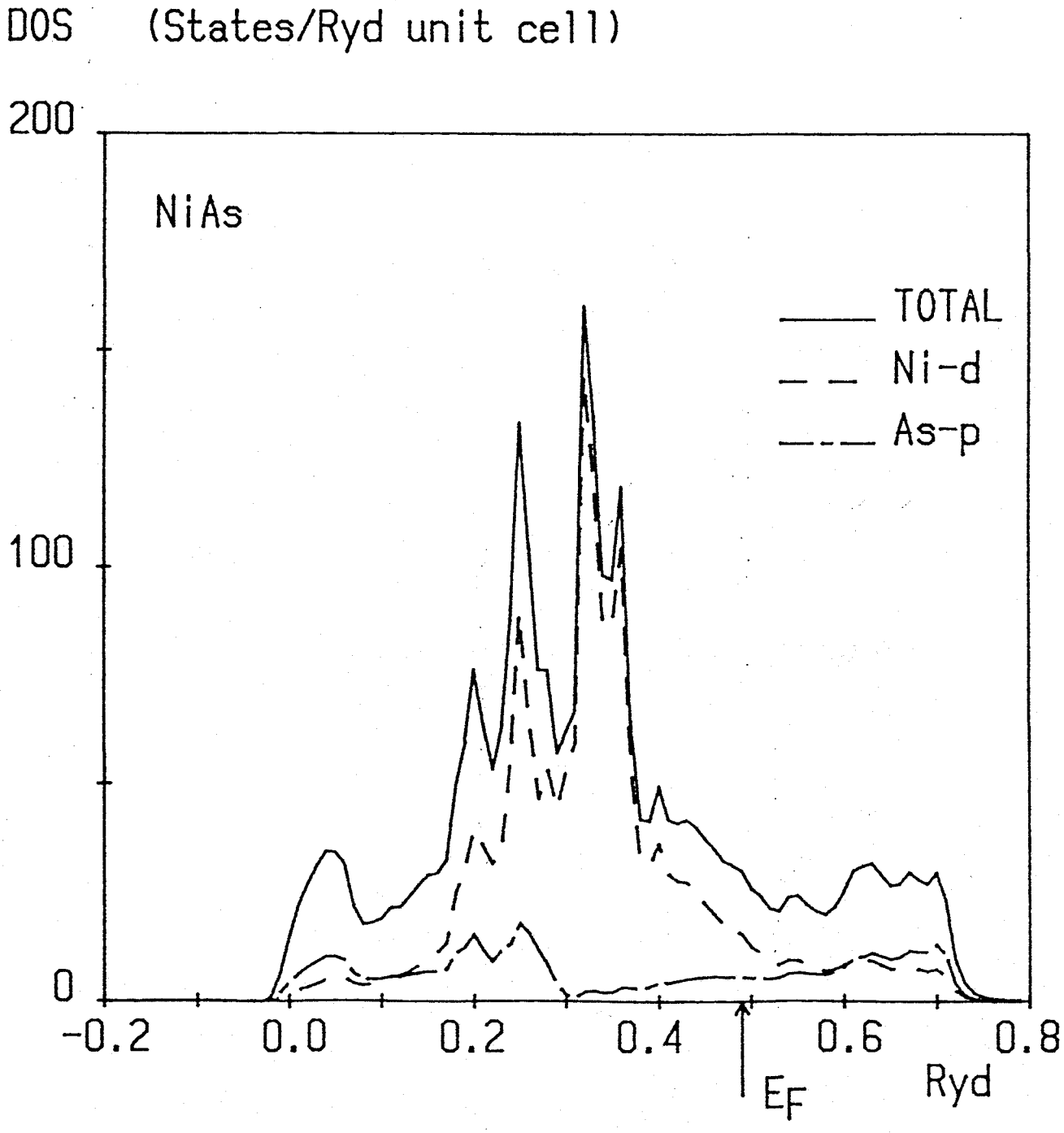

Fig.2-5(b). Density of states of NiAs.

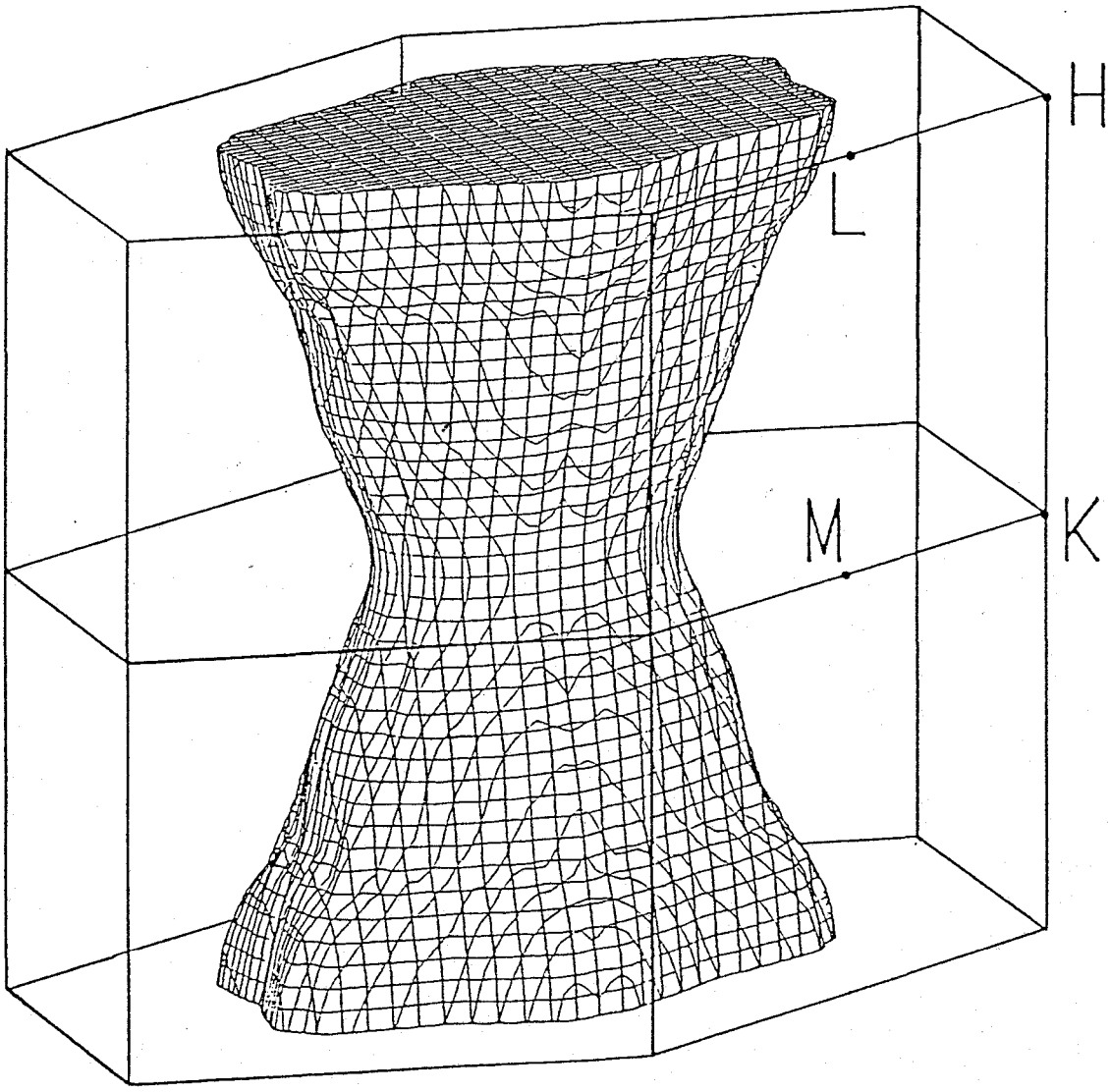

Fig.2-6(a). Fermi surface of CoAs.

The hole surface is shown.

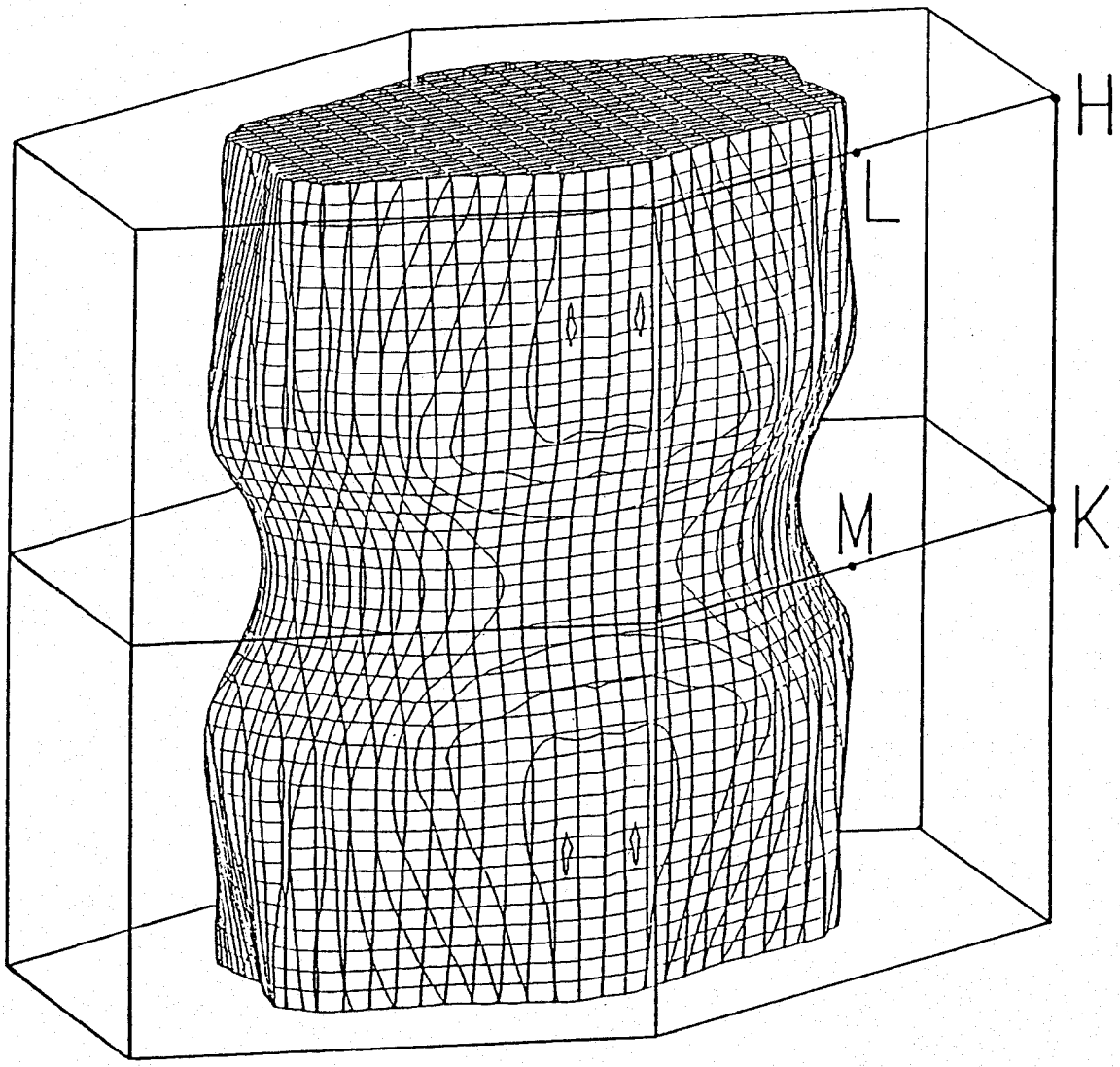

Fig.2-6(b). Fermi surface of CoAs.
The hole surface is shown.

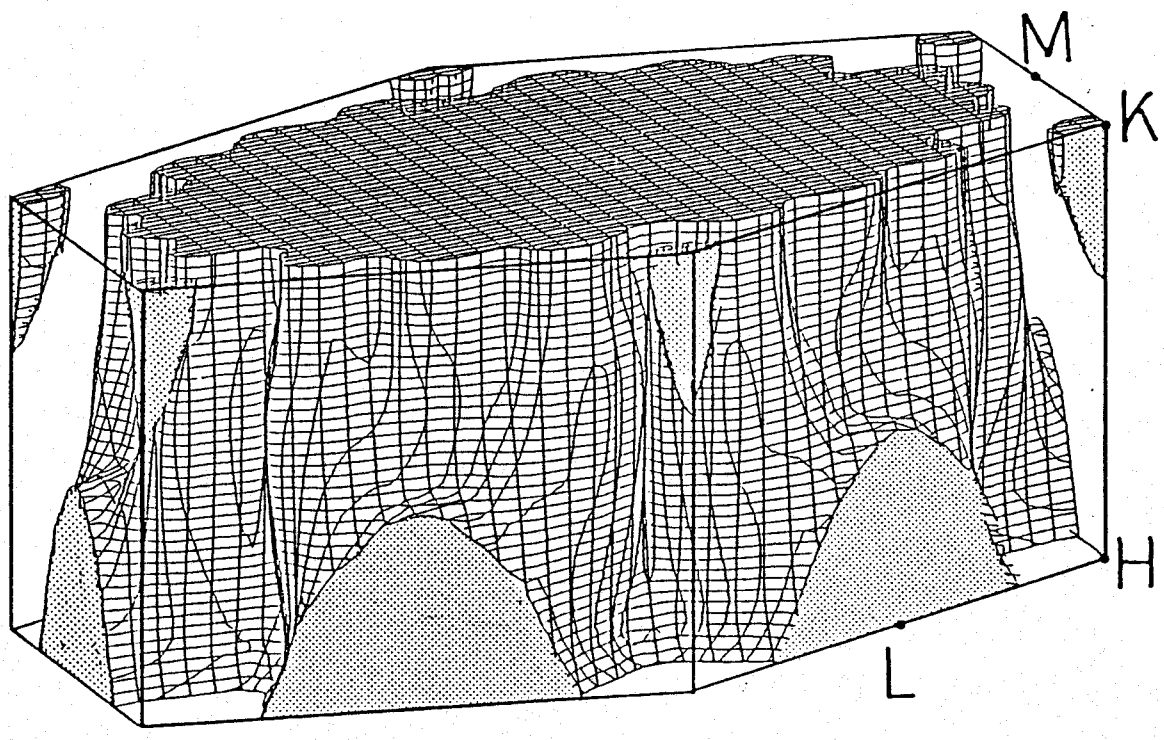

Fig.2-6(c). Fermi surface of CoAs.

The hole surface is shown.

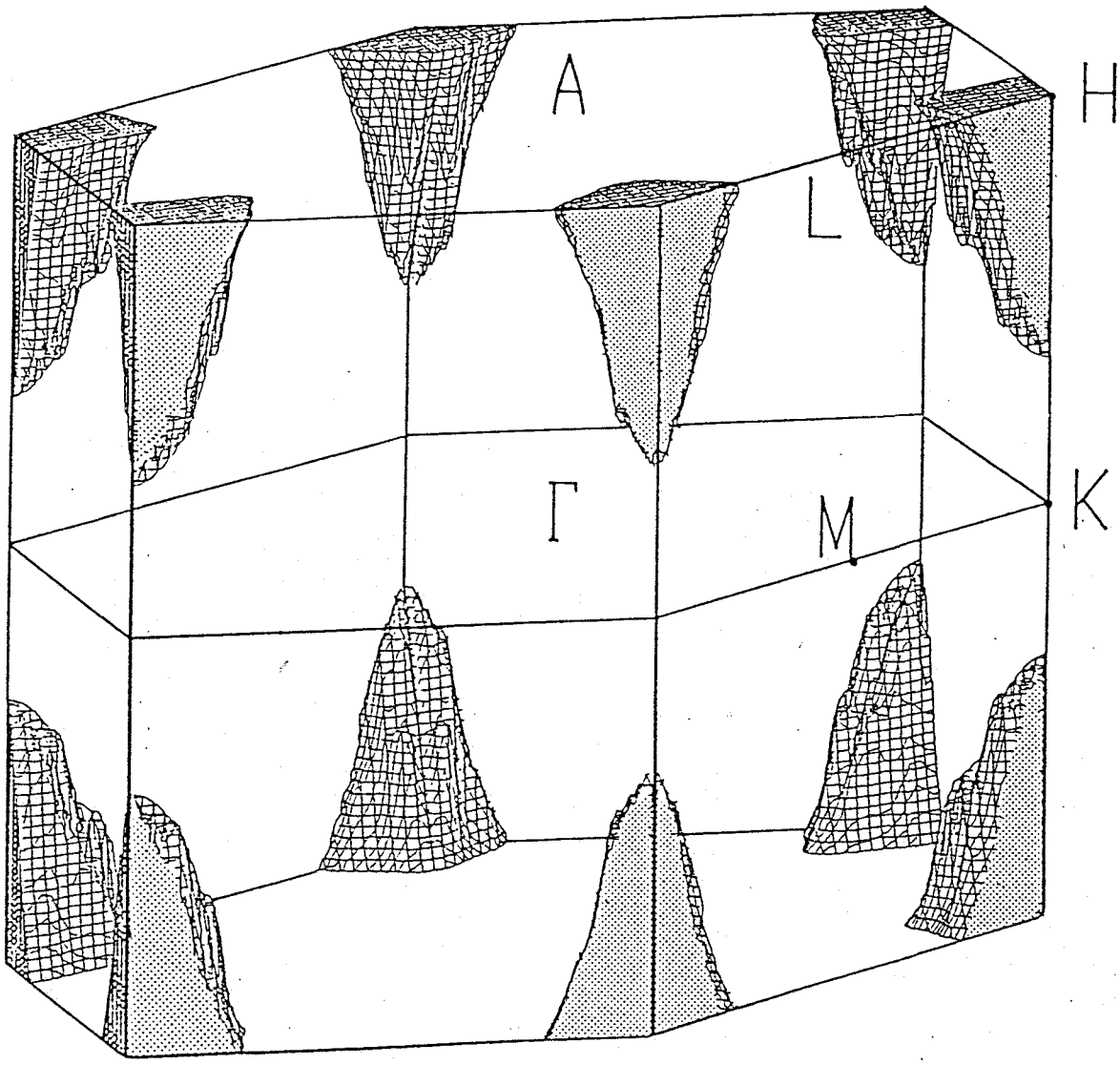

Fig.2-6(d). Fermi surface of CoAs.

The electron surface is shown.

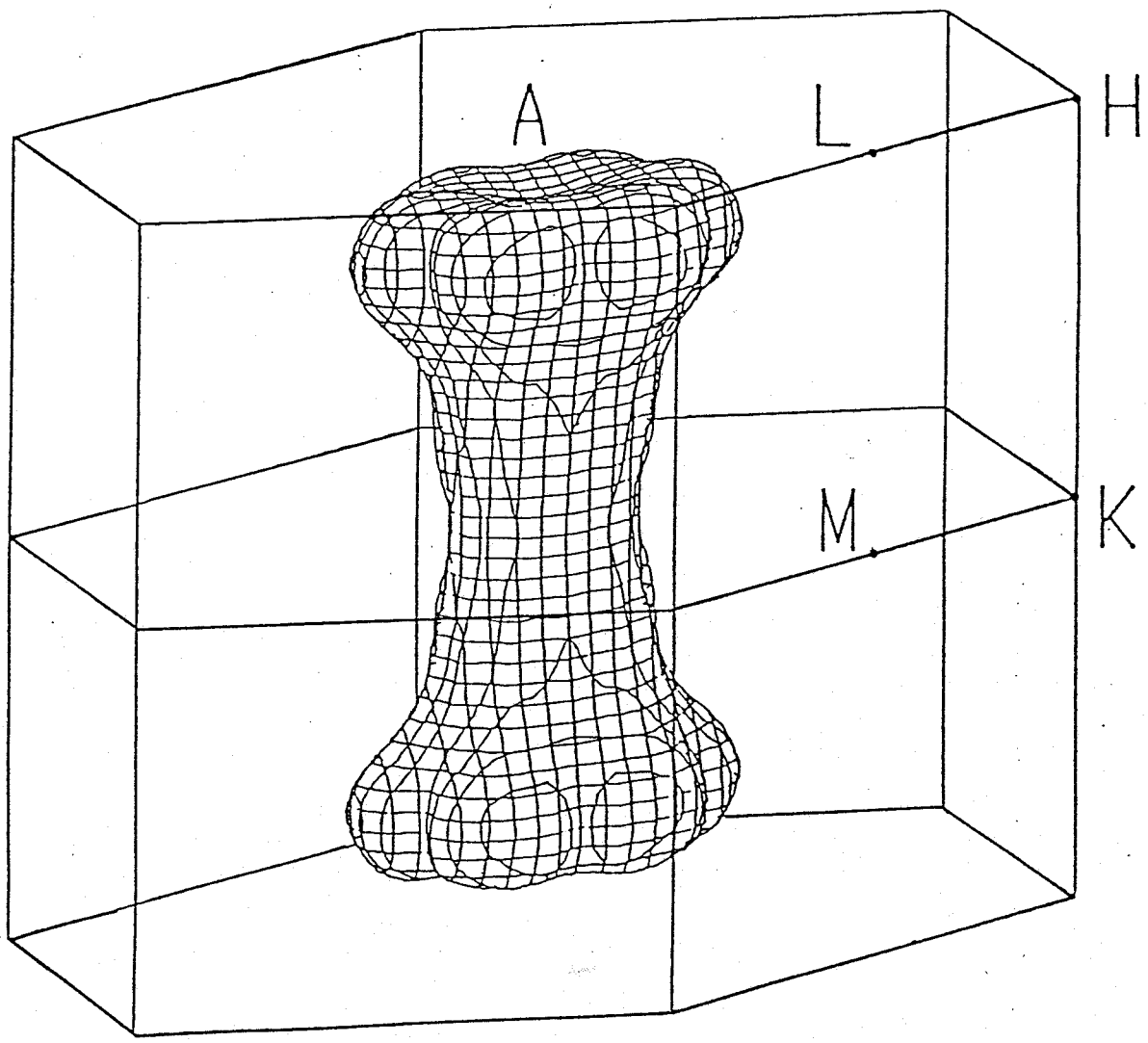

Fig.2-7(a). Fermi surface of NiAs.

The hole surface is shown.

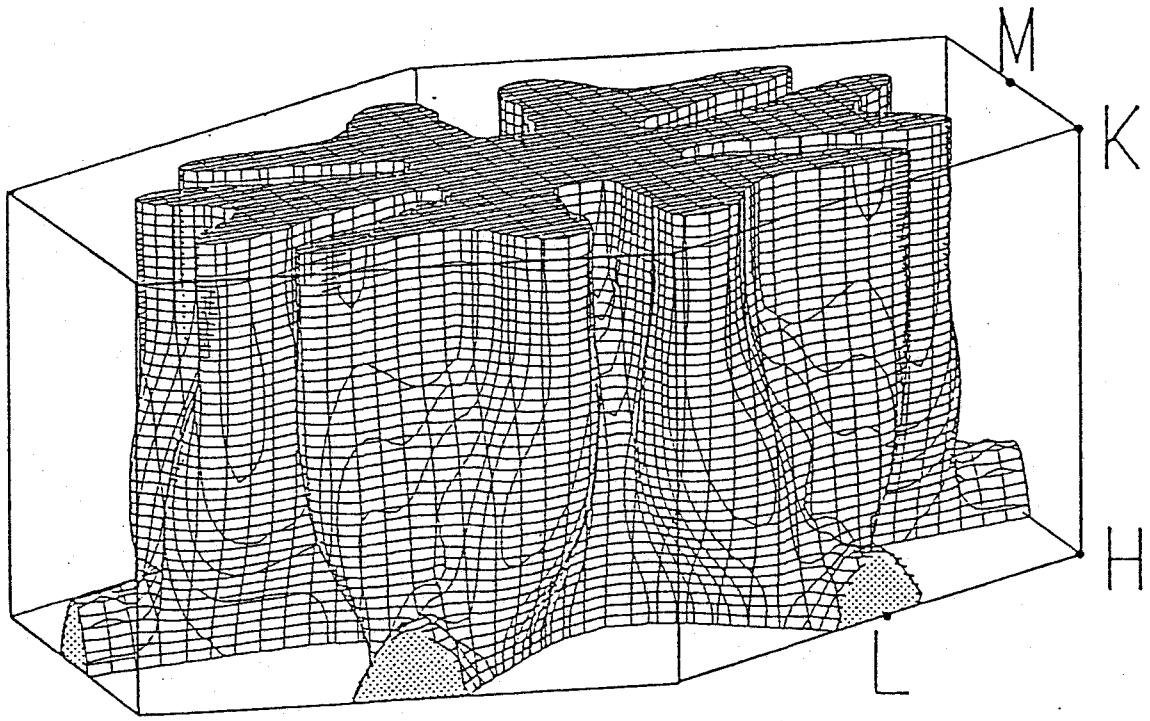

Fig.2-7(b). Fermi surface of NiAs.
The hole surface is shown.

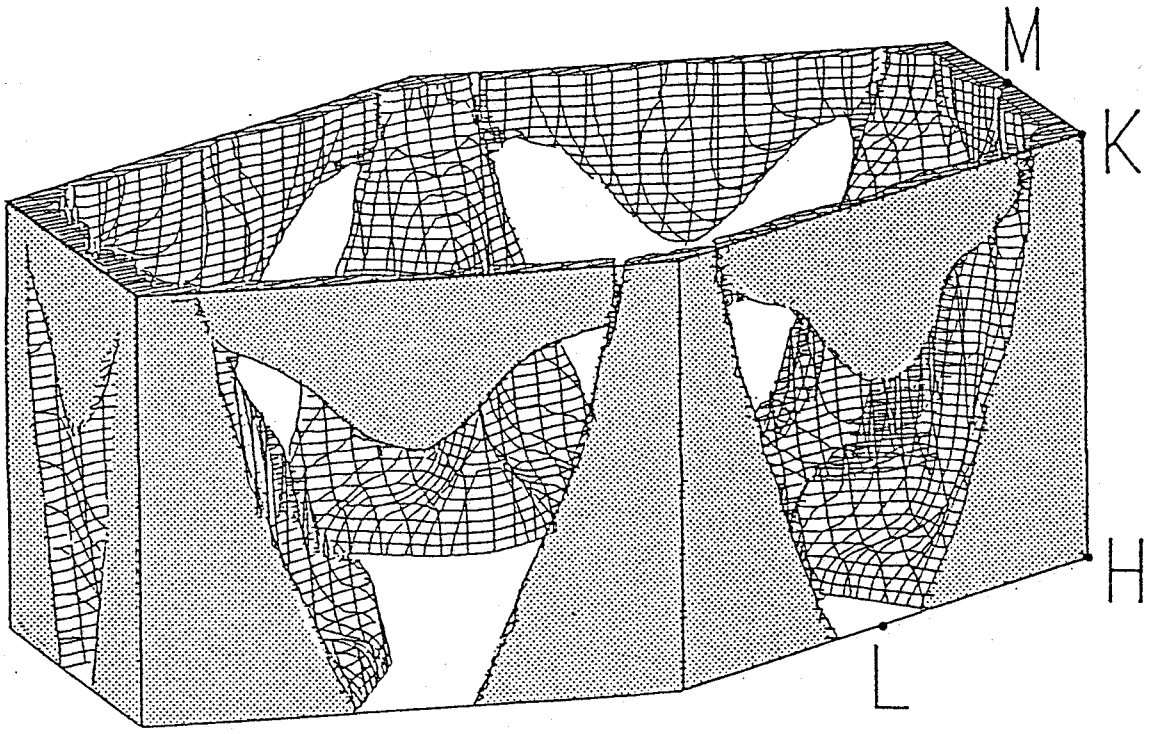

Fig.2-7(c). Fermi surface of NiAs.
The electron surface is shown.

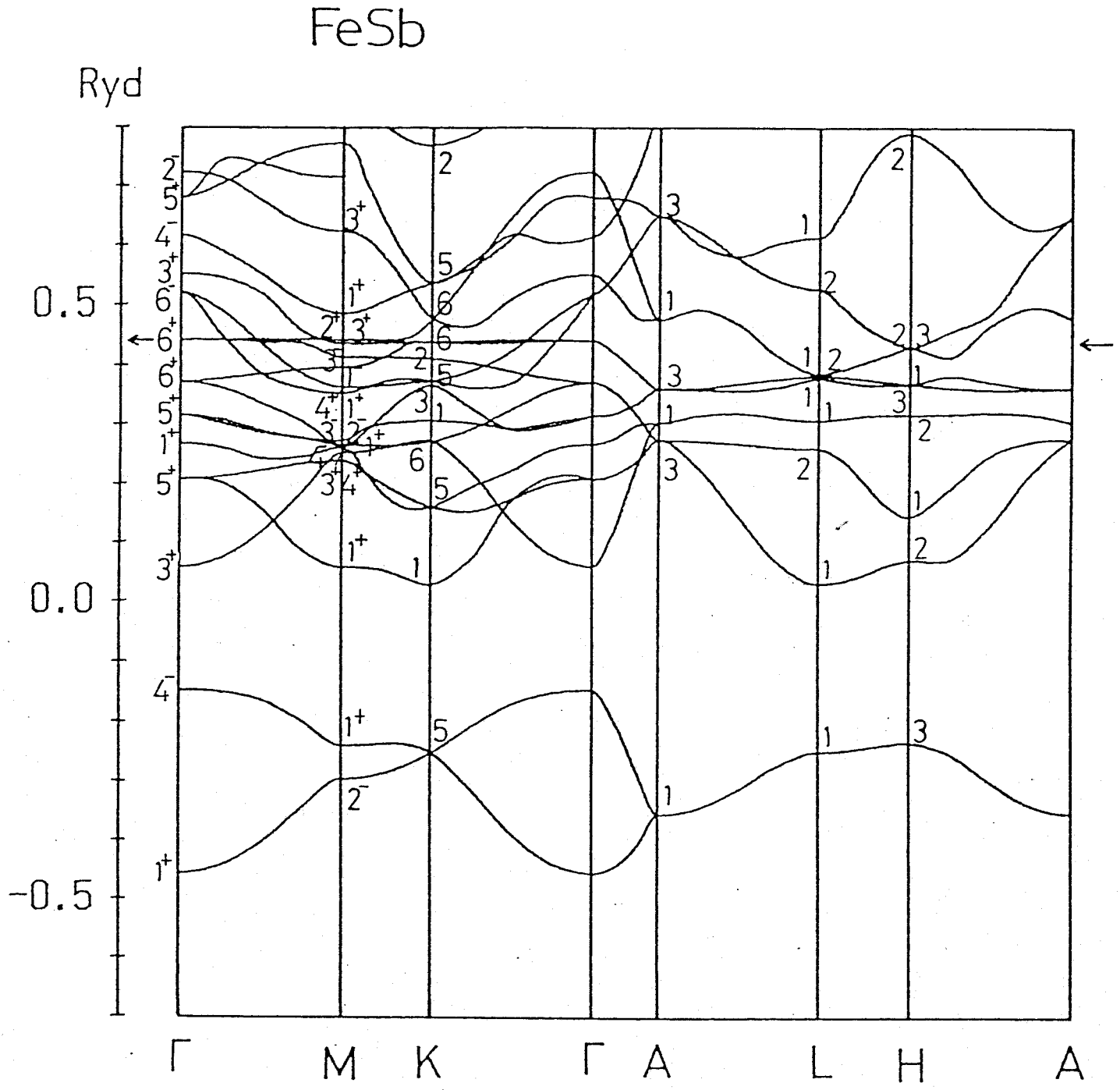

Fig.2-8(a). Dispersion curves of FeSb.

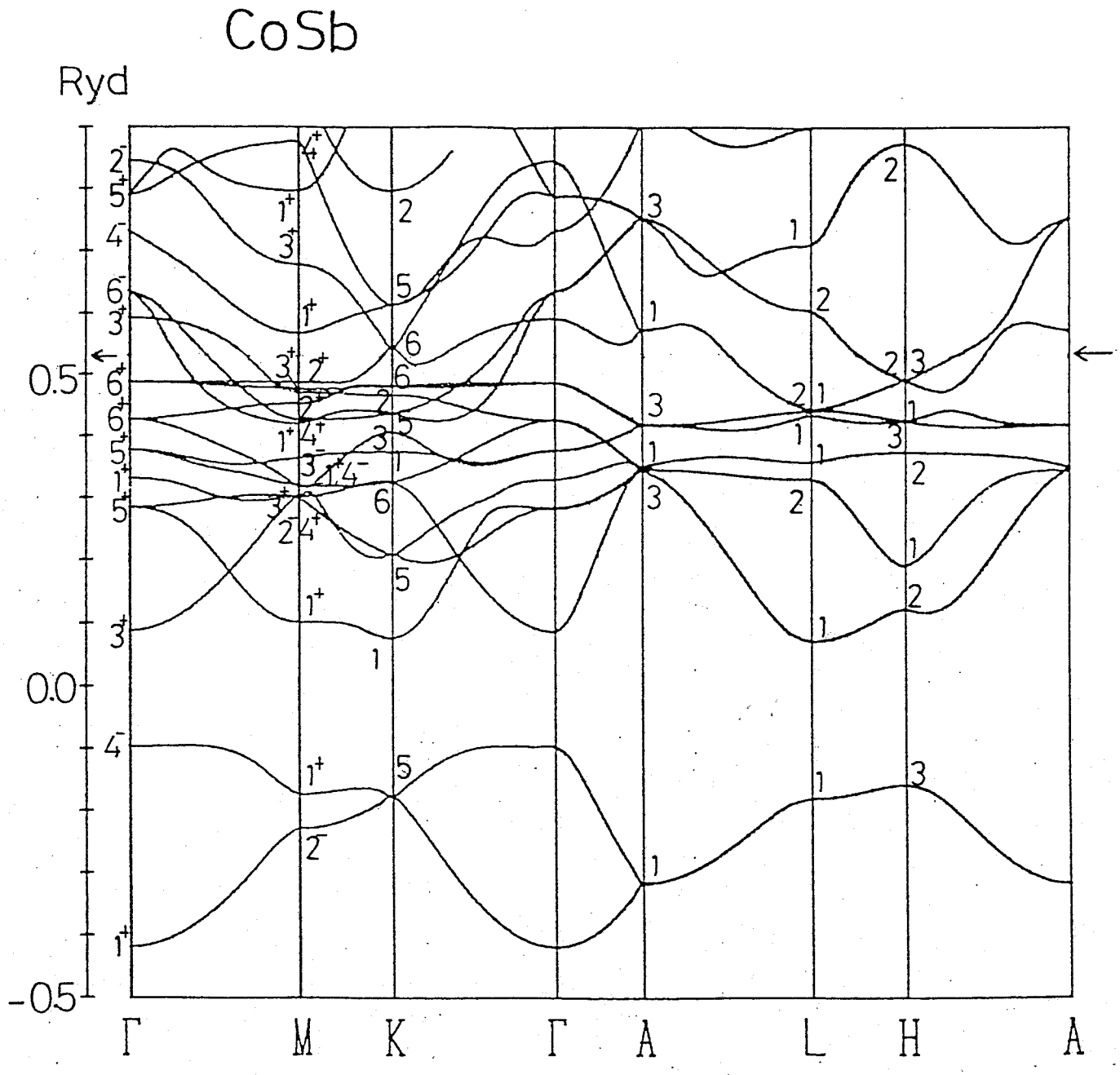

Fig.2-8(b). Dispersion curves of CoSb.

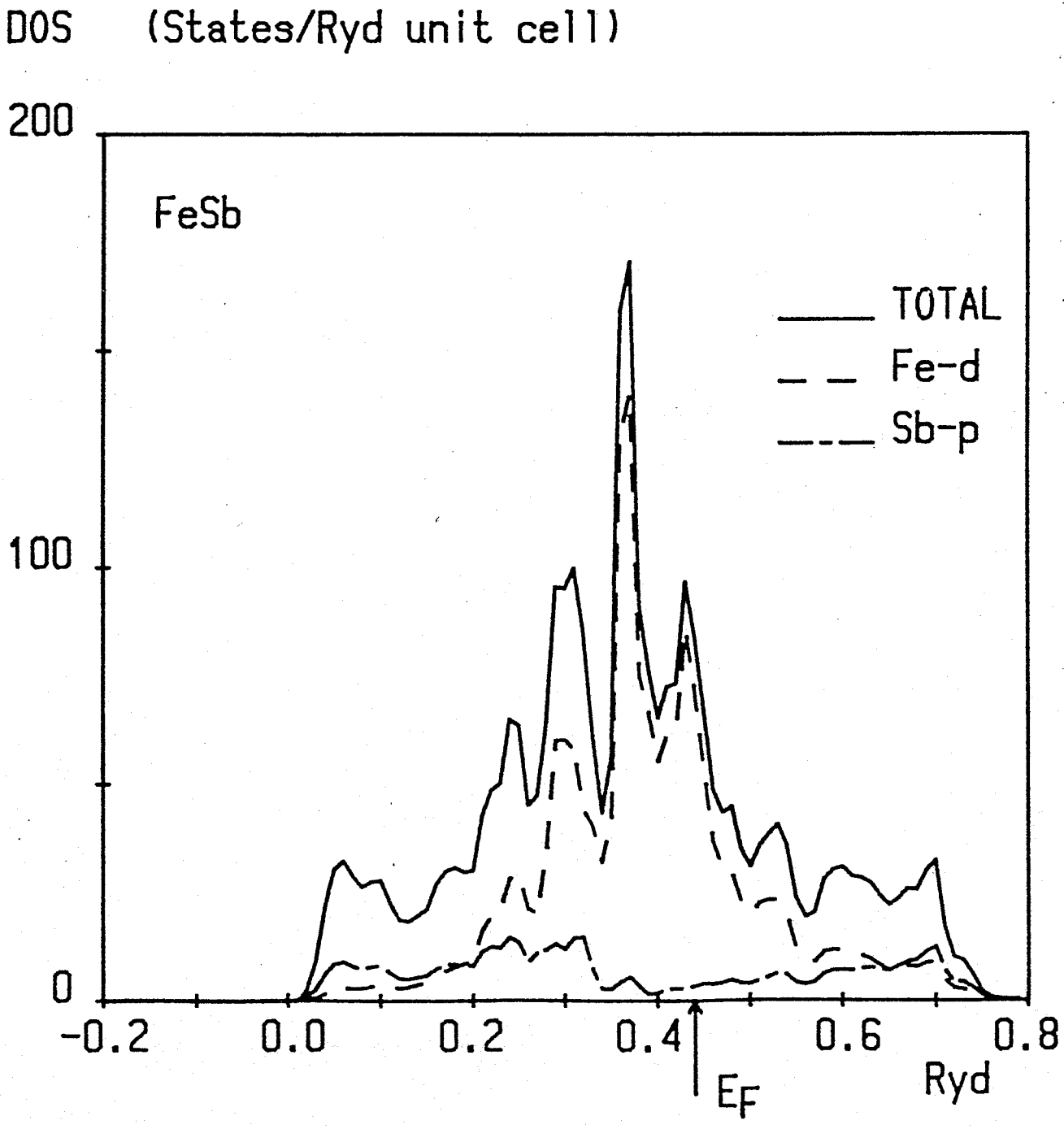

Fig.2-9(a). Density of States of FeSb.

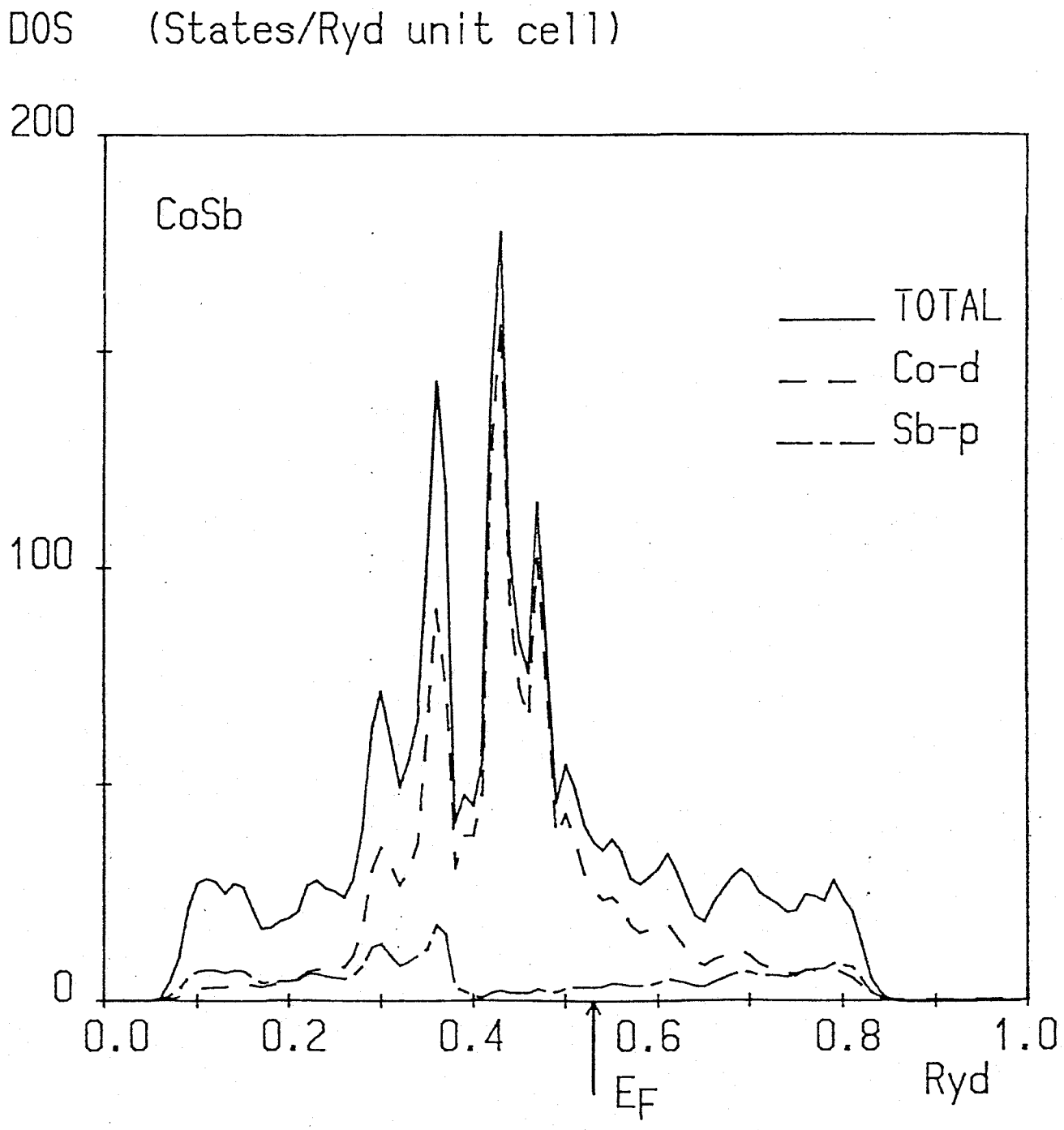

Fig.2-9(b). Density of states of CoSb.

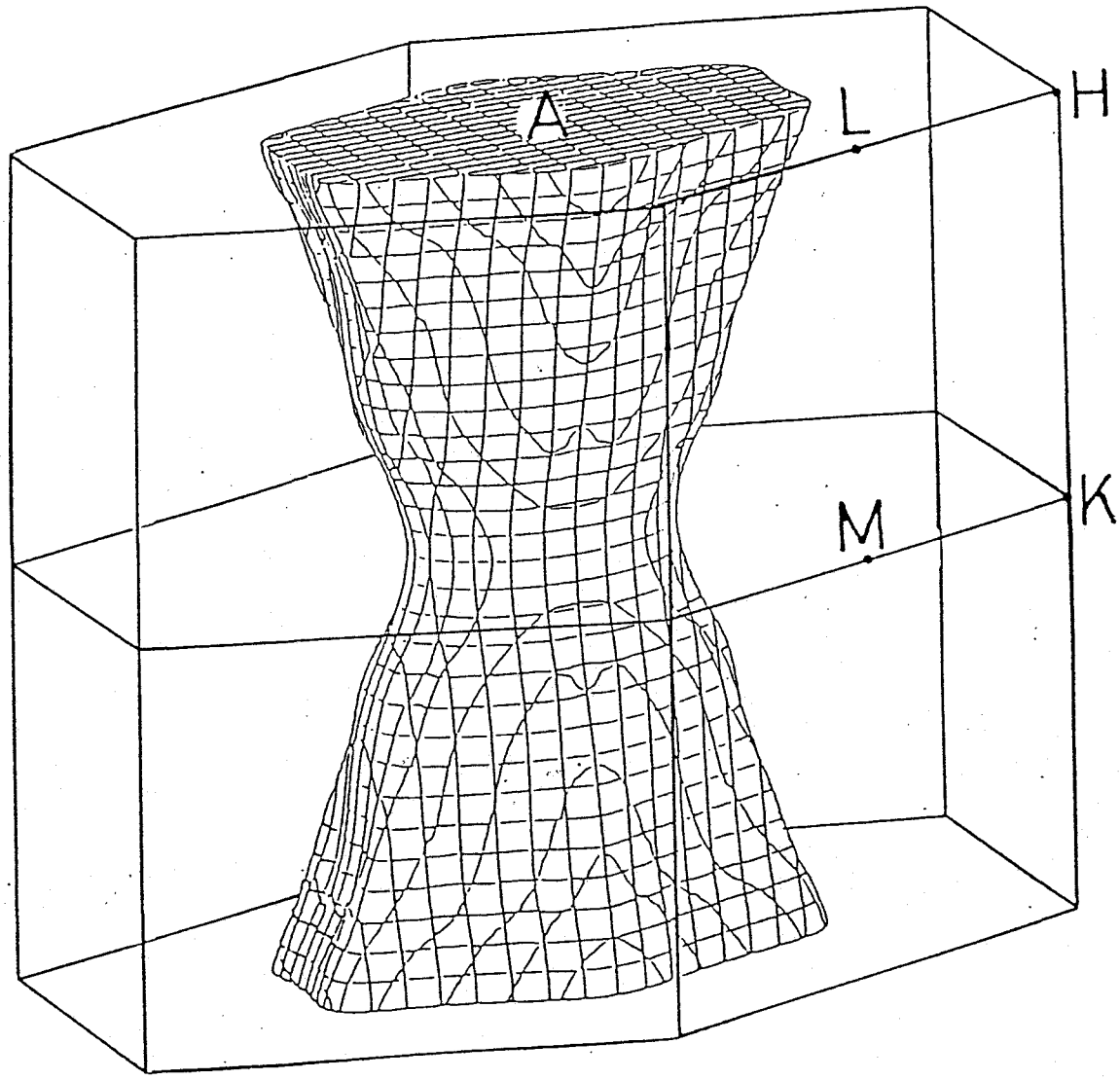

Fig.2-10(a). Fermi surface of CoSb.
The hole surface is shown.

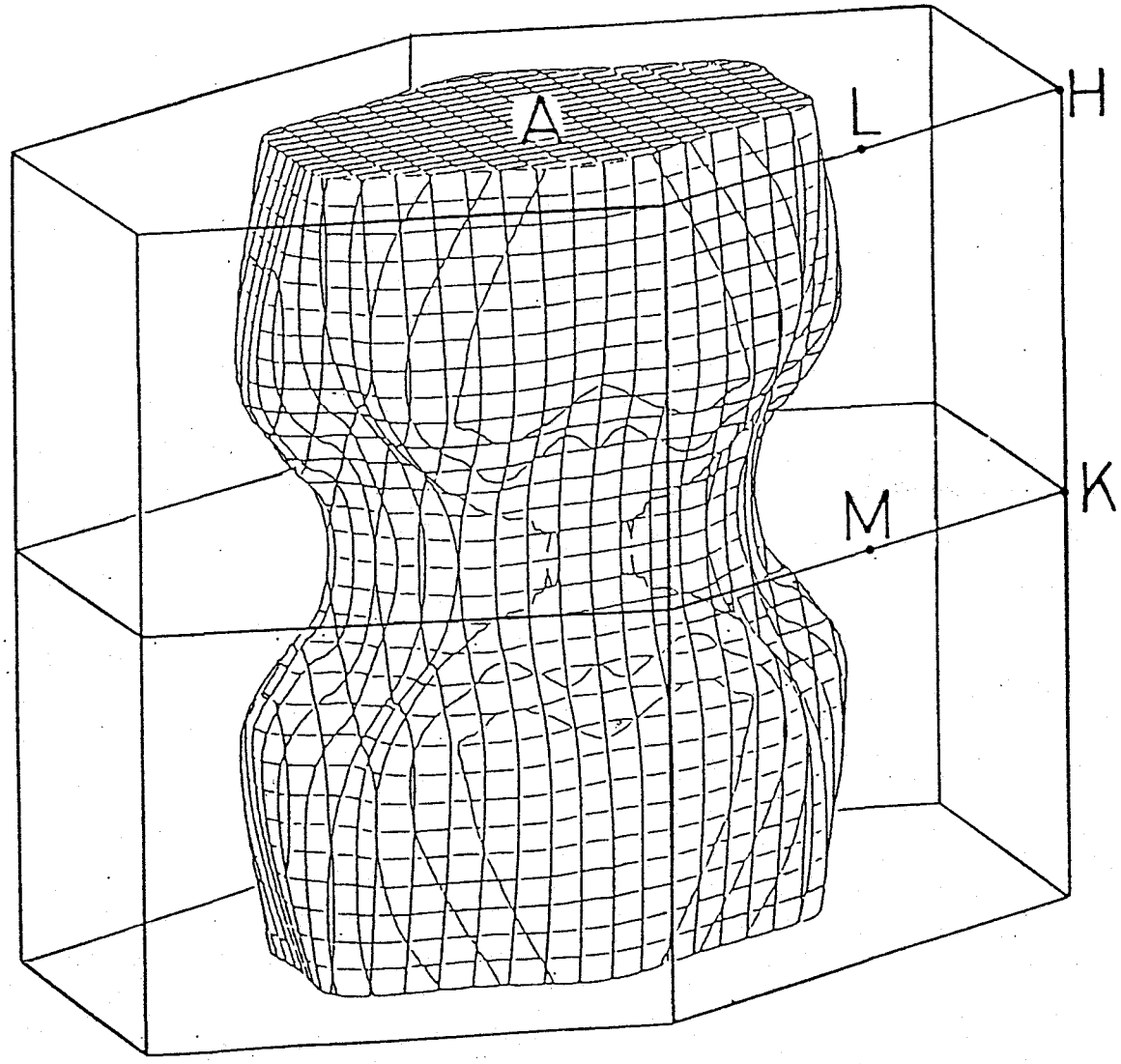

Fig.2-10(b). Fermi surface of CoSb.

The hole surface is shown.

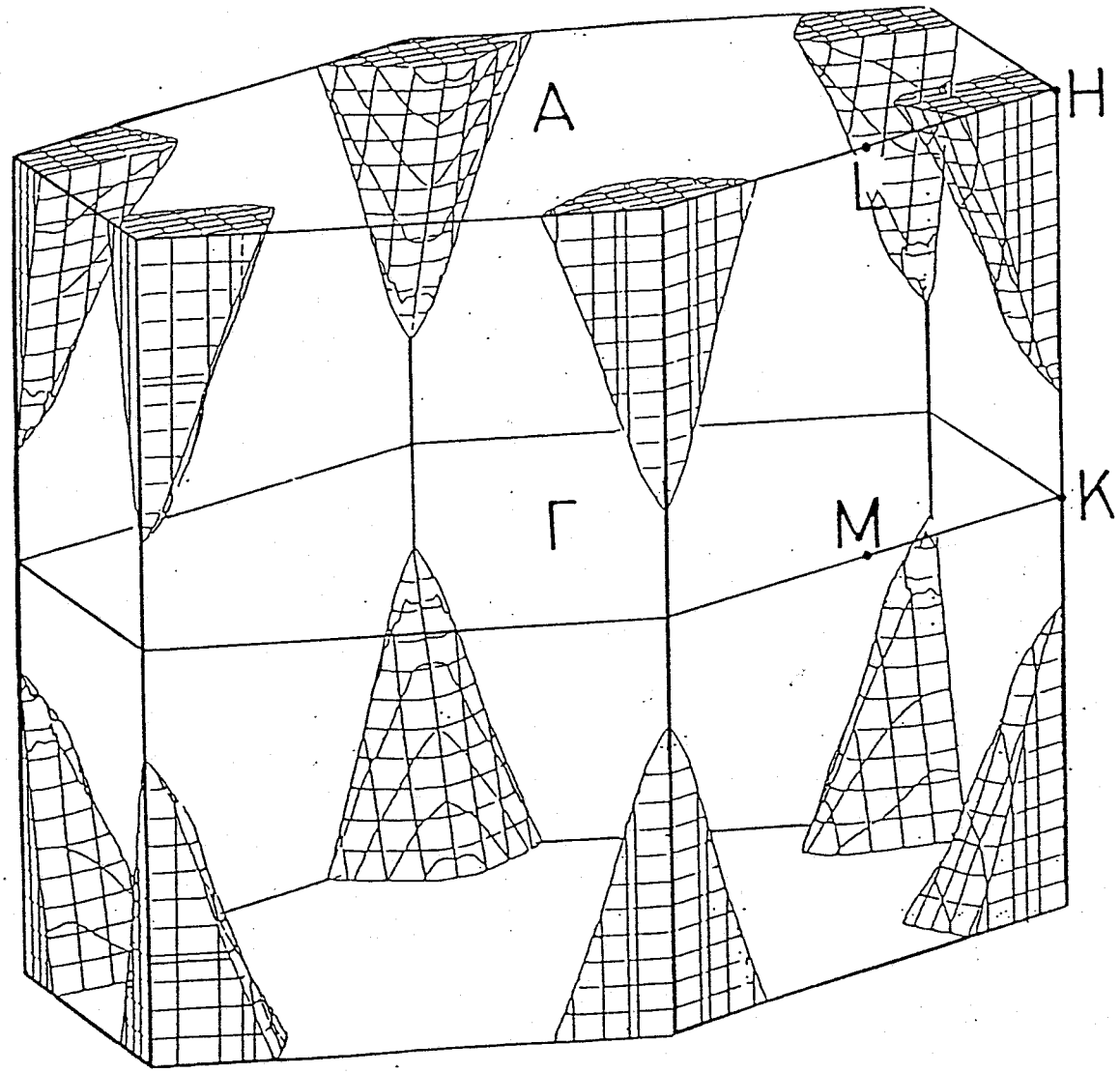

Fig.2-10(c). Fermi surface of CoSb.

The hole surface is shown.

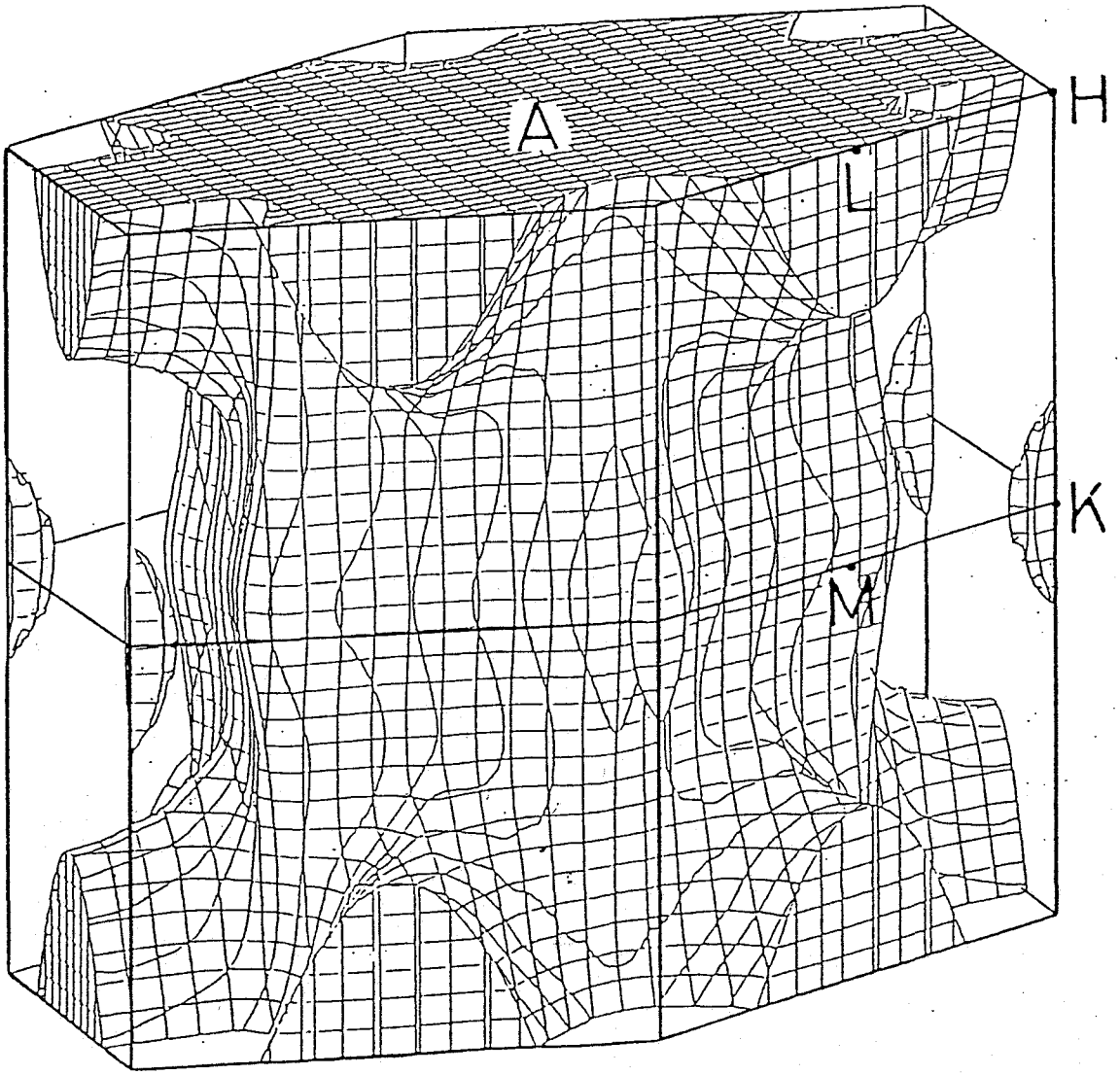

Fig.2-10(d). Fermi surface of CoSb.

The electron surface is shown.

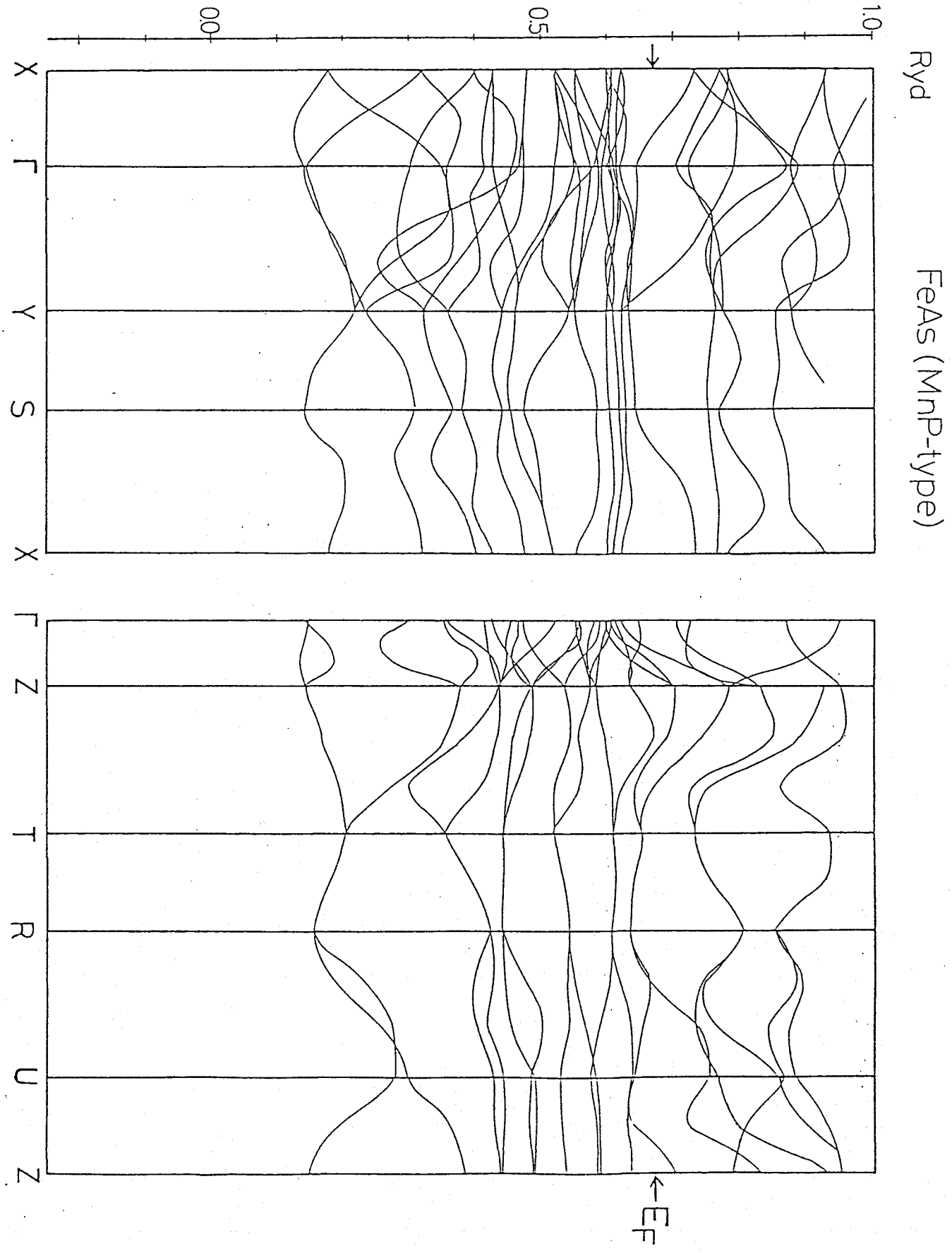

Fig.2-11(a). Dispersion curves of FeAs.

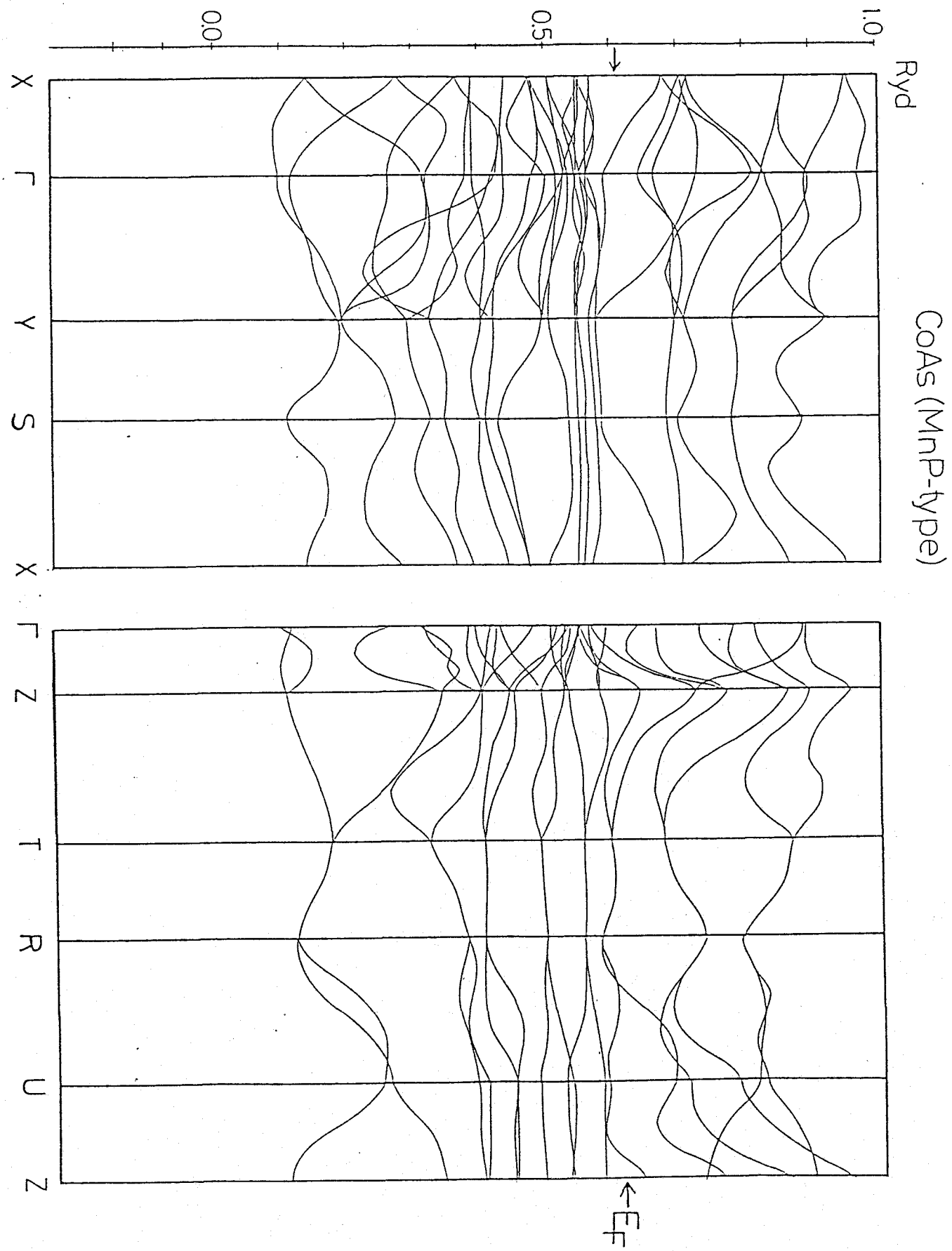

Fig.2-11(b). Dispersion curves of MnP-type CoAs.

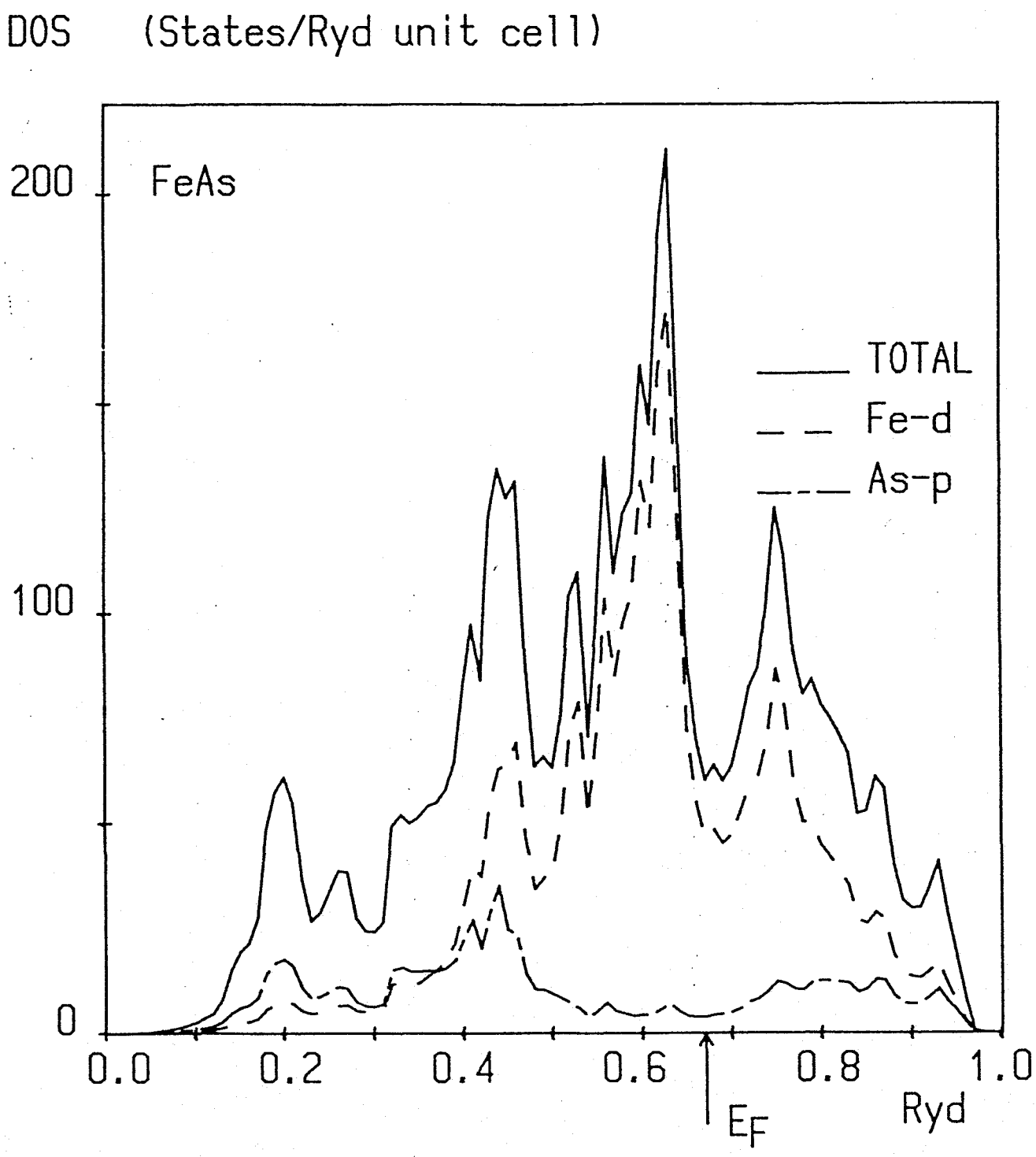

Fig.2-12(a). Density of states of FeAs.

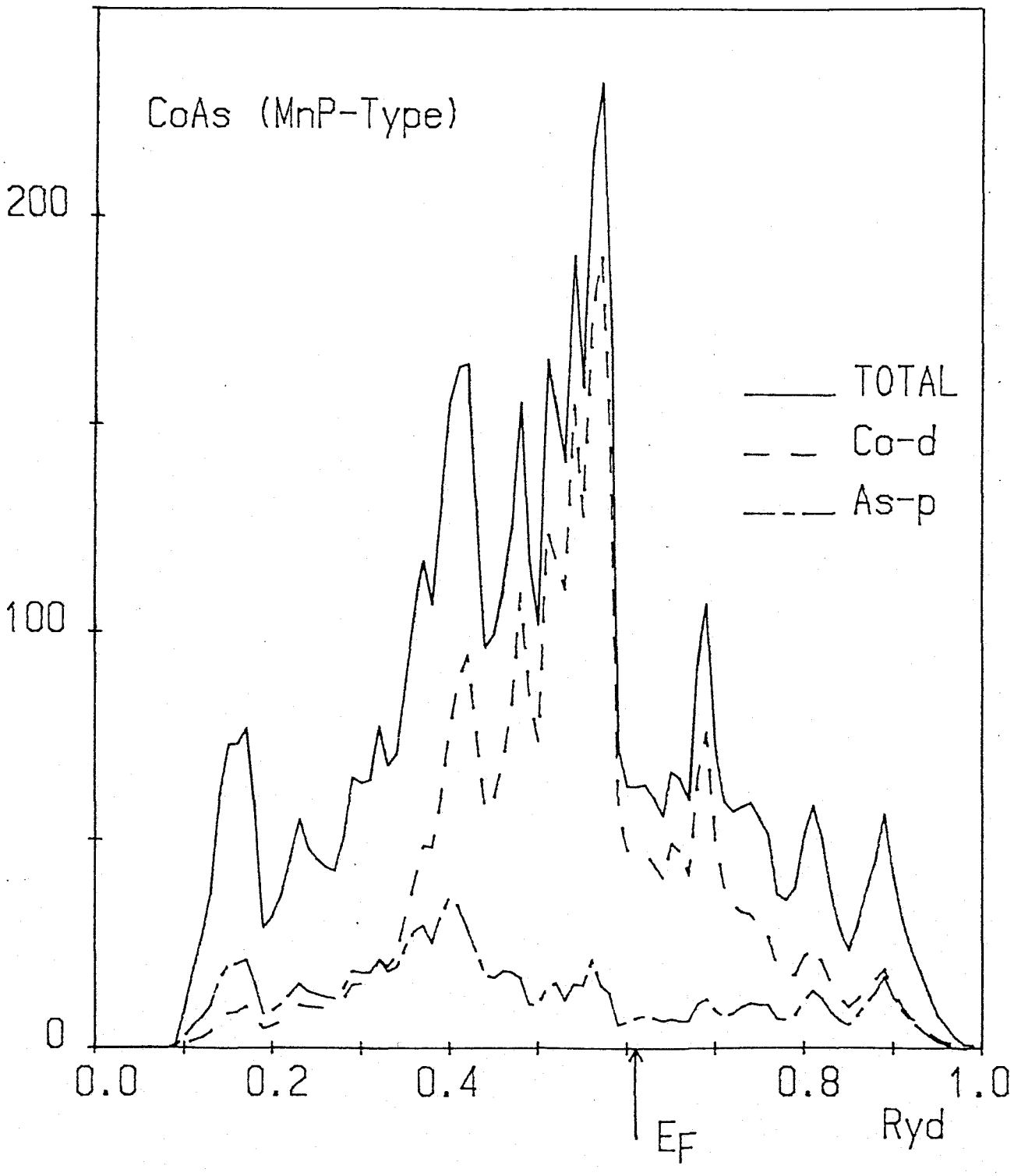

Fig.2-12(b). Density of states of MnP-type CoAs.

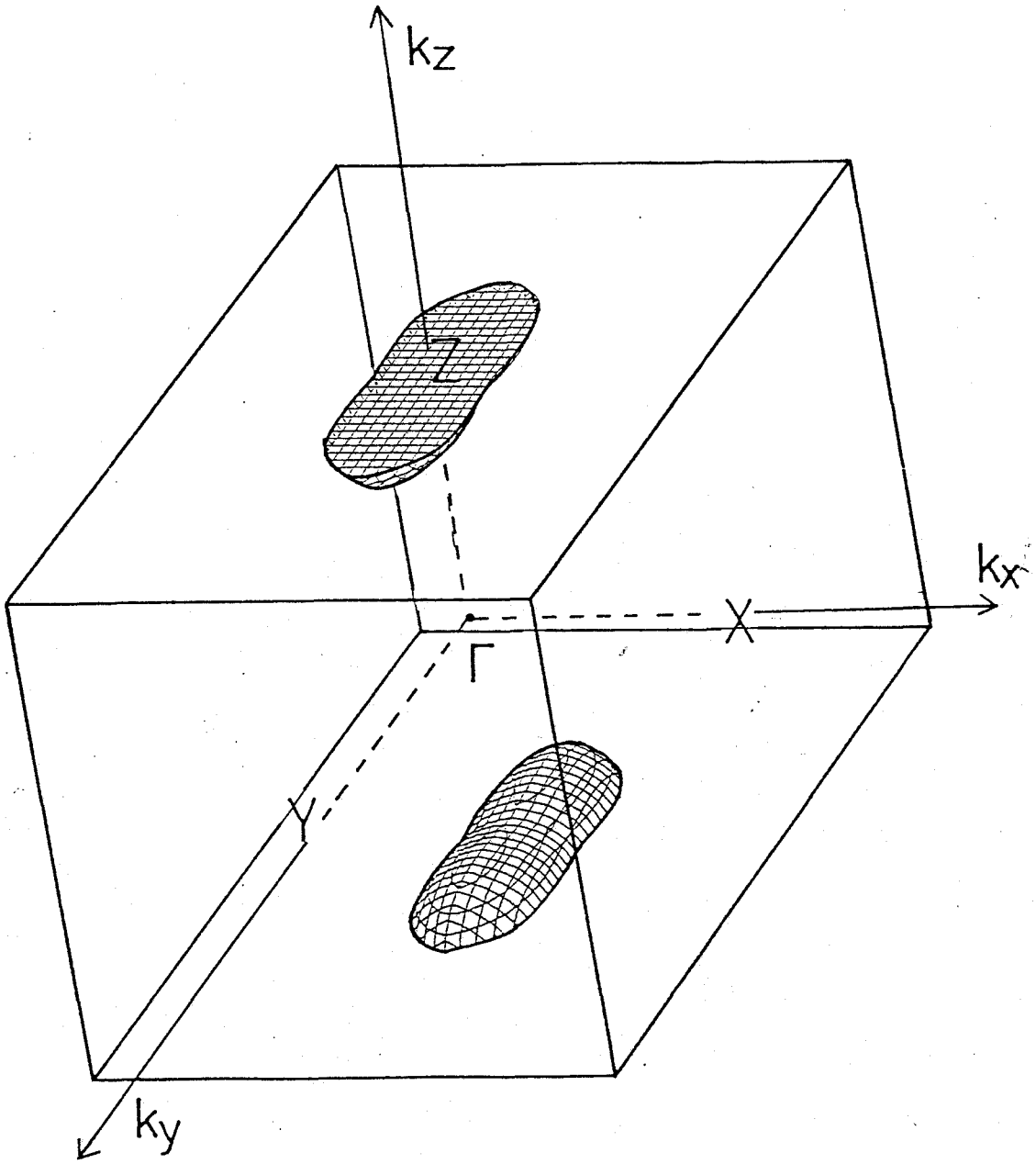

Fig.2-13(a). Fermi surface of FeAs.
The hole surface is shown.

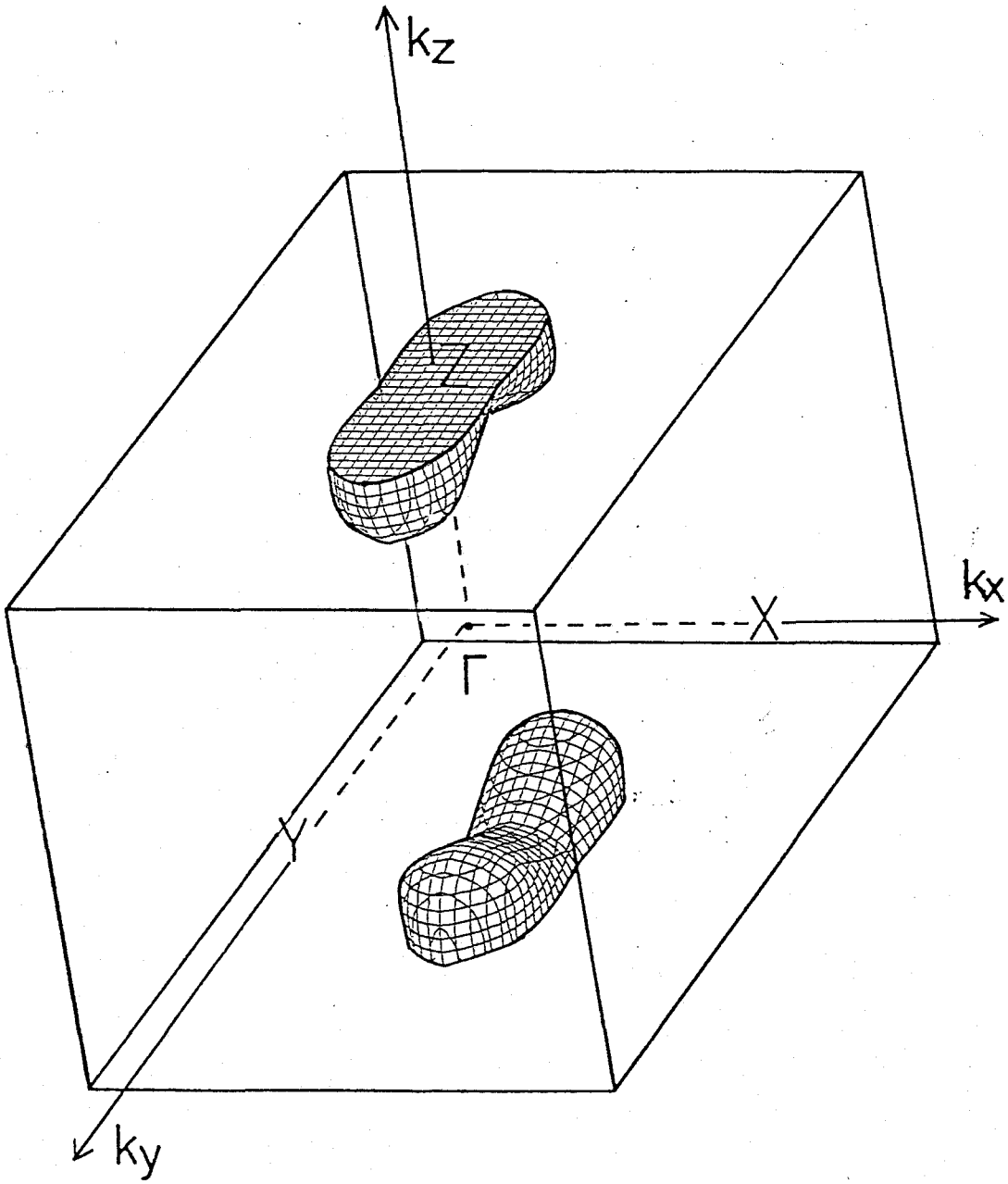

Fig.2-13(b). Fermi surface of FeAs.

The hole surface is shown.

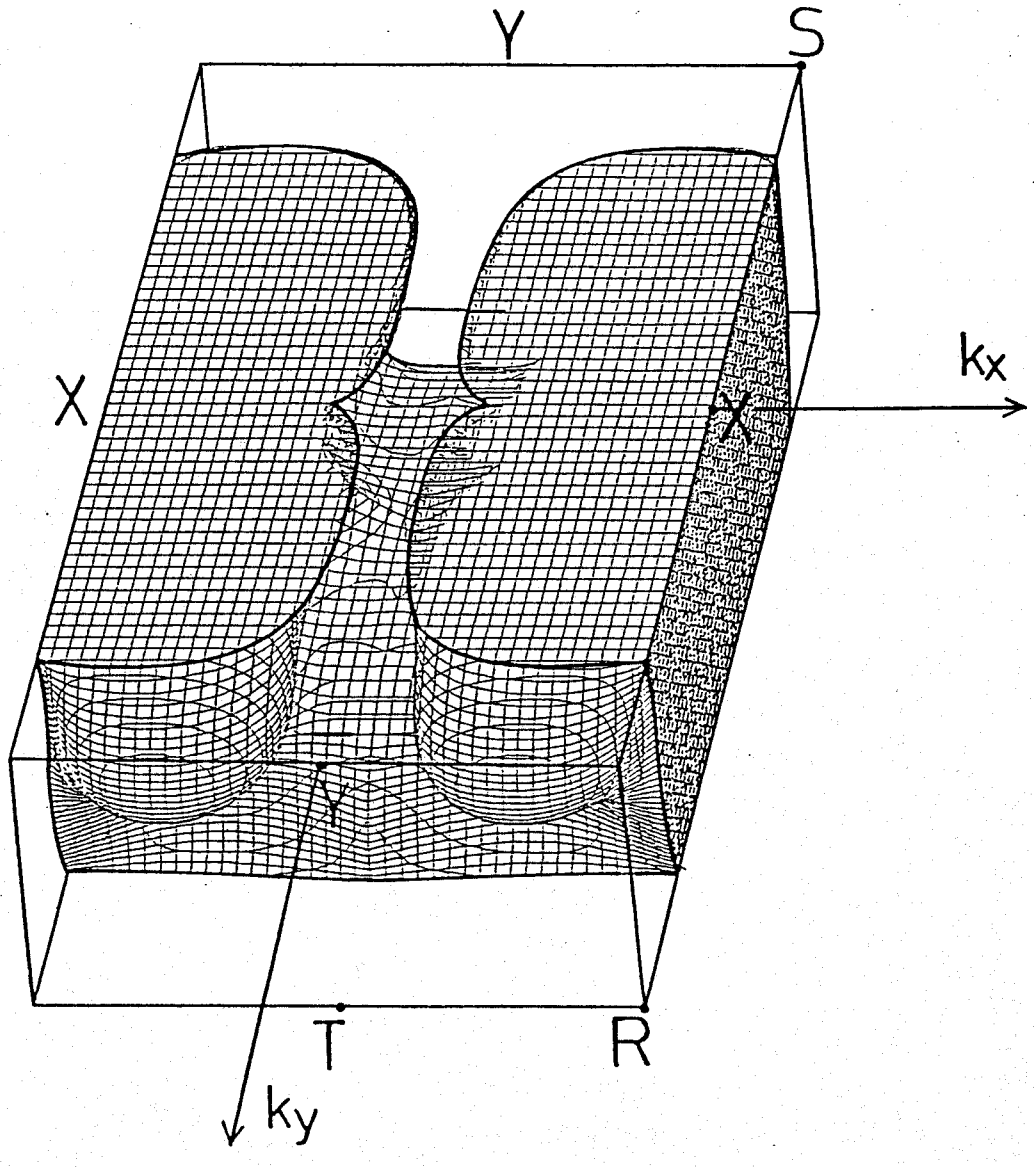

Fig.2-13(c). Fermi surface of FeAs.
The hole surface is shown.

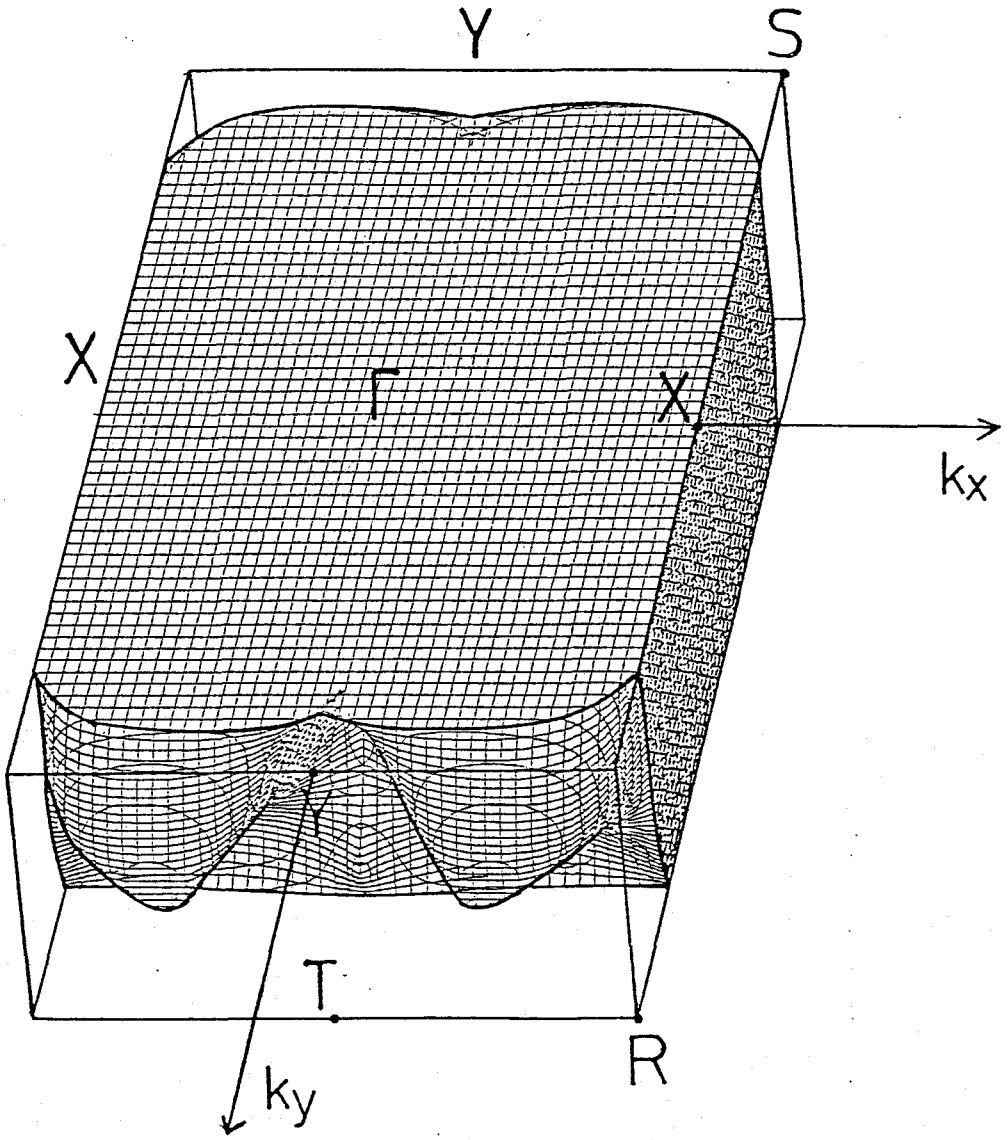

Fig.2-13(d). Fermi surface of FeAs.

The hole surface is shown.

2.3 Bond order

In order to clarify the nature of electronic band structure, we have calculated bond orders within the APW formalism and examined a character of each band. The bond order between two atomic orbitals is defined as follows:[23,24]

$$\mu^{\nu\nu'}_{\ell m;\ell' m'}(n,k) = \langle \phi^{\nu}_{\ell m} | \psi_{nk} \rangle_{\nu} \langle \psi_{nk} | \phi^{\nu'}_{\ell' m'} \rangle_{\nu'} \quad , \tag{2.7}$$

where ψ_{nk} denotes the Bloch function defined by eqs.(2.1) and (2.2), (n and k being the band suffix and a wave vector, respectively). $\phi^{\nu}_{\ell m}$ represents an atomic wave function, which is specified by the quantum number (ℓ,m), centered on the νth muffin-tin sphere and is given by

$$\phi^{\nu}_{\ell m}(r) = R^{\nu}_{\ell}(\rho) Y_{\ell m}(\hat{\rho}) \quad . \tag{2.8}$$

$\langle \ \rangle_{\nu}$ in eq.(2.7) denotes an integration within the νth muffin-tin sphere. Substituting eqs. (2.1), (2.2) and (2.8) into eq. (2.7), eq.(2.7) is written as

$$\mu^{\nu\nu'}_{\ell m;\ell' m'}(n,k) = \{ \sum_i c_i A^{\nu}_{\ell m}(k_i) \} \{ \sum_j c_j A^{\nu'}_{\ell' m'}(k_j) \}^{*} . \tag{2.9}$$

The bond order $\mu^{\nu\nu'}_{\ell m;\ell' m'}$ represents a correlation between two atomic orbitals, $\phi^{\nu}_{\ell m}$ and $\phi^{\nu'}_{\ell' m'}$, in the state ψ_{nk}. When both $\phi^{\nu}_{\ell m}$ and $\phi^{\nu'}_{\ell' m'}$ are much contained in the state ψ_{nk}, the magnitude of $\mu^{\nu\nu'}_{\ell m;\ell' m'}$ becomes large. In general $\mu^{\nu\nu'}_{\ell m;\ell' m'}$ is a complex quantity and its phase indicates the bonding nature between two orbitals.

It is more convenient to specify the real atomic wave

functions by taking linear combinations with regard to the quantum number m as

$$\phi^{\nu}_{\ell a} = \sum_{m} c_{\ell m a}\phi^{\nu}_{\ell m} \ . \tag{2.10}$$

Thus the suffix "a" in eq. (2.10) denotes kind of atomic orbitals such as p_x , d_{xy} etc. Using eq. (2.10) the bond orders between these real atomic wave functions are given by

$$\mu^{\nu\nu'}_{\ell a;\ell' a'}(n,\mathbf{k}) = \sum_{mm'} c_{\ell m a} c^{*}_{\ell' m' a'} \mu^{\nu\nu'}_{\ell m;\ell' m'}(n,\mathbf{k}) \ . \tag{2.11}$$

Considering the degeneracy of two Bloch states $(n,\mathbf{k})$ and $(n,-\mathbf{k})$, we redefine the bond order between two atomic orbitals as follows:

$$\beta^{\nu\nu'}_{\ell a;\ell' a'}(n,\mathbf{k}) = \frac{1}{2}\left[\mu^{\nu\nu'}_{\ell a;\ell' a'}(n,\mathbf{k}) + \mu^{\nu\nu'}_{\ell a;\ell' a'}(n,-\mathbf{k})\right] \ , \tag{2.12}$$

The bond order defined by eq.(2.12) is a real number and the sign of β is related to the bonding- or antibonding-nature. We take appropriate sign of atomic orbitals so that $\beta>0$ means bonding and $\beta<0$ means antibonding.

Using eqs. (2.1), (2.2) and orthogonarity of the spherical harmonic functions, charge density inside the νth muffin-tin sphere is written as

$$\begin{aligned} \langle \psi_{n\mathbf{k}} | \psi_{n\mathbf{k}} \rangle_{\nu} &= \sum_{\ell m} \Big\{ \sum_{i} c_i A^{\nu}_{\ell m}(\mathbf{k}_i) \Big\} \Big\{ \sum_{j} c_j A^{\nu}_{\ell m}(\mathbf{k}_j) \Big\}^{*} \\ &= \sum_{\ell m} \mu^{\nu\nu}_{\ell m;\ell m}(n,\mathbf{k}) \\ &= \sum_{\ell a} \beta^{\nu\nu}_{\ell a;\ell a}(n,\mathbf{k}) \ . \end{aligned} \tag{2.13}$$

Thus we can regard the quantity $\beta^{\nu\nu}_{\ell a;\ell a}(n,\mathbf{k})$ as a contribution of the charge arising from the atomic wave function ,$\phi^{\nu}_{\ell a}$.

We have calculated the bond orders of NiAs-type CoAs for wave vectors along the Σ-line ((1,0,0)- direction). The symmetry of the Σ-line is C_{2v} and there are four irreducible representations. As there are some prominent peaks in the density of states of the p-d mixing bands of CoAs, we have divided the p-d mixing bands into four regions as shown in Fig.2-14:

(i) 0.0-0.2 Ryd,

(ii) 0.2-0.3 Ryd,

(iii) 0.3-0.5 Ryd,

(iv) 0.5-0.8 Ryd.

Firstly, by using eq. (2.13) we have calculated $\beta^{\nu\nu}_{\ell a;\ell a}(n,\mathbf{k})$ for each band in each energy region. We have taken a new coordinate system in which the x'-, y'- and z'- axes are directed from a Co atom toward an As atom as shown in Fig.2-15, because Co atoms are surrounded nearly octahedrally by six As atoms. The calculated results for the bands in the region (i), (ii), (iii) and (iv) are shown in Fig.16(a)-(e). The bands used for the calculation are denoted as thick curves in each figure. The calculated charge in the muffin-tin spheres arising from Co-dγ ($d_{3z'^2-r'^2}$ and $d_{x'^2-y'^2}$) orbitals, Co-dε ($d_{x'y'}$, $d_{y'z'}$ and $d_{z'x'}$) orbitals and As-p orbitals are denoted as a cross, an open circle and a triangle, respectively, in Fig.16(a) -(e). From the results we may say that the kind of atomic orbitals which contribute mainly to the bands in each energy region are as follows :

the region (i) ;As-p orbitals,

the region (ii) ;Co-dγ orbitals and As-p orbitals,

the region (iii);Co-dγ and Co-dε orbitals for the lower energy bands and Co-dε orbitals for the upper energy bands,

the region (iv) ;Co-dγ orbitals and As-p orbitals.

The Fermi level is located at the upper energy part in the region (iii) where the states consist of almost dε orbitals of Co atoms.

Next we have calculated bond orders between the $d_{3z',2-r',2}$ orbital of Co and the $p_{z'}$ orbital of As for some bands. The calculated results shown in Fig.2-18(a) and (b) indicate that the lower energy part of the p-d mixing bands (the region (i) and (ii)) has bonding nature and the upper energy part of the p-d mixing bands (the region (iv)) has antibonding nature. On the other hand the middle part of the p-d mixing bands (the region (iii)) has non-bonding nature because As-p orbitals are not contained in the states of this region.

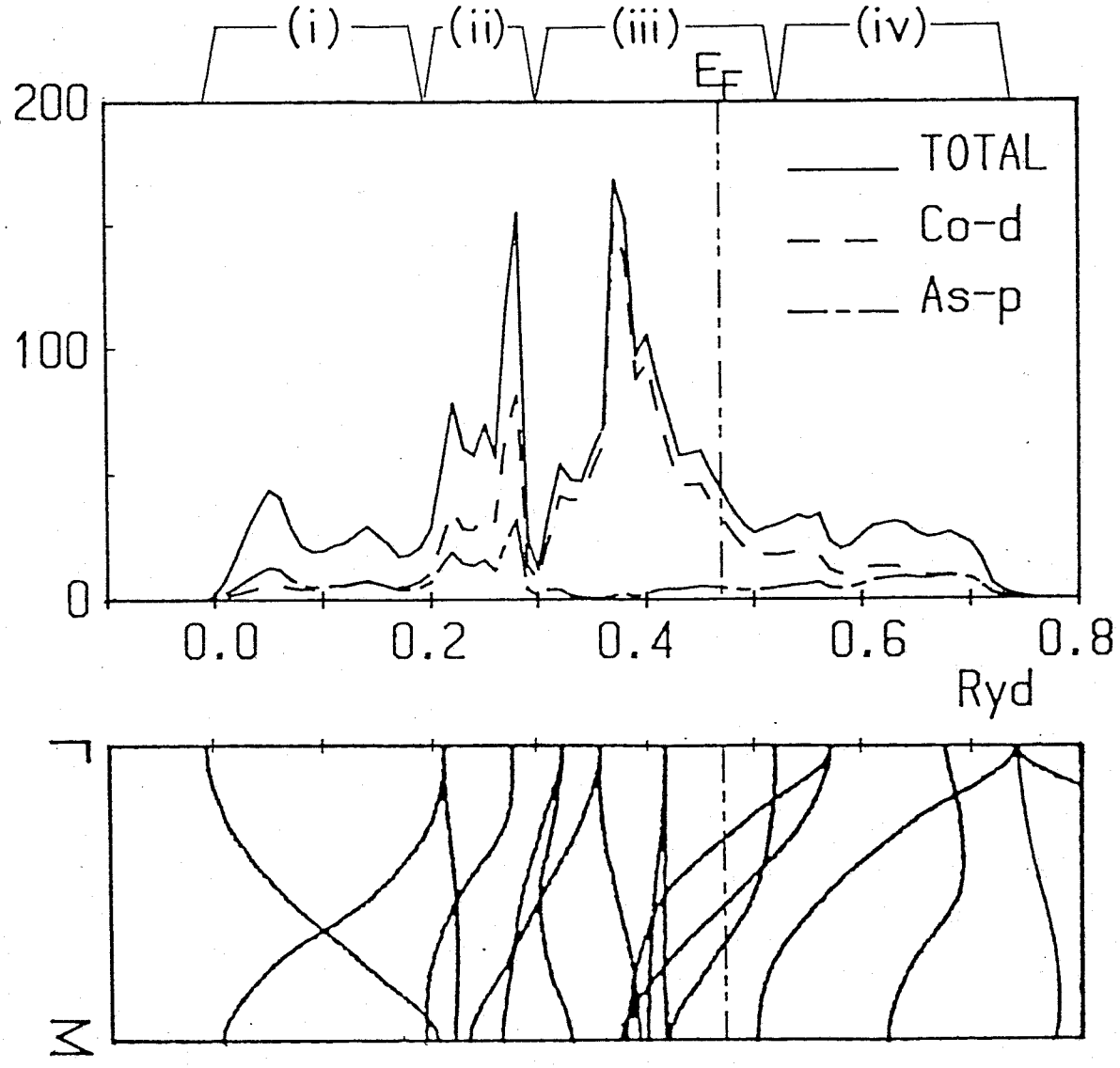

Fig.2-14. The density of states and the dispersion curves along the ΓM line of NiAs-type CoAs.

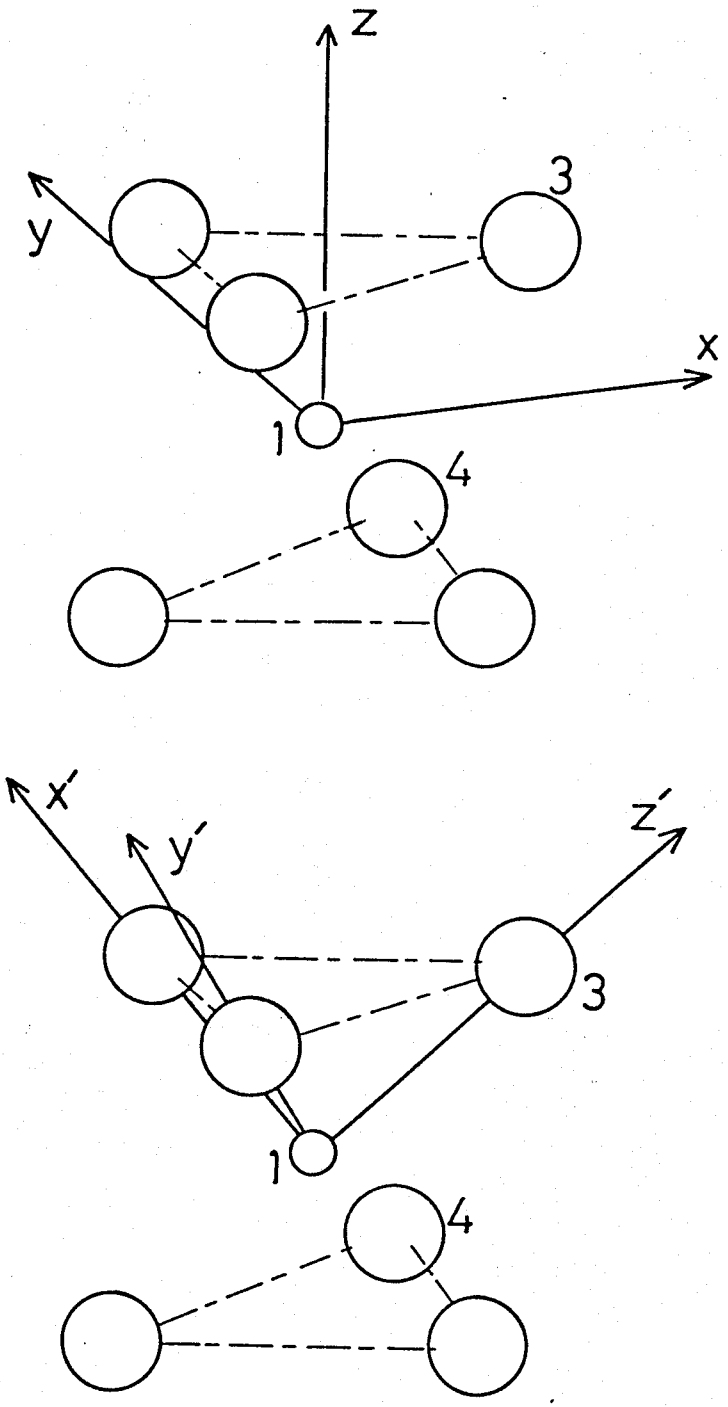

Fig.2-15. The coordinate system fixed to the crystal (a) and local coordinate system (b). The metal atoms and As atoms are denoted by small and large circles.

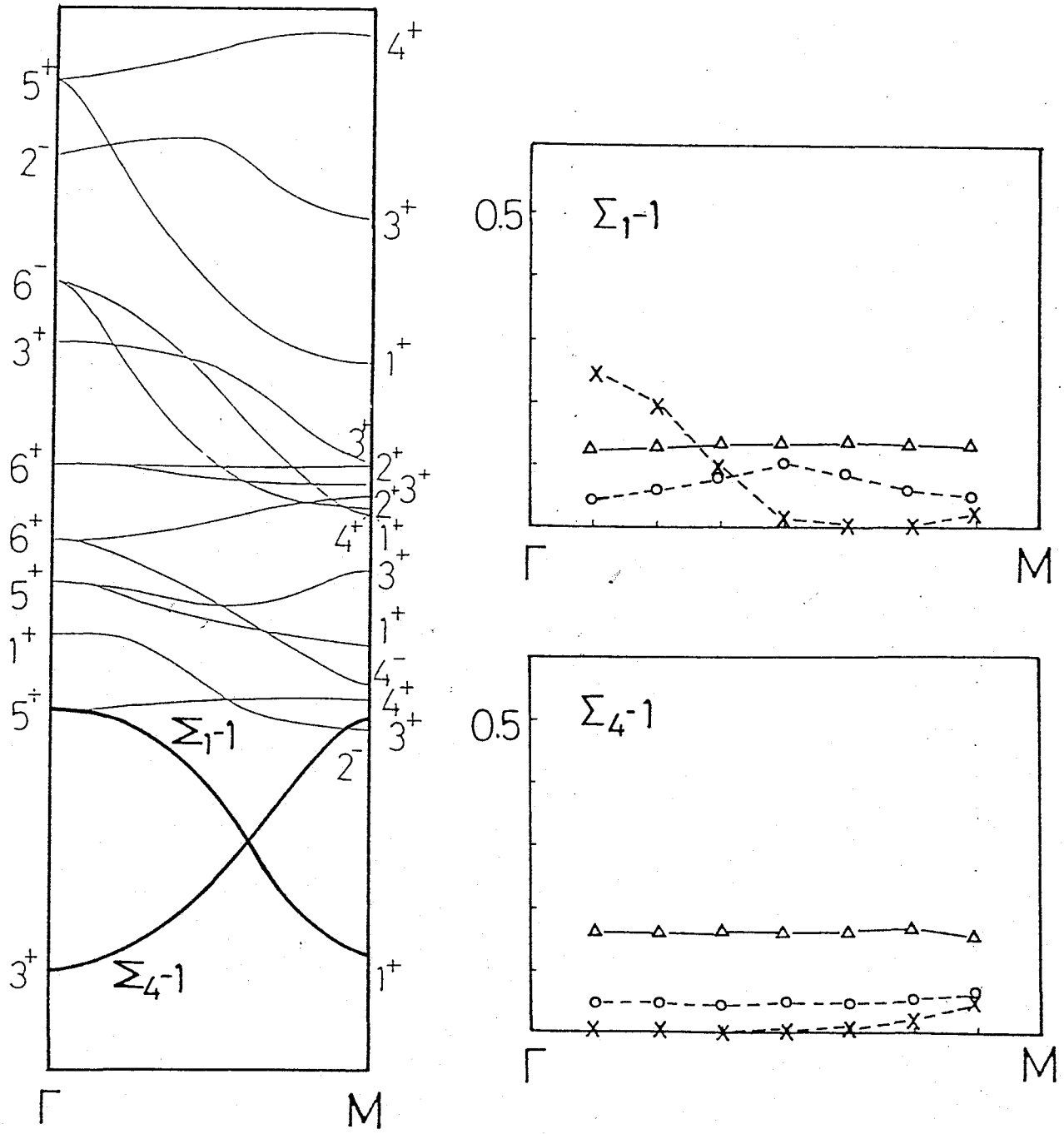

Fig.2-16(a). The bond order $\beta^{\nu;\nu}_{\ell a;\ell a}(n,k)$ for Co-dγ orbitals(x), Co-dε orbitals(o) and As-p orbitals(Δ), respectively, for the bands in the energy region (i).

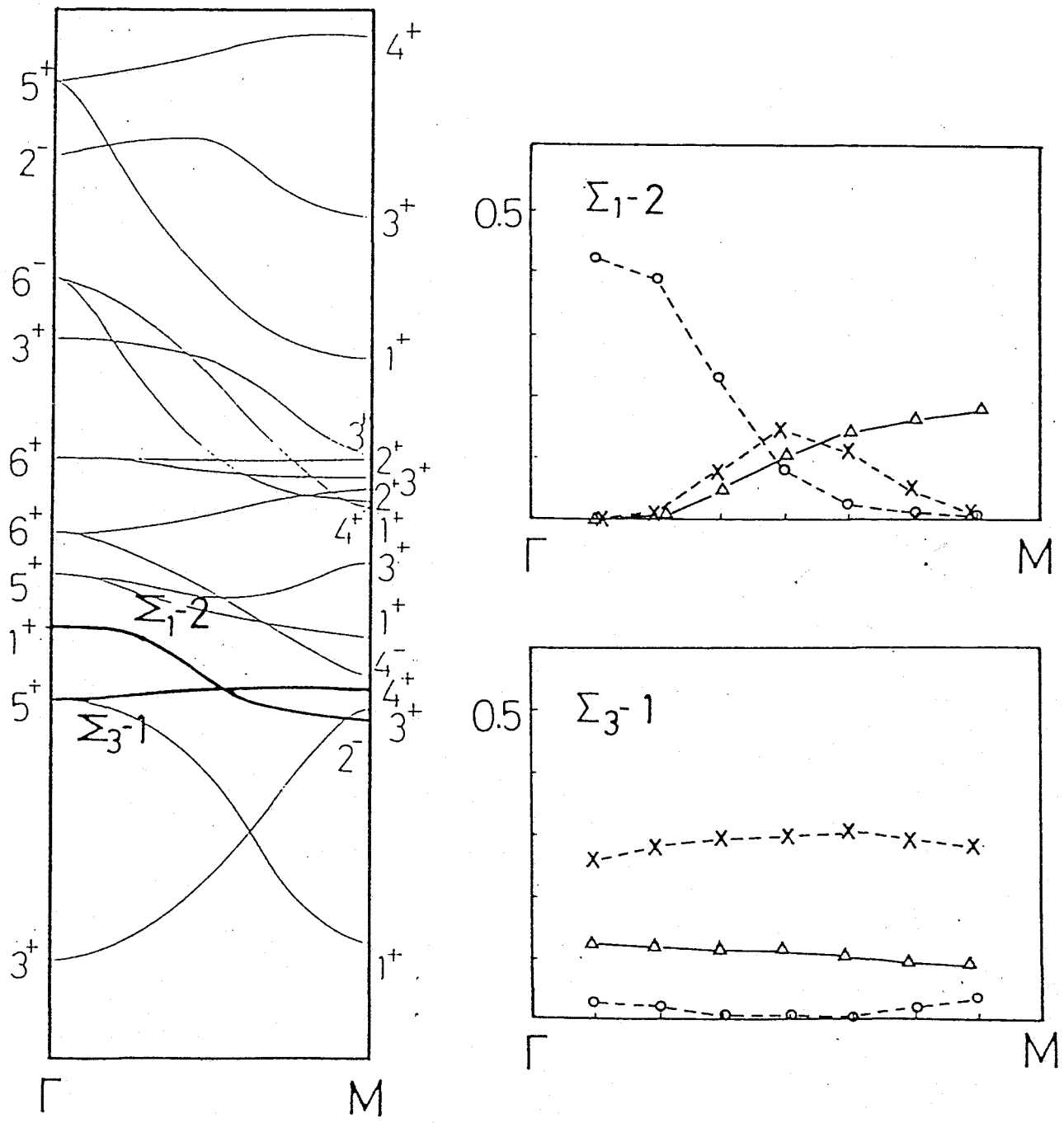

Fig.2-16(b). The bond order $\beta^{\nu;\nu}_{\ell a;\ell a}(n,k)$ for Co-dγ orbitals(x), Co-dε orbitals(o) and As-p orbitals(△), respectively, for the bands in the energy region (ii).

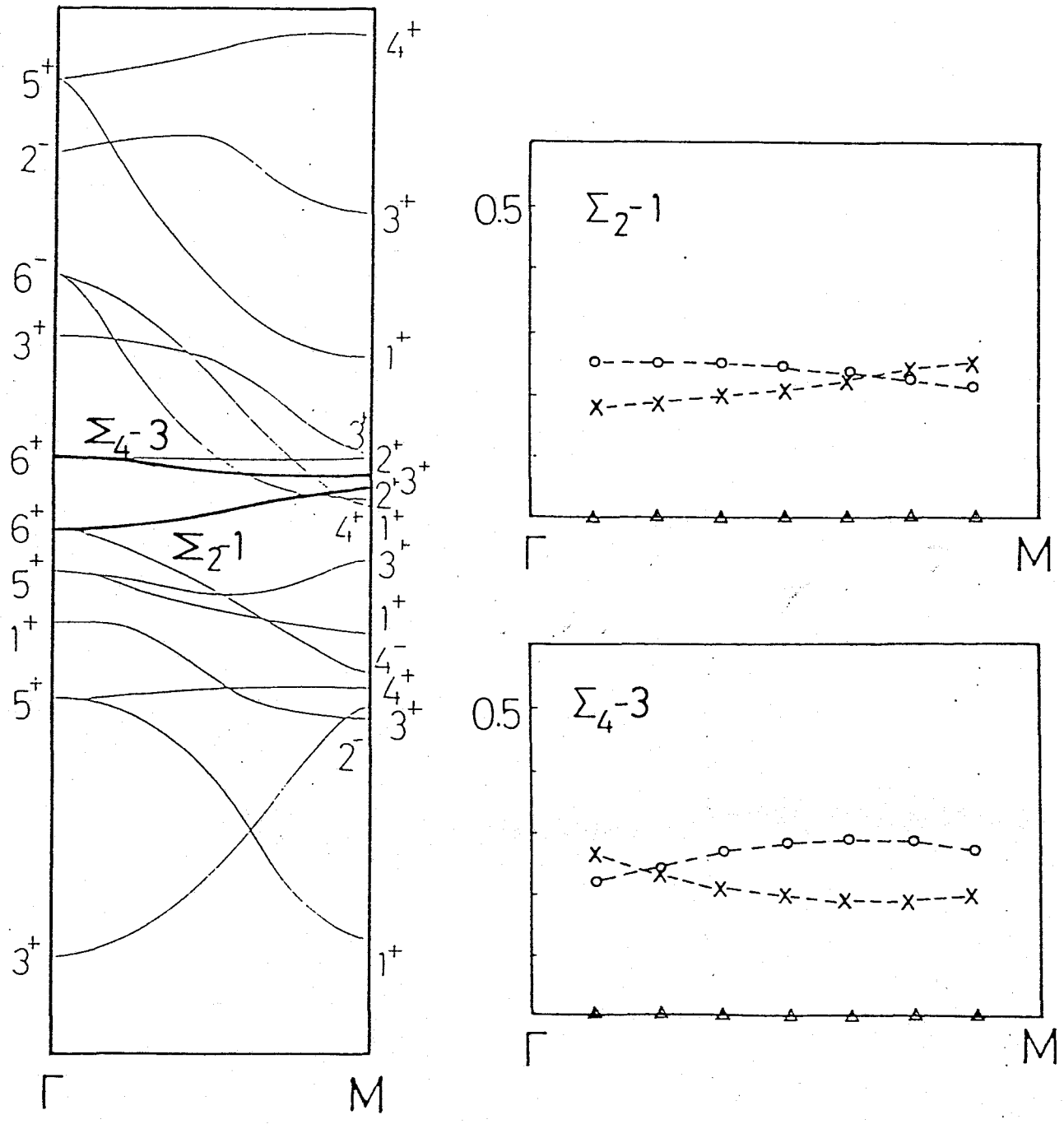

Fig.2-16(c). The bond order $\beta^{\nu;\nu}_{\ell a;\ell a}(n,k)$ for Co-dγ orbitals(x), Co-dε orbitals(o) and As-p orbitals(Δ), respectively, for the bands in the energy region (iii).

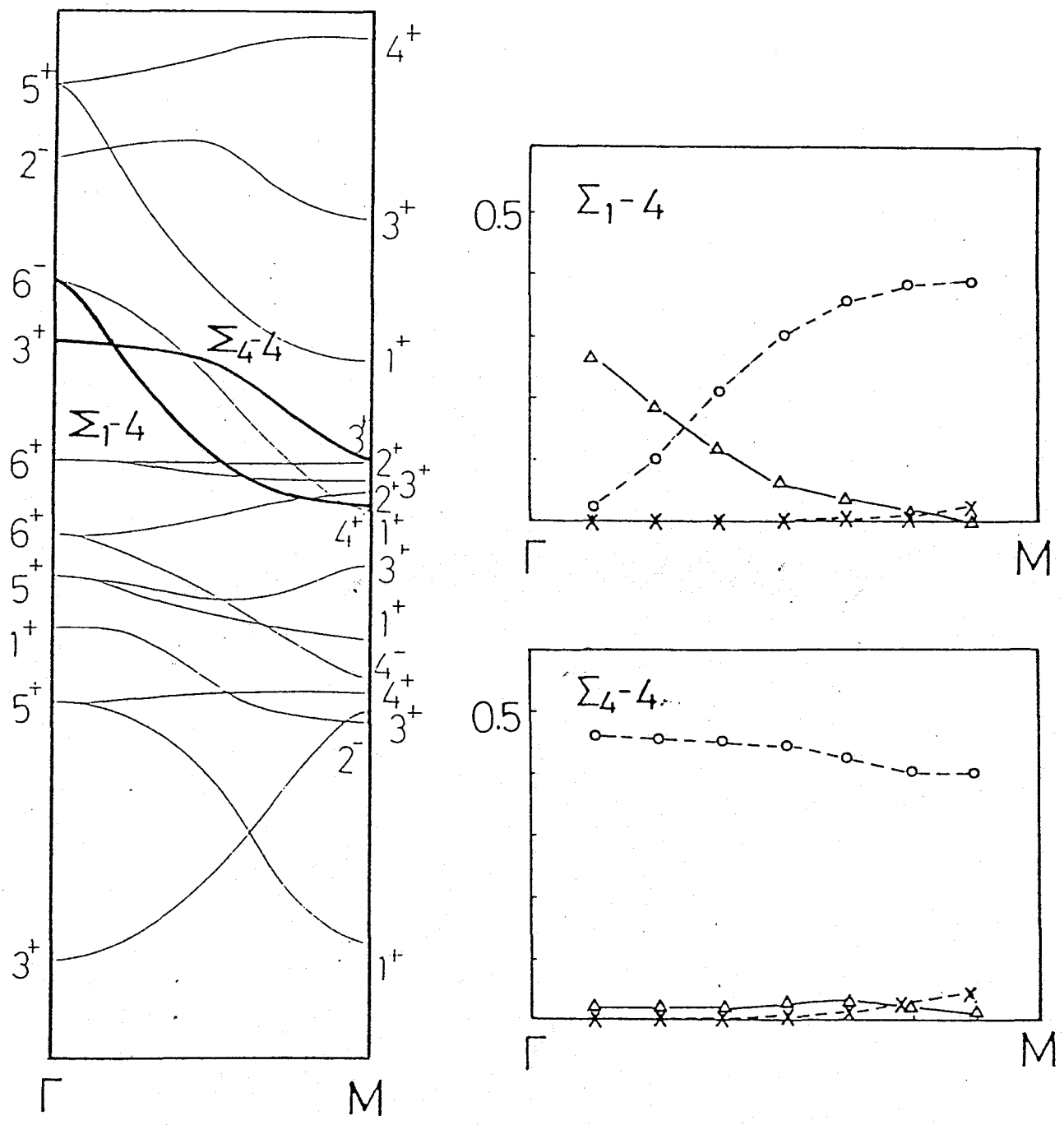

Fig.2-16(d). The bond order $\beta^{\nu;\nu}_{\ell a;\ell a}(n,k)$ for Co-dγ orbitals(X), Co-dε orbitals(o) and As-p orbitals(Δ), respectively, for the bands in the energy region (iii).

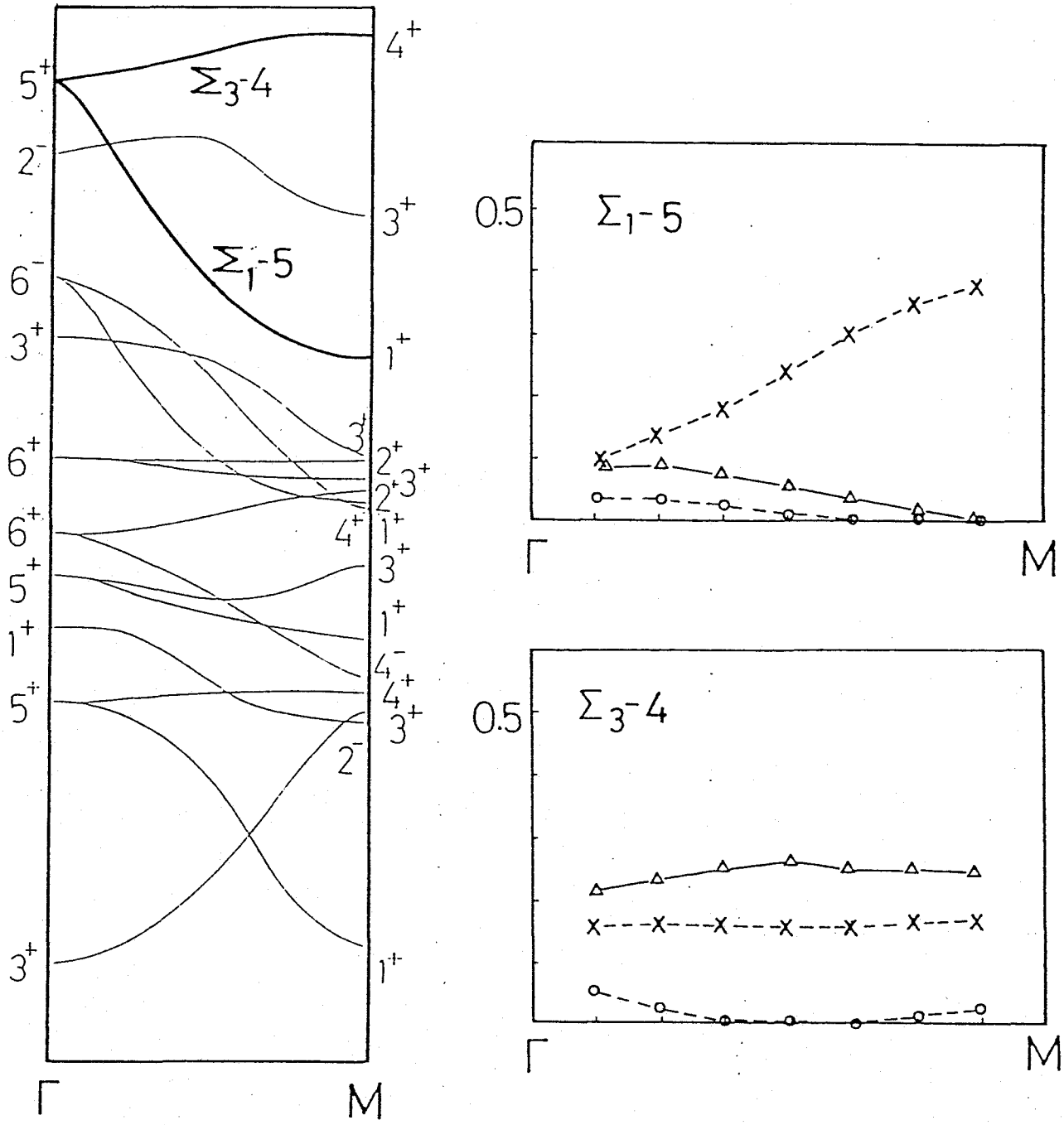

Fig.2-16(e). The bond order $\beta^{\nu;\nu}_{\ell a;\ell a}(n,k)$ for Co-dγ orbitals(x), Co-dε orbitals(o) and As-p orbitals(Δ), respectively, for the bands in the energy region (iv).

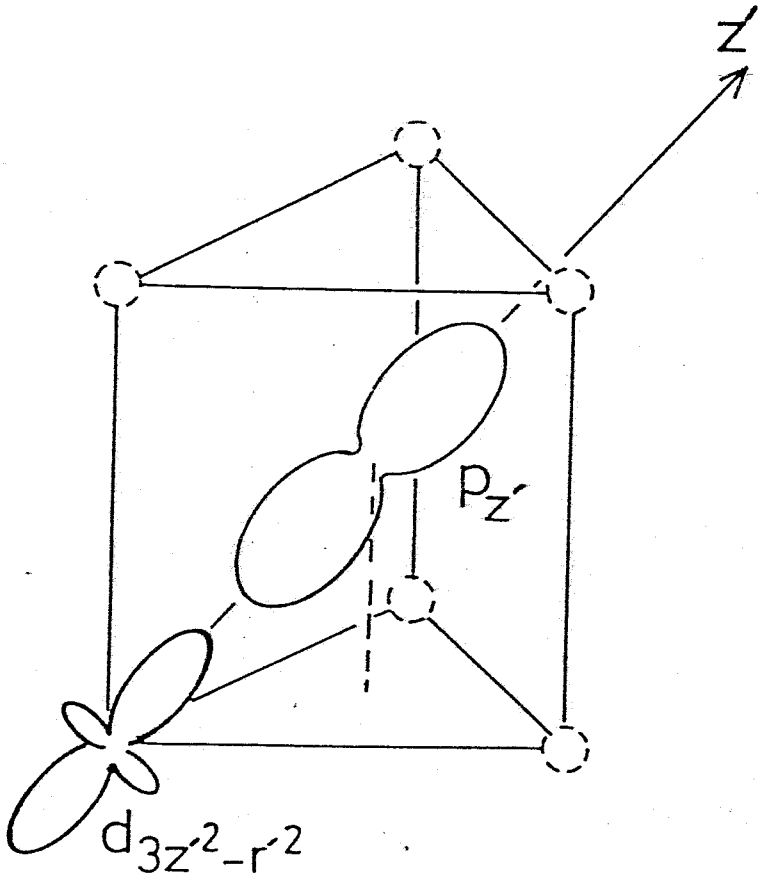

Fig.2-17. A schematic spatial arrangement of a $d_{3z',2-r',2}$ orbital of Co and $p_{z'}$ orbital of As. Bond orders between these orbitals are calculated.

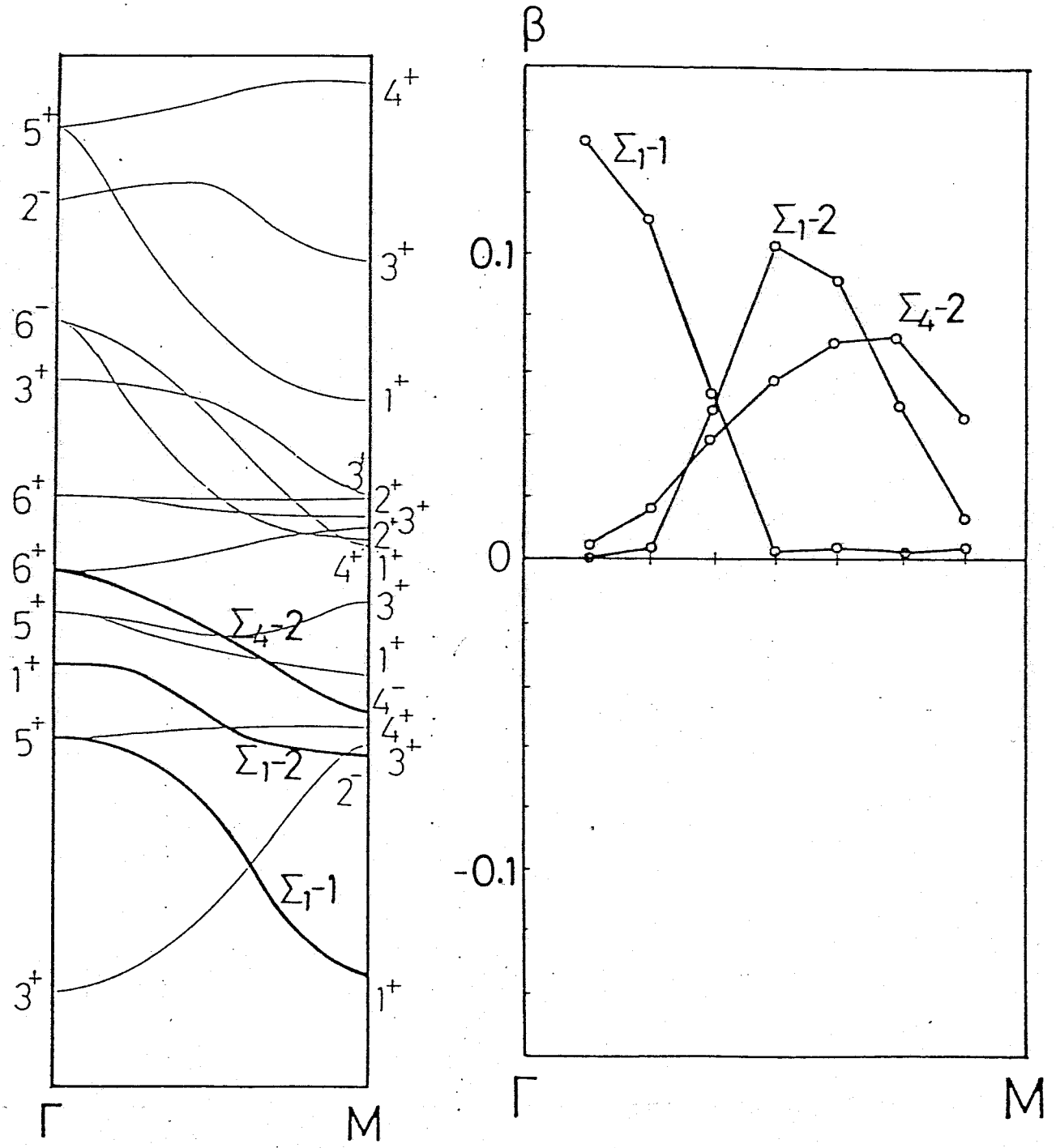

Fig.2-18(a). The bond order $\beta^{Co1;As3}_{d_{z^2-r^2};p_z}(n,k)$ for the bands denoted as thick curves. These bands have bonding nature.

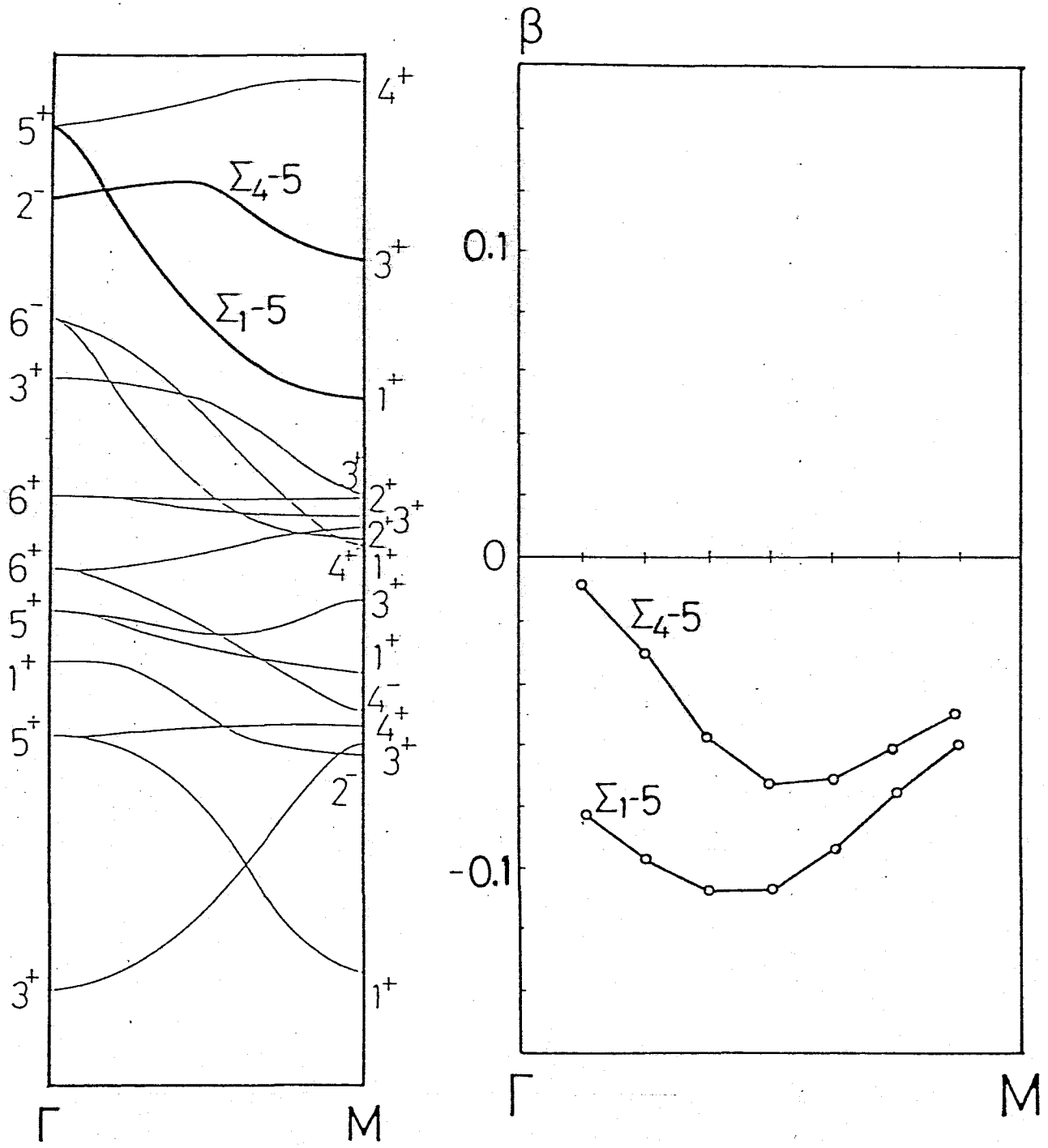

Fig.2-18(b). The bond order $\beta^{Co1;As3}_{d_{z^2-r^2};p_z}(n,k)$ for the bands denoted as thick curves. These bands have anti-bonding nature.

§3. Structural Transformaton from NiAs-type to MnP-type of CoAs and NiAs.

Among Fe-, Co- and Ni-pnictides CoAs[1] shows 2nd order structural phase transition from the NiAs-type structure to the MnP-type structure at $T_t = 1250$ K. On the other hand the crystal structures of FeAs[4] and NiAs[5] are the MnP-type and the NiAs-type, respectively, at all temperatures. Lattice distortion from the NiAs-type structure to the MnP-type structure is described as a frozen longitudinal phonon of M_4^- mode at the M point in the Brillouin zone of the NiAs-type structure.

A microscopic theory of the structural transformation of NiAs-type compounds has been developed by Katoh and Motizuki[9]. They calculated the electron-lattice matrix elements from the first principle by using the electronic bands obtained by using a self-consistent APW method. The results explained well why the structural transformation from the NiAs-type to the MnP-type structure occurs in MnAs, CrAs and VS, but not in MnSb, CrSb and TiSe.

In the present thesis we study microscopically the structural transformation of CoAs and NiAs, on the basis of their electronic bands obtained in §2. The effect of the wave number and mode dependence of the electron-lattice matrix elements are taken into account as well as the effect of nesting of the Fermi surface. We calculate the electron-lattice matrix elements and the generalized electronic susceptibility. From the results we

make clear why the structural change from the NiAs-type to the MnP-type occurs in CoAs but not in NiAs.

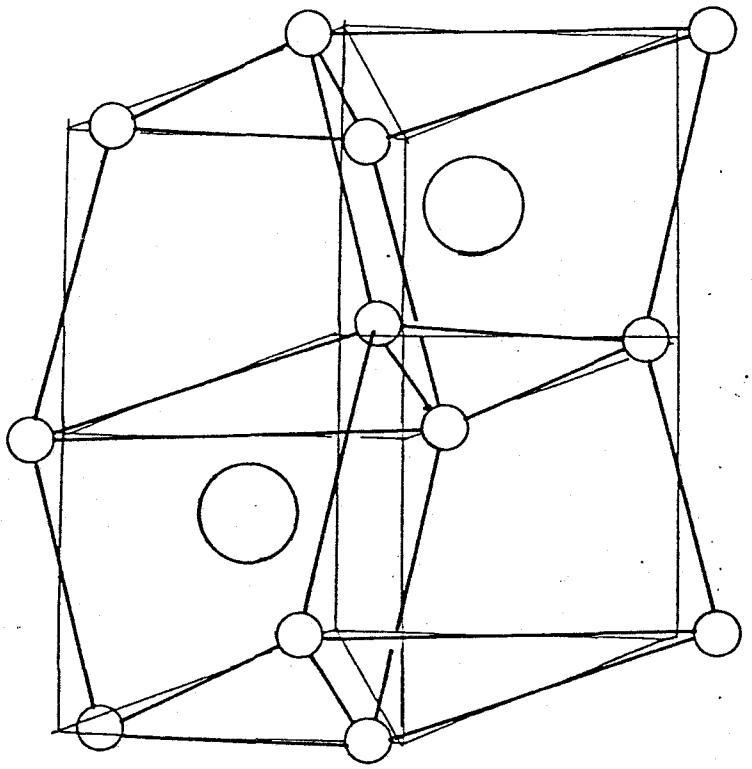

Fig.3-1. MnP-type crystal structure. Thin lines denote the unit cell of the NiAs-type structure.

3.1 Formulation

The displacement of the νth atom in the ℓth unit cell is expressed as

$$\mathbf{u}_{\ell\nu} = \frac{1}{\sqrt{NM_\nu}} \sum_{\mathbf{q}} Q_{\mathbf{q}\lambda} \varepsilon(\mathbf{q}\lambda,\nu) e^{i\mathbf{q}\cdot\mathbf{R}} \quad , \tag{3.1}$$

where N is the number of unit cells in the crystal, M_ν is the mass of the νth atom, $Q_{\mathbf{q}\lambda}$ is the normal coordinate of a phonon with wave vector $\mathbf{q}$ and mode λ, and $\varepsilon(\mathbf{q}\lambda,\nu)$ is the phonon polarization vector. As a crystal potential we consider the following muffin-tin potential:

$$V_0(\mathbf{r}) = \sum_{\ell\nu} V(|\mathbf{r}-\mathbf{R}_{\ell\nu}|)$$

$$V(|\mathbf{r}-\mathbf{R}_{\ell\nu}|) = \begin{cases} V_\nu(|\boldsymbol{\rho}|) & (|\boldsymbol{\rho}| < S_\nu) \\ 0 & (|\boldsymbol{\rho}| > S_\nu) \end{cases} \tag{3.2}$$

S_ν represents a muffin-tin radius of the νth atom. In the rigid muffin-tin approximation in which the potential moves rigidly with associated nuclei, the crystal potential in the distorted lattice is given by

$$V_d(\mathbf{r}) = V_0(\mathbf{r}) - \sum_{\ell\nu\alpha} \frac{dV_\nu}{d|\boldsymbol{\rho}|} \frac{\rho_\alpha}{|\boldsymbol{\rho}|} \delta R^\alpha_{\ell\nu} \ . \tag{3.3}$$

The matrix elements of $V_d(\mathbf{r})-V_0(\mathbf{r})$ between Bloch states $\psi_{n\mathbf{k}}$ and $\psi_{n'\mathbf{k}+\mathbf{q}}$ where $\mathbf{k}$ and $\mathbf{q}$ represent the wave vectors and n and n' specify the bands, are expressed as

$$I^{\nu\alpha}_{nk;n'k+q} = N \int \psi^{*}_{nk}(r_\nu+\rho)\left(\frac{-\rho_\alpha}{|\rho|}\right)\frac{dV_\nu}{d|\rho|}\,\psi_{n'k+q}(r_\nu+\rho)dr, \quad (3.4)$$

where the vector r_ν represents the position of the νth atom in the unit cell. The integration in eq. (3.4) is taken within the νth muffin-tin sphere. $I^{\nu\alpha}_{nk;n'k+q}$ is called the electron-lattice matrix element and it represents the strength of coupling between the electronic states (n,k) and $(n',k+q)$ caused by displacement of the νth atom in the α-direction. For the numerical calculation we use the explicit expression of $I^{\nu\alpha}_{nk;n'k+q}$ obtained by Katoh and Motizuki.

A change of the electronic free energy due to a lattice distortion characterized by a particular phonon normal coordinate $Q_{q\lambda}$ (q denotes the wave vector and λ the mode) is expressed as

$$\Delta F = -\chi(q\lambda)|Q_{q\lambda}|^2 \quad (3.5)$$

$$\chi(q\lambda) = -\frac{1}{N}\sum_{\nu\nu'}\sum_{\alpha\beta}\frac{1}{\sqrt{M_\mu M_\nu}}\,\varepsilon^{\alpha}(q\lambda,\nu)\varepsilon^{\beta *}(q\lambda,\nu')$$

$$\times 2\sum_{nn'}\sum_{k} I^{\nu\alpha *}_{nk;n'k+q} I^{\nu'\beta}_{nk;n'k+q}\frac{f(E^0_{nk})-f(E^0_{n'k+q})}{E^0_{nk}-E^0_{n'k+q}},$$

where E^0_{nk} is the electronic energy of undistorted bands and $f(E)$ is the Fermi distribution function. The quantity $\chi(q\lambda)$ is called the generalized electronic susceptibility. If the k and q dependences of the electron-lattice matrix elements are neglected, $\chi(q\lambda)$ becomes proportional to

$$\chi^0(q)=\frac{1}{N}\sum_{nn'k}\frac{f(E^0_{nk})-f(E^0_{n'k+q})}{E^0_{n'k+q}-E^0_{nk}}, \qquad (3.6)$$

which is called the bare electronic susceptibility. The wave vector dependence of $\chi^0(q)$ comes only through the electronic band structure and reflects the effect of Fermi surface nesting. On the other hand the wave vector dependence of $\chi(q\lambda)$ comes not only from the electronic band structure but also from the wave vector dependence of the electron-lattice matrix elements.

3.2. Results and discussion

First, we have calculated the bare electronic susceptibility, $\chi^0(q)$, for NiAs-type CoAs. Reflecting a good nesting of the Fermi surface, there is a remarkable peak at the M point as shown in Fig.3-2. This result indicates that the lattice distortion described as a frozen phonon at the M point is likely to be realized in CoAs.

The MnP-type distortion is described as a frozen longitudinal phonon of M_4^- mode at the M point in the Brillouin zone. This (M_4^-) mode consists of displacements of metal ions in the x- and z-directions and those of anions in the z-direction as follows:

$$M_4^- : c_1(x_1-x_2) + c_2(z_1+z_2) + c_3(z_3-z_4).$$

We have calculated $I^{\nu\alpha}_{nk;n'k+q}$ for the phonon wave vector q=ΓM as functions of the wave vector k.

The numerical calculation of the electron-lattice matrix elements has been made for three cases of k-points in the

Brillouine zone as shown in Fig.3-3 : case a) **k**-points are along the ΓM, AB, CD, EF-line in the k_z=0 plane, case b) **k**-points are along the ΓA/3, ML/3, A'B', C'D', E'F'-lines in the k_z=ΓA/3 plane. case c) **k**-points are along the 2ΓA/3, 2ML/3, A"B", C"D", E"F"-lines in the k_z=2ΓA/3 plane. In each case the electronic bands of CoAs and NiAs have the dispersion curves near the Fermi level as shown in Fig.3-4 and 3-5, respectively. Since, we confine our consideration to the M_4^- mode, it is necessary to calculate the matrix elements between two bands whose product representation has a compatibility relation with the M_4^- representation. Two bands denoted by thick curves in each figure satisfy this relation. The hatched regions in Fig.3-4 and 3-5 denote the regions in which one of the electronic states (n,**k**) and (n',**k**+**q**) is above the Fermi level and another is below the Fermi level. In these regions the coupling between the electronic states (n,**k**) and (n',**k**+**q**) can contribute to the electronic energy gain. In the case a), the electron-lattice matrix is obtained in the following form :

	x	y	z
metal 1	(0,a)	(0,e)	(0,b)
metal 2	(0,-a)	(0,-e)	(0,b)
anion 3	0	0	(d,c)
anion 4	0	0	(d,-c),

(3.7)

where a,b etc. denote real numbers and a+ib is abbreviated as (a,b). The Cartesian coordinates x, y and z are shown in Fig.2-1. The z-axis corresponds to the hexagonal c-axis.

Introducing the matrix

$$\tilde{I}^{\alpha\beta}(\nu\nu',\mathbf{q}) = (I^{\nu\alpha *}_{n\mathbf{k};n'\mathbf{k}+\mathbf{q}} I^{\nu'\beta}_{n\mathbf{k};n'\mathbf{k}+\mathbf{q}} + I^{\nu\alpha *}_{n-\mathbf{k};n'-\mathbf{k}+\mathbf{q}} I^{\nu'\beta}_{n-\mathbf{k};n'-\mathbf{k}+\mathbf{q}})/2 \tag{3.8}$$

and making the transformation by the use of the unitary matrix U given by

$$U=\frac{1}{\sqrt{2}}\begin{pmatrix} 1 & 1 & & & & \\ 1 & -1 & & & & \\ & & 1 & 1 & & \\ & & 1 & -1 & & \\ & & & & & \\ & & & & & \end{pmatrix}, \tag{3.9}$$

we obtain the following transformed matrix:

$$U^{-1}\tilde{I}U=\begin{array}{c} \begin{matrix} x_1-x_2 & z_1+z_2 & z_3-z_4 & y_1-y_2 & z_3+z_4 & \cdots \end{matrix} \\ \begin{pmatrix} 2a^2 & 2ab & 2ac & 2ae & & 0 \\ 2ab & 2b^2 & 2bc & 2be & & \\ 2ac & 2bc & 2c^2 & 2ce & & \\ 2ae & 2be & 2ce & 2e^2 & & \\ & & & & 2d^2 & \\ 0 & & & & & 0 \end{pmatrix} \end{array}. \tag{3.10}$$

This result indicates that the M_4^- mode, M_3^+ mode (z_3+z_4) and M_1^- mode (y_1-y_2) remain. In this paper we consider only the M_4^- mode. So, we call $|a|$,$|b|$ and $|c|$ as the metal x-component, the metal z-component and the anion z-component of the electron- lattice matrix elements, respectvely. We mention that for the wave vector $\mathbf{k}$ along the ΓM-line, the matrix element e appeared in

eq.(3.7) vanishes and therefore the transformed matrix given by eq.(3.10) does not include the matrix elements which contribute to the M_1^- mode. $|a|$,$|b|$ and $|c|$ calculated for CoAs and NiAs are shown in Fig.3-6(a) and 3-7(a) as functions of **k**. The calculated results for wave vectors **k** which are inside and outside the hatched regions of Fig.3-4 and 3-5 are denoted by solid and dashed lines, respectively. To examine a reduction of the free energy due to the lattice distortion, we have calculated the quantities, $|a|^2/|E_{n\mathbf{k}}-E_{n'\mathbf{k}+\mathbf{q}}|$, $|b|^2/|E_{n\mathbf{k}}-E_{n'\mathbf{k}+\mathbf{q}}|$ and $|c|^2/|E_{n\mathbf{k}}-E_{n'\mathbf{k}+\mathbf{q}}|$ as functions of **k**. The results for CoAs and NiAs are shown in Fig.3-8(a) and 3-9(a), respectively. Similar calculation has been made for the case b) and case c). In each case the diagonal parts of the transformed matrix $U^{-1}\tilde{I}U$ are obtained in the form

$$[U^{-1}\tilde{I}U]_{\xi\xi} = 2a'^2 \quad \text{for } \xi = x_1 - x_2 ,$$

$$[U^{-1}\tilde{I}U]_{\xi\xi} = 2b'^2 \quad \text{for } \xi = z_1 + z_2 ,$$

$$[U^{-1}\tilde{I}U]_{\xi\xi} = 2h^2 \quad \text{for } \xi = z_3 - z_4 .$$

$|a'|$,$|b'|$ and $|h|$ calculated as functions of wave vector **k** are shown in Fig.3-6(b) and (c) for CoAs and 3-7(b) and (c) for NiAs. Furthermore we have calculated the quantities $|a'|^2/|E_{n\mathbf{k}}-E_{n'\mathbf{k}+\mathbf{q}}|$, $|b'|^2/|E_{n\mathbf{k}}-E_{n'\mathbf{k}+\mathbf{q}}|$ and $|h|^2/E_{n\mathbf{k}}-E_{n'\mathbf{k}+\mathbf{q}}|$ which represent a reduction of the free energy due to displacements of metal ions in the x-direction and in the z-direction and those of anions in the z-direction, respectively. The results are shown in Fig.3-8(b) and (c) and 3-9(b) and (c). The results shown in Fig.3-6 and 3-4 indicate that in the wide hatched region of the

wave vector k the metal x-component |a| has a larger value than the metal z- and anion z-components |b| and |c|. This means that the displacements of the metal atoms are most likely to be realized in the x-direction as observed. Furthermore, from the results for CoAs and NiAs shown in Fig.3-8 and 3-9, we have found that the reduction of the free energy in CoAs is larger than that in NiAs. This is consistent with the observations that CoAs reveals the transformation from the NiAs-type to the MnP-type but NiAs does not.

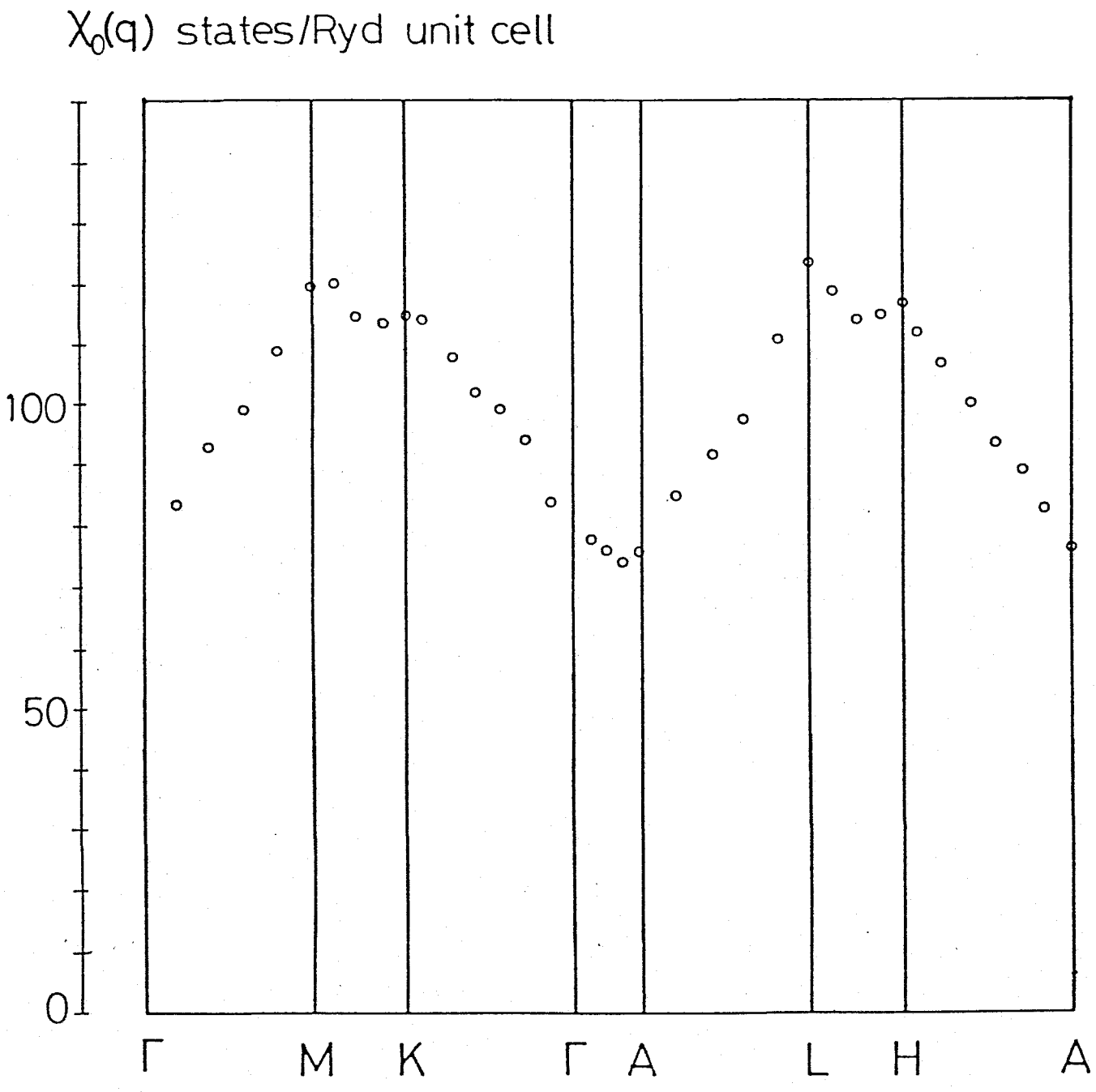

Fig.3-2. The bare electronic susceptibility $\chi_0(q)$ of CoAs. There are peaks at the M point and the L point.

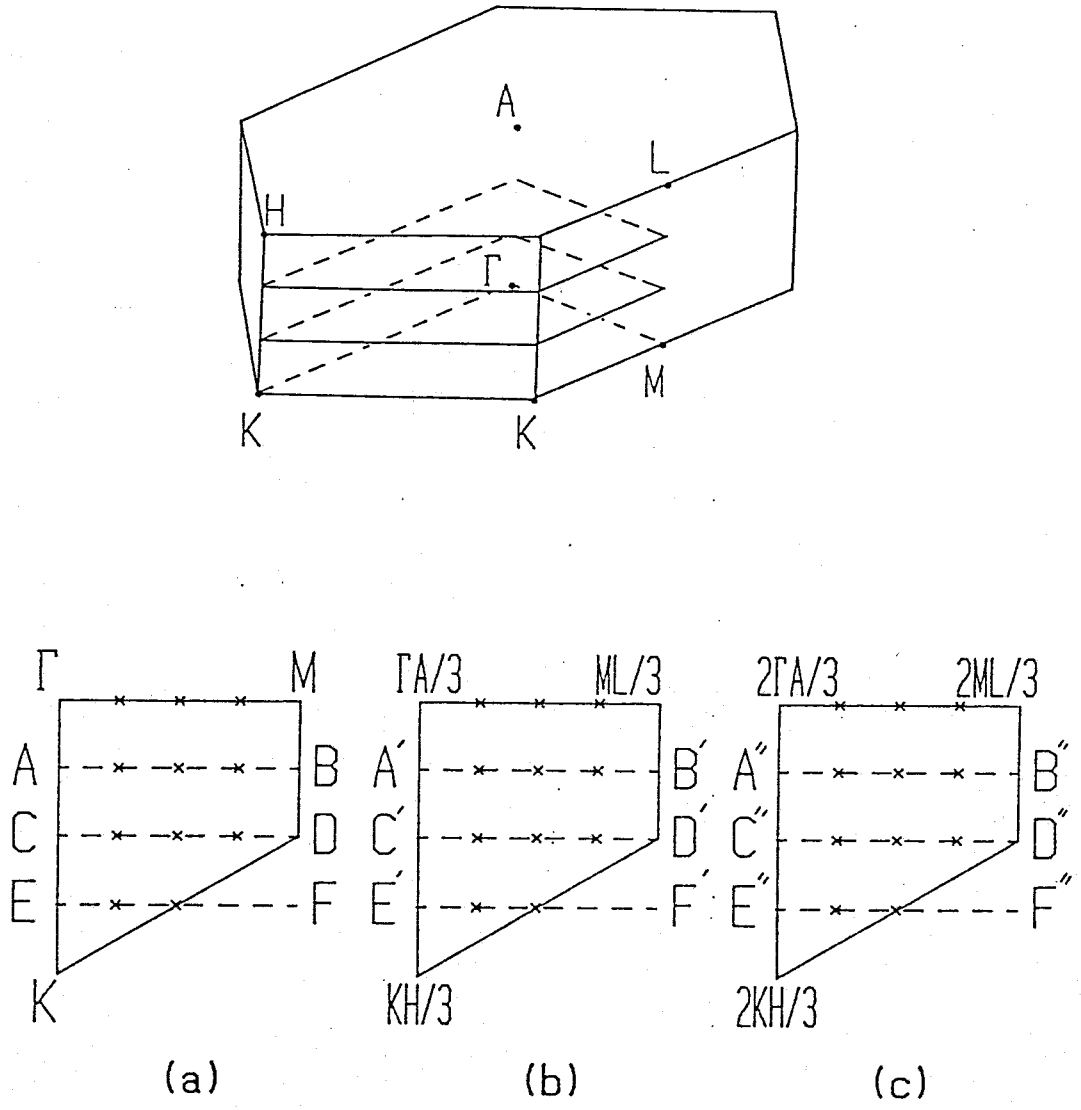

Fig.3-3. **k**-points used in the calculation of the electron-lattice matrix elements are denoted by cross points.

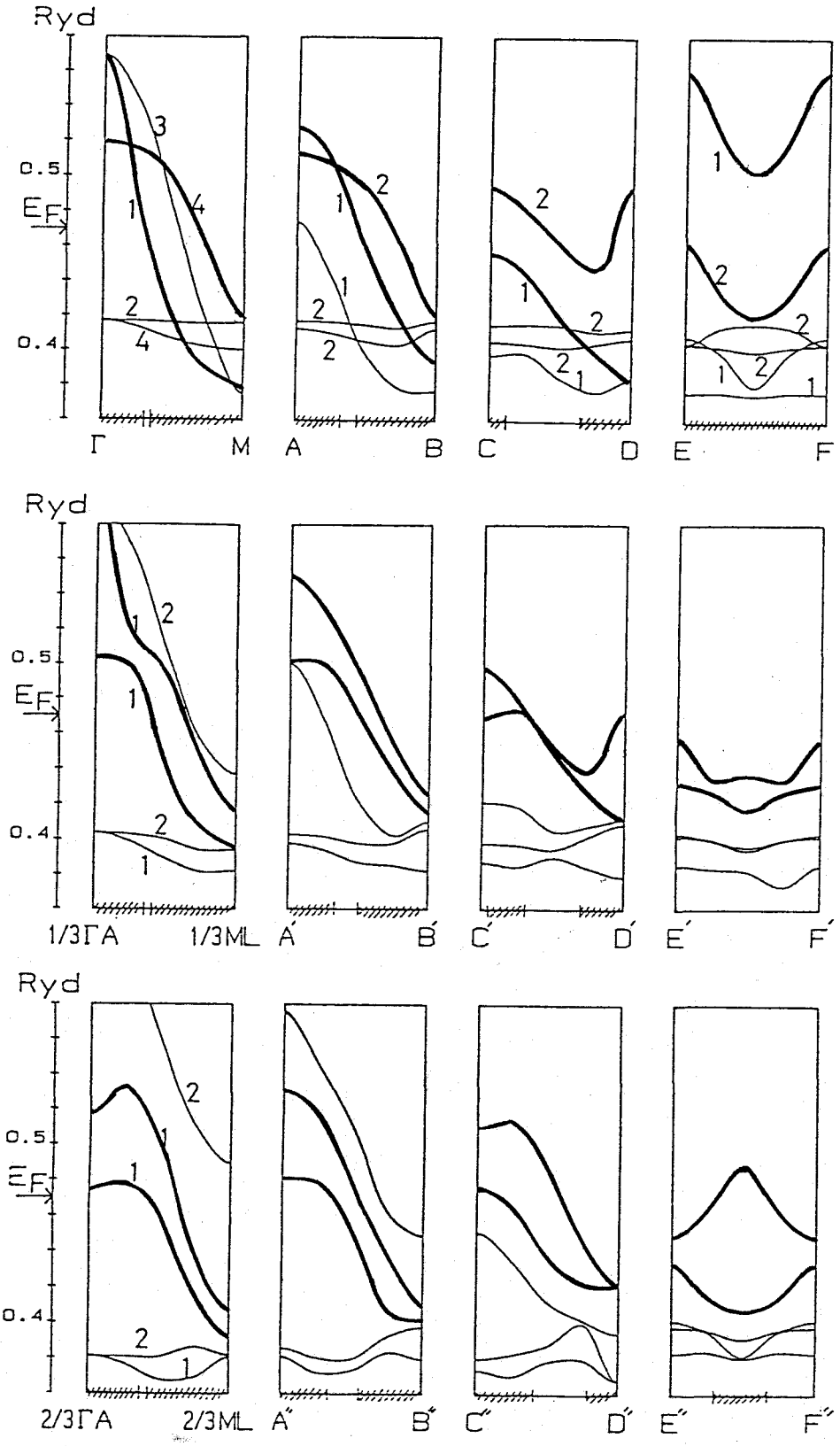

Fig.3-4. Dispersion curves of the band of CoAs near the Fermi level along the directions denoted by the dotted lines in Fig.3-3.

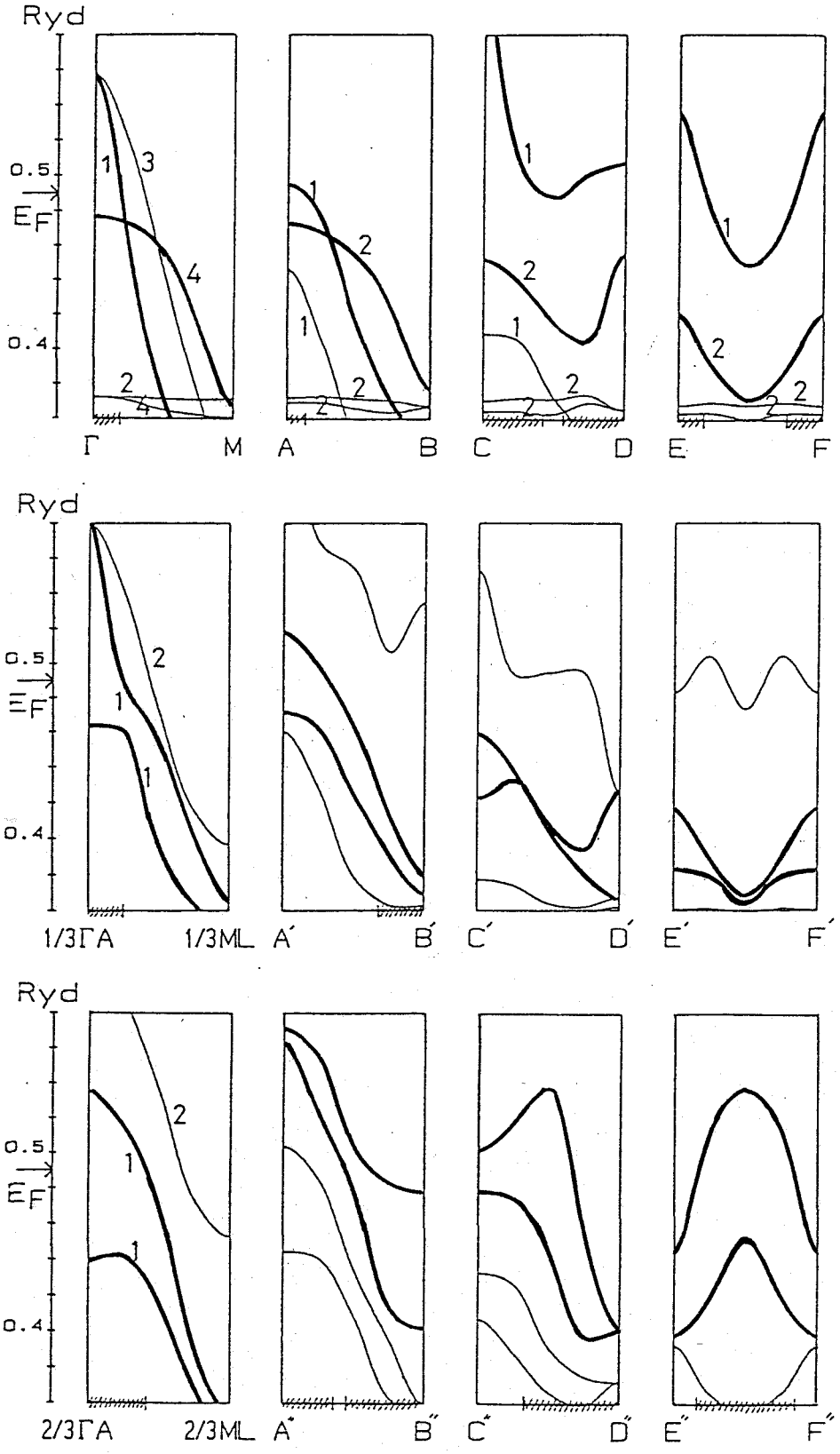

Fig.3-5. Dispersion curves of the band of NiAs near the Fermi level along the directions denoted by the dotted lines in Fig.3-3.

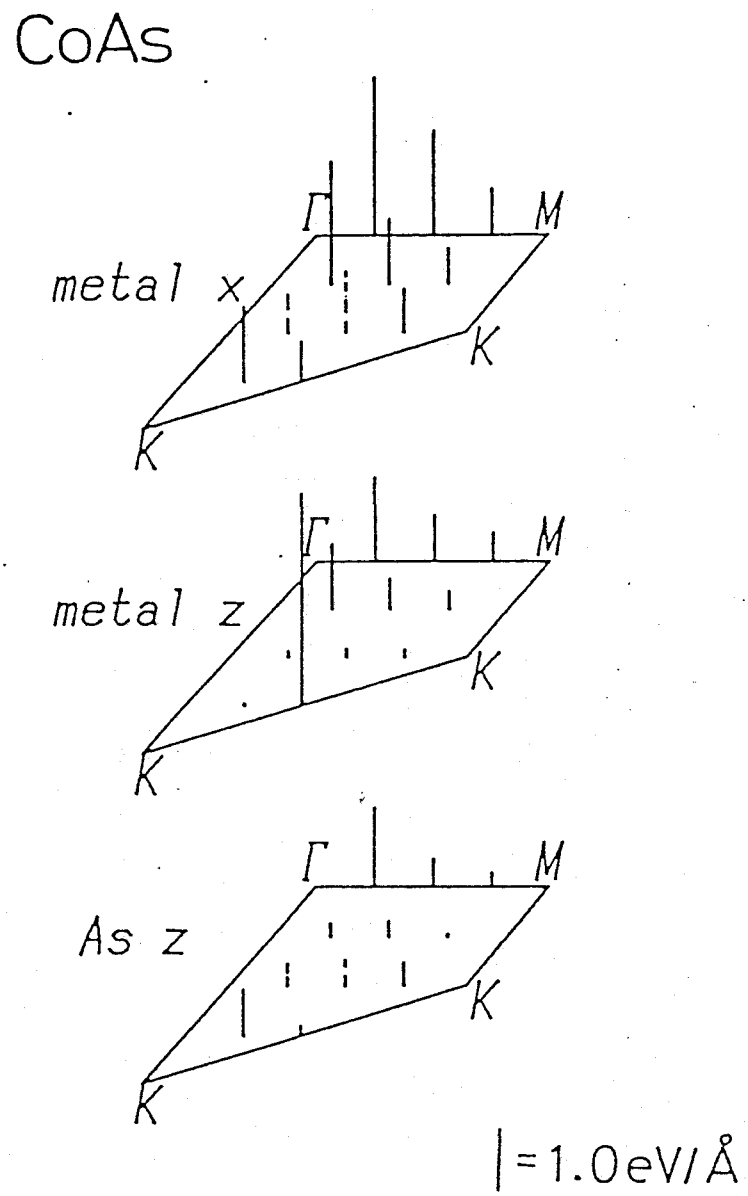

Fig.3-6(a). Electron-lattice matrix elements calculated for CoAs as functions of wave vectors **k** denoted in Fig.3-3 for the case a). The metal x-, metal z- and As z-components of the electron-lattice matrix elements represent the quantities |a|,|b| and |c|, respectively

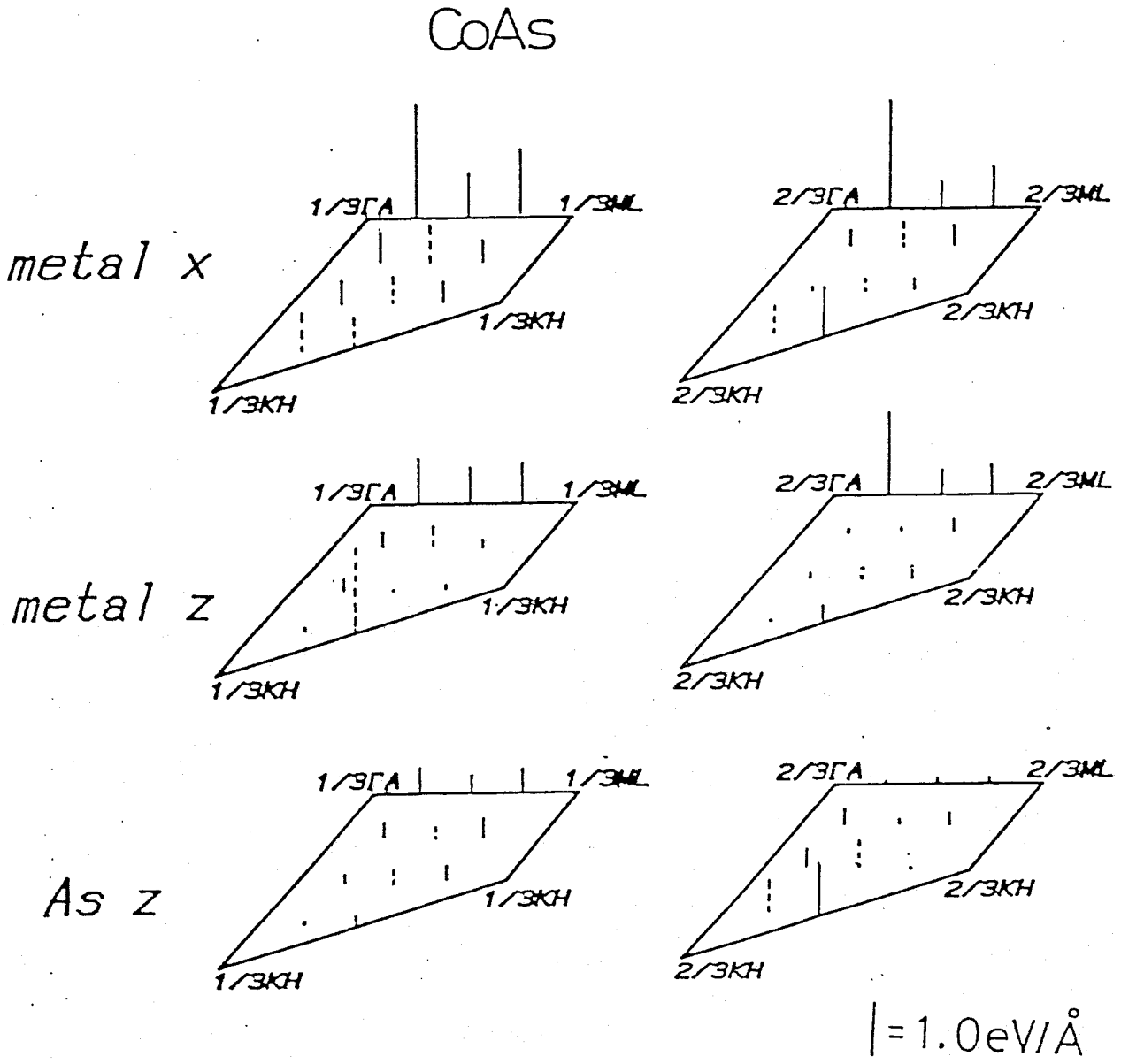

Fig.3-6(b) and (c). Electron-lattice matrix elements calculated for CoAs as functions of wave vectors k denoted in Fig.3-3 for the case b) and the case c). The metal x-, metal z- and As z-components of the electron-lattice matrix elements represent the quantities |a'|, |b'|and |h|, respectively.

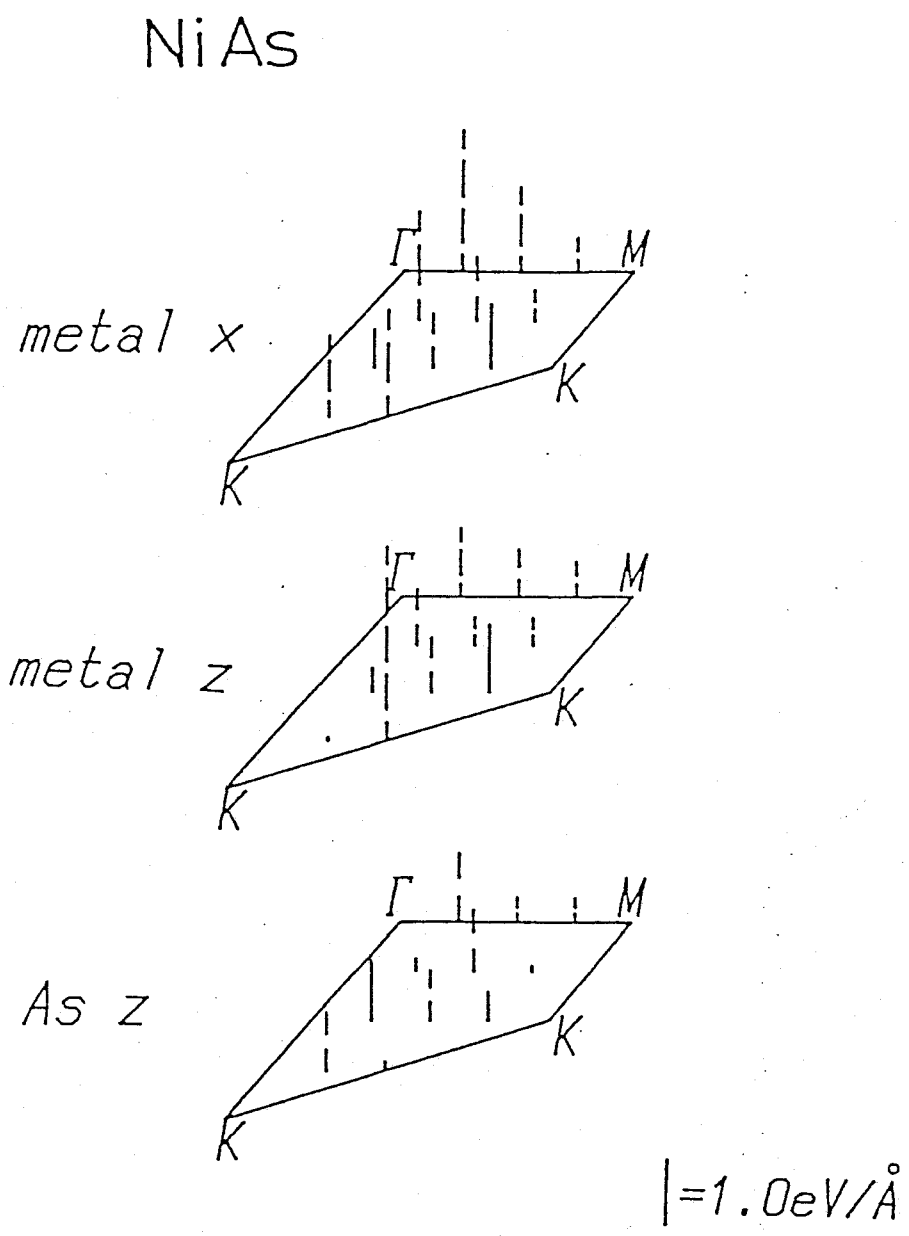

Fig.3-7(a). Electron-lattice matrix elements calculated for NiAs as functions of wave vectors k denoted in Fig.3-3 for the case a).

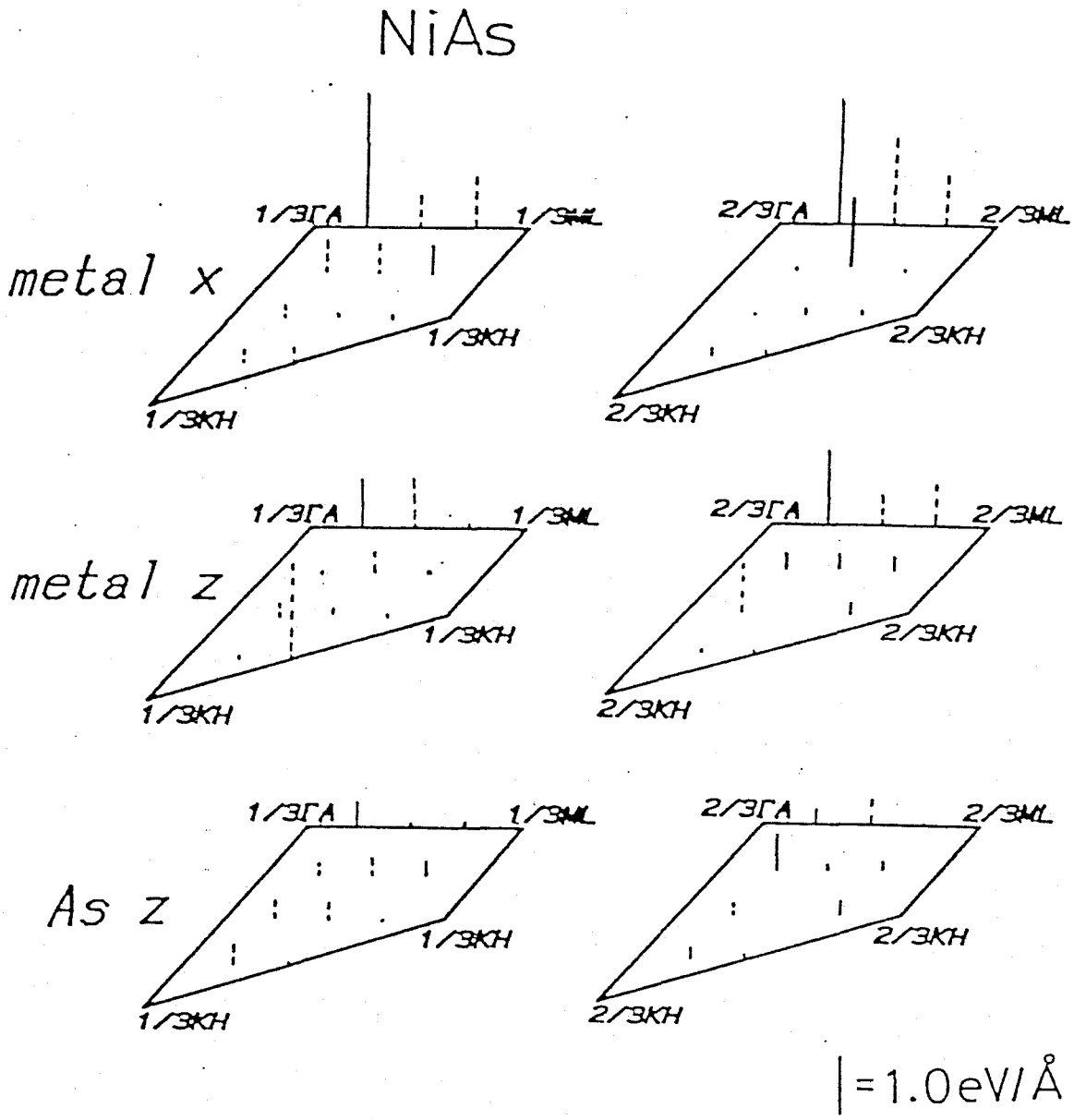

Fig.3-7(b) and (c) Electron-lattice matrix elements calculated for NiAs as functions of wave vectors k denoted in Fig.3-3 for the case b) and the case c).

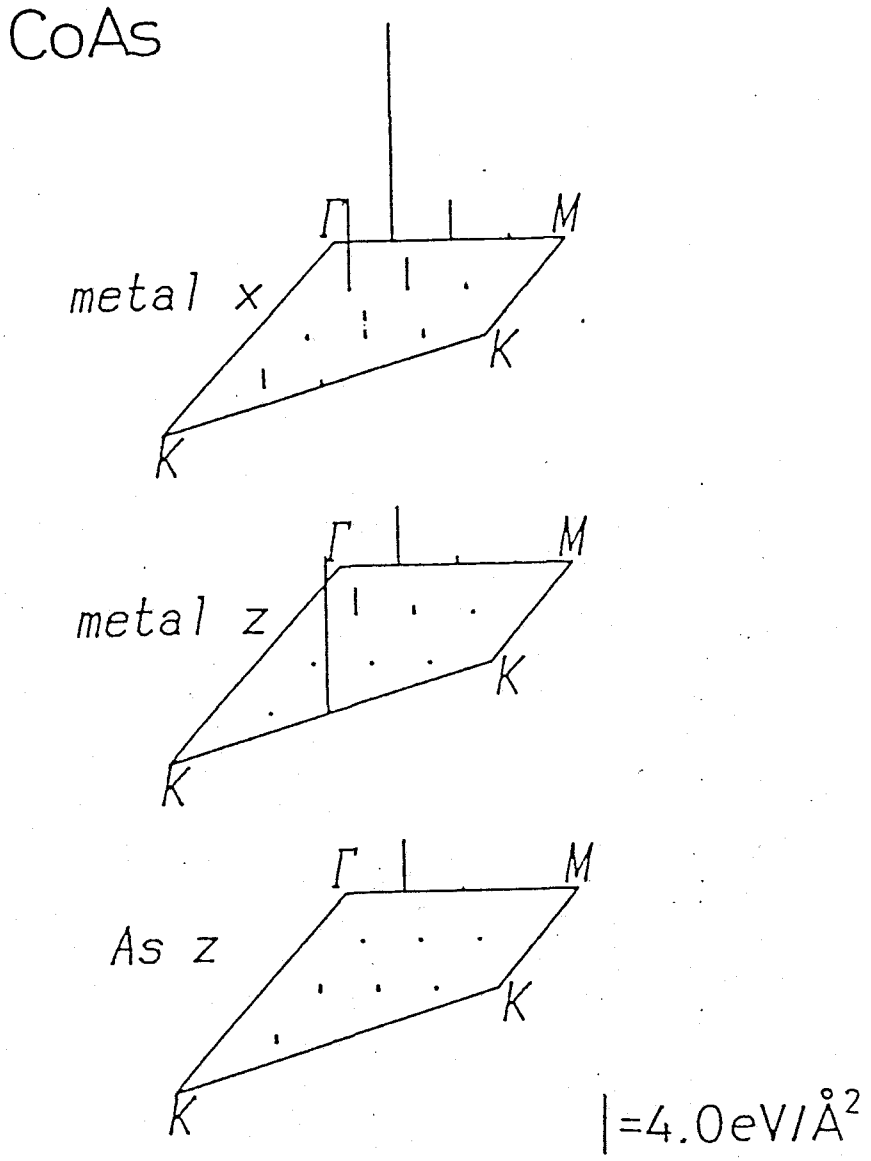

Fig.3-8(a). $|a|^2/|E_{nk}-E_{n'k+q}|$, $|b|^2/|E_{nk}-E_{n'k+q}|$, $|c|^2/|E_{nk}-E_{n'k+q}|$ calculated for CoAs as functions of k for the case a).

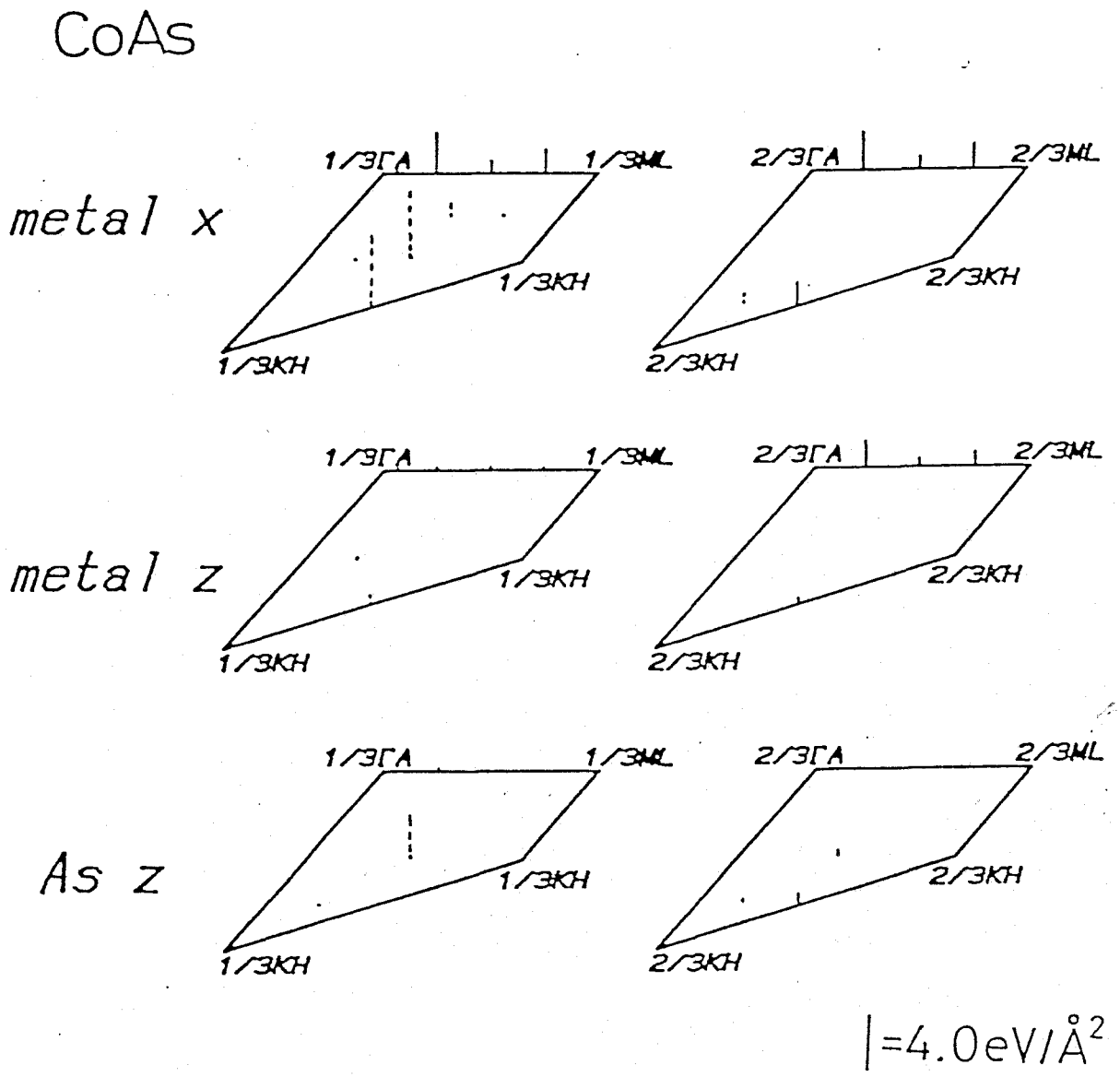

Fig.3-8(b) and (c). $|a'|^2/|E_{nk}-E_{n'k+q}|$, $|b'|^2/|E_{nk}-E_{n'k+q}|$, $|h|^2/|E_{nk}-E_{n'k+q}|$ calculated for CoAs as functions of k for the case b) and the case c).

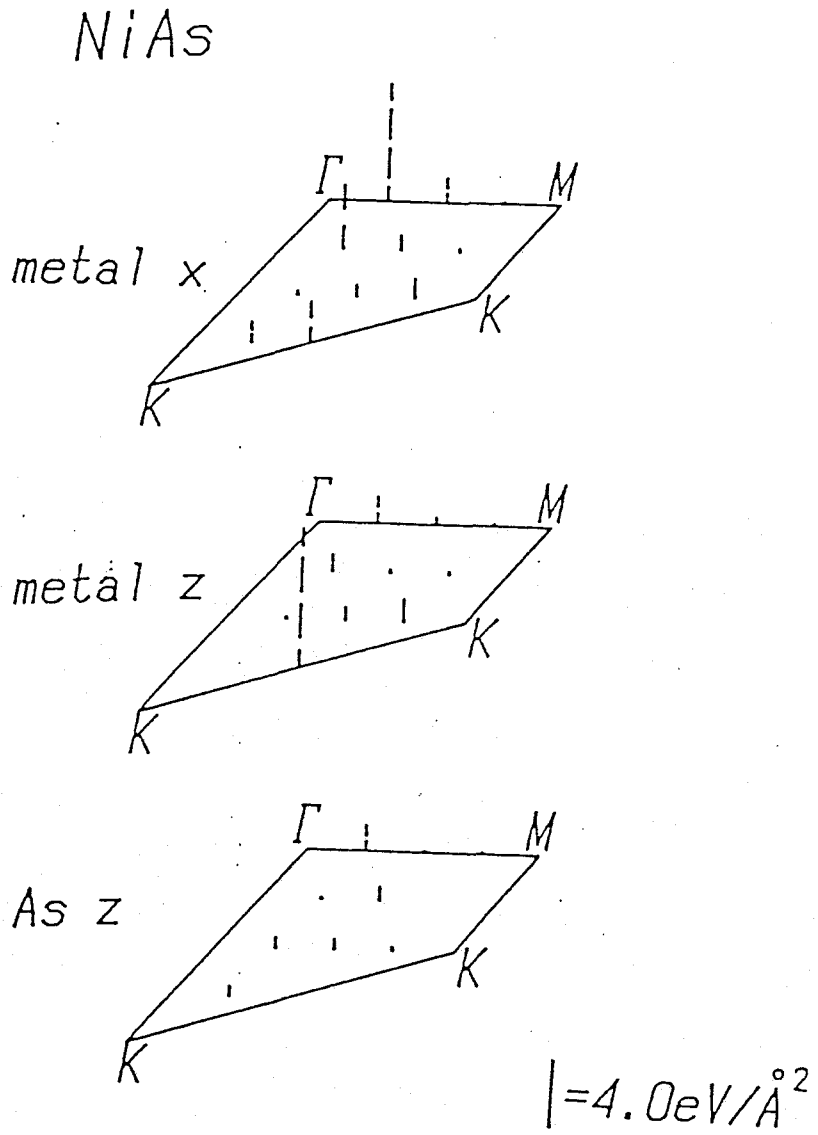

Fig.3-9(a). $|a|^2/|E_{nk}-E_{n'k+q}|$, $|b|^2/|E_{nk}-E_{n'k+q}|$, $|c|^2/|E_{nk}-E_{n'k+q}|$ calculated for NiAs as functions of k for the case a).

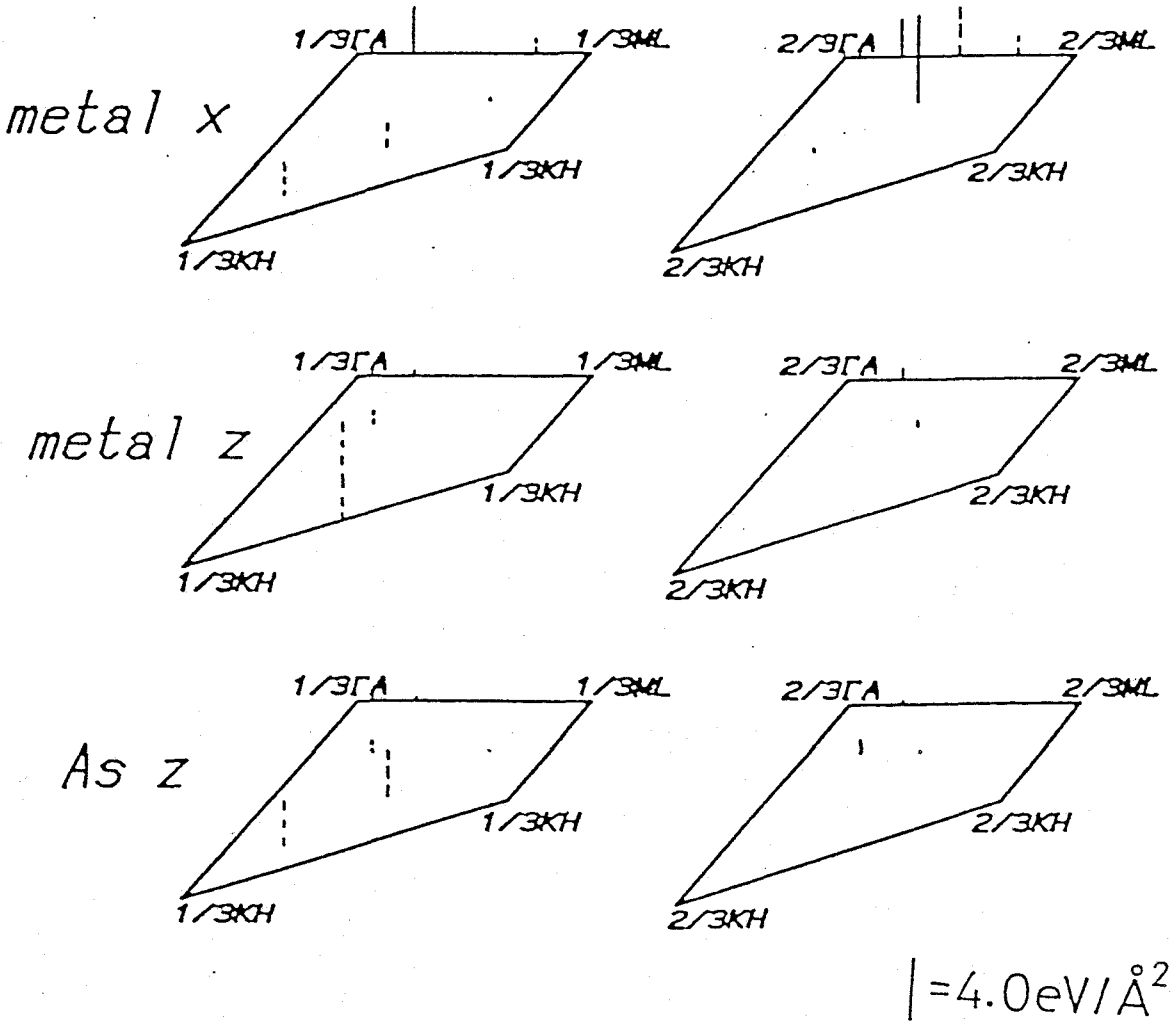

Fig.3-9(b) and (c). $|a'|^2/|E_{nk}-E_{n'k+q}|$, $|b'|^2/|E_{nk}-E_{n'k+q}|$, $|h|^2/|E_{nk}-E_{n'k+q}|$ calculated for NiAs as functions of k for the case b) and the case c).

§4. Magnetic properties of FeAs, CoAs and NiAs.

Among FeAs, CoAs and NiAs, FeAs becomes a double helical magnet below T_N= 77 K with a helical propagation vector of $\mathbf{Q}=0.375\times(2\pi/c)$ along the c-axis[4]. The unit cell of FeAs whose crystal structure is of MnP-type at all temperatures contains four metal atoms 1, 2, 3 and 4 as shown in Fig.4-1. By a neutron diffraction experiment it has been found that the magnetic moment on each Fe atom is in the plane perpendicular to the helical axis and the phase angles ϕ_{ij} between the magnetic moment on the ith atom and the jth atom in the unit cell are given by $\phi_{12}=\phi_{34}=140^0$ and $\phi_{23}=\phi_{41}=-72.5^0$(see Fig.4-1). The magnetic moment observed at 12 K is $0.5\mu_B$/Fe. On the other hand, CoAs and NiAs do not show any magnetic ordering.

The paramagnetic susceptibilities of FeAs[4] and CoAs[15] show anomalous temperature dependence: in the high temperature range the paramagnetic susceptibility χ obeys the Curie-Weiss law and as temperature decreases χ^{-1} vs. T curve shows a positive deviation from the Curie-Weiss law and it passes through a broad minimum at a certain temperature (about 200-300 K). On the other hand, the paramagnetic susceptibility of NiAs whose crystal structure is of NiAs-type is almost temperature-independent in the whole temperature range[16]. These facts indicate that the temperature dependence of the paramagnetic susceptibility is closely related to the crystal structure. The magnetic moment of FeAs estimated from the Curie constant is $3.1\mu_B$/Fe, which is much

larger than the moment obtained by a neutron diffraction measurement at 12 K. This fact indicates an itinerant character of d electrons in these compounds. Further, the magnitudes of paramagnetic susceptibilities of FeAs and CoAs are much larger than the values estimated from the calculated density of states at the Fermi level, $\rho(E_F)$. This fact suggests a strong electron correlation in these compounds.

Our purpose is to make clear whether these magnetic properties of FeAs, CoAs and NiAs can be explained or not on the basis of the electronic band structures obtained by the APW method. In §4.1, we study the paramagnetic susceptibilities of FeAs, CoAs and NiAs. The observed anomalous temperature dependence of the paramagnetic susceptibilities of FeAs and CoAs are very similar to that of FeSi[25] which is a nearly ferromagnetic semiconductor. Takahashi and Moriya explained the observed peculiar paramagnetic susceptibility of FeSi by their spin-fluctuation theory[26], in which the longitudinal spin-fluctuation that is called temperature-induced local moment plays an important role. They pointed out that the negative mode-mode coupling at low temperatures gives rise to a rapid decrease of χ^{-1} with increasing temperature at temperatures lower than the temperature of the minimun of χ^{-1}, and that the effect of saturation of the local amplitude of spin-fluctuation leads to the Curie-Weiss behavior in the high temperature side[27]. Furthermore, for a semiconducting FeSi a characteristic shape of the density of states arround the Fermi level[28] plays an

important role in causing the negative mode-mode coupling.

As shown in §2, in MnP-type CoAs and FeAs the density of states of the p-d mixing bands reveals a characteristic behavior: the Fermi level is located at a dip of the density of states $\rho(E)$ and below the Fermi level $\rho(E)$ increases steeply. Therefore, for the paramagnetic susceptibilities of FeAs and CoAs we can expect a similar explanation to that for FeSi. We calculate the paramagnetic susceptibilities of CoAs and FeAs, by taking account of spin-fluctuations and a characteristic feature of the density of states[29].

In §4.2, we explain the double helical magnetic ordering of FeAs by using the model Hamiltonian based on the tight-binding approximation. The transfer terms included in the model Hamiltonian are determined so as to reproduce the electronic band of FeAs obtained by the APW method. The Hartree-Fock approximation is adopted to the Coulomb interaction terms. First, we study the instability of the paramagnetic phase against the formation of a magnetic ordering. Secondly, the wave vector $\mathbf{Q}$ and the phase angle ϕ of the most stable double helical spin density wave (SDW) state at 0 K are calculated by minimizing the total electronic energy. From the amplitude of the SDW determined self-consistently, we evaluate the magnetic moment.

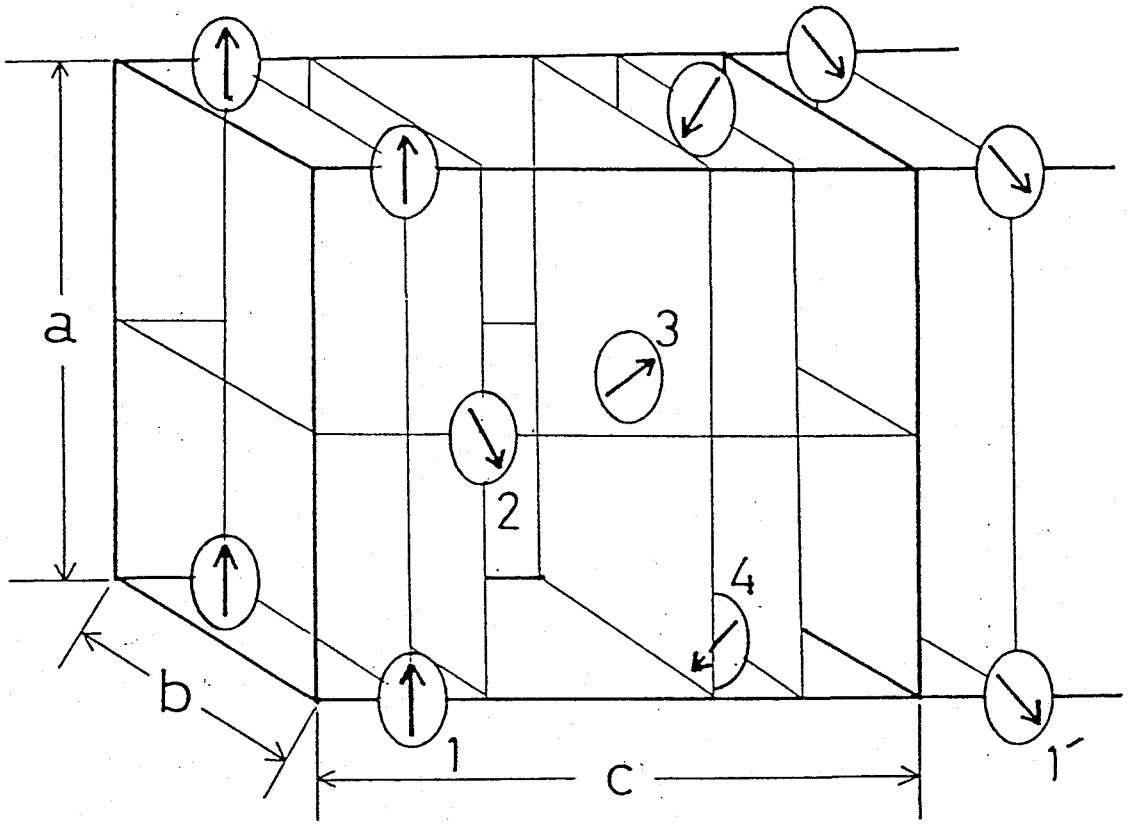

Fig.4-1. Double helical magnetic structure of FeAs. $\phi_{11'}=135^0$ ($q=0.375\times 2\pi/c$), $\phi_{12}=\phi_{34}=140^0$, $\phi_{23}=\phi_{41'}=-72.5^0$.

4.1 Paramagnetic susceptibilities of FeAs, CoAs and NiAs

4.1.1 Formulation

For the purpose of explaining the anomalous temperature dependence of paramagnetic susceptibilities of FeAs and CoAs, we adopt the unified theory of spin-fluctuation developed by Moriya and Takahashi. The starting Hamiltonian is a single-band Hubbard Hamiltonian :

$$H = H_0 + H_I + H' , \tag{4.1}$$

$$H_0=\sum_{ij\sigma} t_{ij} a^{\dagger}_{i\sigma} a_{j\sigma} , \tag{4.2a}$$

$$H_I= U\sum_{j} n_{j\uparrow} n_{j\downarrow}, \tag{4.2b}$$

$$H'=(h_0/2)\sum_{j}(n_{j\uparrow}-n_{j\downarrow}), \tag{4.2c}$$

where $a_{i\sigma}(a^{\dagger}_{i\sigma})$ is an annihilation (creation) operator of an electron with spin σ at the ith site, $n_{j\sigma}$ is the number operator , t_{ij} is the transfer integral, U is the intra-atomic Coulomb integral and h_0 is the magnetic field applied along the z-direction. We rewrite H_I as

$$H_I=\frac{U}{4}\sum_{j}[(n_{j\uparrow}+n_{j\downarrow})^2 -(n_{j\uparrow}-n_{j\downarrow})^2]. \tag{4.3}$$

The first and the second terms of eq.(4.3) denote charge and spin density operators, respectively. Using eqs.(4.1) and (4.2), the partition function Z (or free energy F) of the system is written

as

$$Z = e^{-\beta F} = \mathrm{Tr}[e^{-\beta(H_0+H_I+H')}] = e^{-\beta(F_0+\Delta F)}, \tag{4.4}$$

where

$$\beta = 1/T \ (T : \text{temperature}), \tag{4.5a}$$

$$e^{-\beta F_0} = \mathrm{Tr}\, e^{-\beta H_0}, \tag{4.5b}$$

$$e^{-\beta \Delta F} = \langle T_\tau \exp[-\int_0^\beta H_I(\tau)+H'(\tau)d\tau] \rangle, \tag{4.5c}$$

$$H_I(\tau) = e^{\beta H_0} H_I e^{-\beta H_0}, \quad H'(\tau) = e^{\beta H_0} H' e^{-\beta H_0}, \tag{4.5d}$$

T_τ is a time-ordering operator with respect the imaginary time τ, and $\langle \ \rangle$ denotes average value defined as

$$\langle A \rangle = \frac{\mathrm{Tr}[Ae^{-\beta(H_0+H_I)}]}{\mathrm{Tr}[e^{-\beta(H_0+H_I)}]}. \tag{4.6}$$

By evaluating ΔF, we can calculate the paramagnetic susceptibility as a function of temperature. The self-consistent equations to obtain the paramagnetic susceptibility are as follows[26,30,31] (see Appendix B) :

$$\chi = \frac{\bar{\chi}_{00}}{1 - 2I\bar{\chi}_{00}}, \tag{4.7a}$$

$$\bar{\chi}_{qm} = N[X_{qm} - \frac{1}{2U}\frac{\partial L(x)}{\partial x}] , \tag{4.7b}$$

$$x = \frac{3T}{2N\pi}\sum_{qm}\frac{1}{1 - 2I\bar{\chi}_{qm}} , \tag{4.7c}$$

$$NX_{qm} = \bar{\chi}_{qm} - \frac{1}{N}\sum_{q}\bar{\chi}_{qm} , \tag{4.7d}$$

$$L(x) = -\frac{T}{\pi N}\sum_{\sigma=\pm 1}\int_{-\infty}^{\infty} d\varepsilon\rho(\varepsilon)\log[1+e^{-\beta(\varepsilon-\sigma B)}] , \tag{4.7e}$$

$$B=(\pi Ux)^{1/2},$$

where $\rho(\varepsilon)$ denotes the density of states and m is an integer which is related to the frequency as $\omega_m = 2\pi mT$. The quantity x represents the average square amplitude of the local field and is related to the average square amplitude of local spin density as follows :

$$\langle s_j^2\rangle = \frac{\pi}{U}(x - \frac{3T}{2\pi}) \tag{4.8}$$

Furthermore, we replace $\bar{\chi}_{qm}$ by the following expanded form[32] :

$$\frac{\bar{\chi}_{qm}}{\bar{\chi}_{00}} = 1 - Aq^2 - i\bar{c}\frac{\omega}{q} , \tag{4.9}$$

for $0 \leqq q \leqq q_0$, $0 \leqq \omega \leqq vq$,

where A, $\bar{c}$, q_0 and v are parameters. Among them, q_0 and v are determined as

$$\frac{4\pi}{3} q_0^3 = \frac{(2\pi)^3}{V} \quad \text{(V: volume of the unit cell)},$$

$$vq = D \qquad \text{(D: band width)}.$$

For convenience of the calculation we use the following non-dimensional parameters instead of A and $\bar{c}$:

$$\langle\sigma\rangle = \frac{3}{5} A q_0^2 \quad , \quad c = \frac{\bar{c}D}{q_0} \; .$$

4.1.2 Results and discussion

Using eqs. (4.7) and (4.9), we have calculated the paramagnetic susceptibilities of FeAs and CoAs as functions of temperature. In order to take account of the band structure calculated by the APW method, we have replaced the density of states by model density of states which consists of a set of straight lines as shown in Fig.4-2(a) and (b), respectively. The characteristic behavior of the density of states, such as the Fermi level is located at a dip of $\rho(\varepsilon)$ and $\rho(\varepsilon)$ increases steeply below the Fermi level, is well reproduced by the model density of states. The calculated χ^{-1} of FeAs and CoAs are shown in Fig.4-3(a) and (b), respectively. For each compound, the observed anomalous temperature dependence of χ^{-1} is qualitatively explained. Quantitatively, however, the minimum position of the calculated χ^{-1} is shifted to higher temperature side compared with observation, and the calculated absolute values of χ^{-1} are larger compared with the observed ones.

We also calculated paramagnetic susceptibility of NiAs whose crystal structure is of NiAs-type. In NiAs the density of states near the Fermi level is quite different from that of FeAs. The calculated paramagnetic susceptibility is almost temperature independent as shown in Fig.4-3(c).

In order to clarify the origin of anomalous temperature dependence of the paramagnetic susceptibility observed in FeAs and CoAs, we have calculated average square amplitude of local

field x as functions of temperature. x is related to the local moment as shown in eq.(4.8). From the results shown in Fig.4-4, we can see that x increases as the temperature increases. In FeAs and CoAs x increases rapidly at about 300-400 K and is saturated at much higher temperatures. On the other hand, in NiAs x increases slowly as the temperature increases and it is not saturated. These results indicate the existence of a temperature-induced local moment in FeAs and CoAs, but not in NiAs. Both the rapid increase of x at low temperatures and the saturation of the longitudinal spin-fluctuation at high temperatures play an essential role in the bahavior of the paramagnetic susceptibility. The physical picture of the anomalous temperature dependence of the paramagnetic susceptibilities of FeAs and CoAs is as follows: at low temperatures, due to an increase of an amplitude of the longitudinal spin-fluctuation, χ^{-1} decreases (χ increases) with increasing temperature. At higher temperatures, however, the local moment is induced by the saturation effect of the longitudinal spin-fluctuation, and therefore χ^{-1} obeys the Curie-Weiss law as a function of temperature.

Such behavior of the longitudinal spin-fluctuation is strongly related to a shape of the density of states near the Fermi level. In order to examine the relation between the density of states and the paramagnetic susceptibility, we consider two functions as follows:

$$\frac{\partial L(x)}{\partial x} = -\int_{-\infty}^{\infty} d\varepsilon \rho(\varepsilon)\frac{\pi U}{2B}[f(\varepsilon-B)-f(\varepsilon+B)] \ , \qquad (4.10a)$$

$$\frac{\partial^2 L(x)}{\partial x^2} = \int_{-\infty}^{\infty} d\varepsilon \rho(\varepsilon)\left(\frac{\pi U}{2B}\right)^2 \{\frac{1}{B}[f(\varepsilon+B)-f(\varepsilon-B)]-[\delta(\varepsilon+B)+\delta(\varepsilon-B)]\}, \qquad (4.10b)$$

where f and δ denote the Fermi distribution function and $-\partial f/\partial B$, respectively. As seen from eq.(4.7a) and (4.7b) a behavior of $\partial L(x)/\partial x$ is explicitly reflected in the behavior of the paramagnetic susceptibility. $\partial^2 L(x)/\partial x^2$ is related to the coefficient of mode-mode coupling. When $\partial^2 L(x)/\partial x^2$ is negative, a longitudinal spin-fluctuation is strongly developed as temperature increases because of negative mode-mode coupling, and therefore the temperature-induced local moment easily arises. From eq.(4.10a) and (4.10b), we can see that

(1) When $\rho(\varepsilon_F)$ is small and the Fermi level is located at a steep dip of the density of states, $-\partial L(x)/\partial x$ increases rapidly with increasing temperature at low temperatures.

(2) When $\partial^2 \rho(\varepsilon)/\partial \varepsilon^2|_{\varepsilon=\varepsilon_F}$ is positive, $\partial^2 L(x)/\partial x^2$ becomes negative.

If a band has a characteristic shape of the density of states as denoted in (1) and (2), we can expect the anomalous temperature dependence of the paramagnetic susceptibility as observed in FeAs and CoAs. In fact, in FeAs and CoAs, the density of states obtained by the APW band calculation satisfies both conditions denoted in (1) and (2). On the other hand in

NiAs the calculated density of states does not satisfy both (1) and (2).

The self-consistent equations (4.7) and (4.9) contain three parameters A, $\bar{c}$ and U. For the Coulomb integral we have adopted the values of U=0.5 - 0.7 Ryd. This is reasonable for 3d-transition metals such as Fe, Co and Ni. Moriya pointed out that the parameter A can be estimated from the spin wave dispersion curve and A was estimated to be 0.35 [$\mathring{A}^2$] for Co and 0.77 [$\mathring{A}^2$] for Ni[33]. In the present work we have adopted 0.7 [$\mathring{A}^2$] for A and 0.05 [$\mathring{A}^{-1}Ryd^{-1}$] for $\bar{c}$.

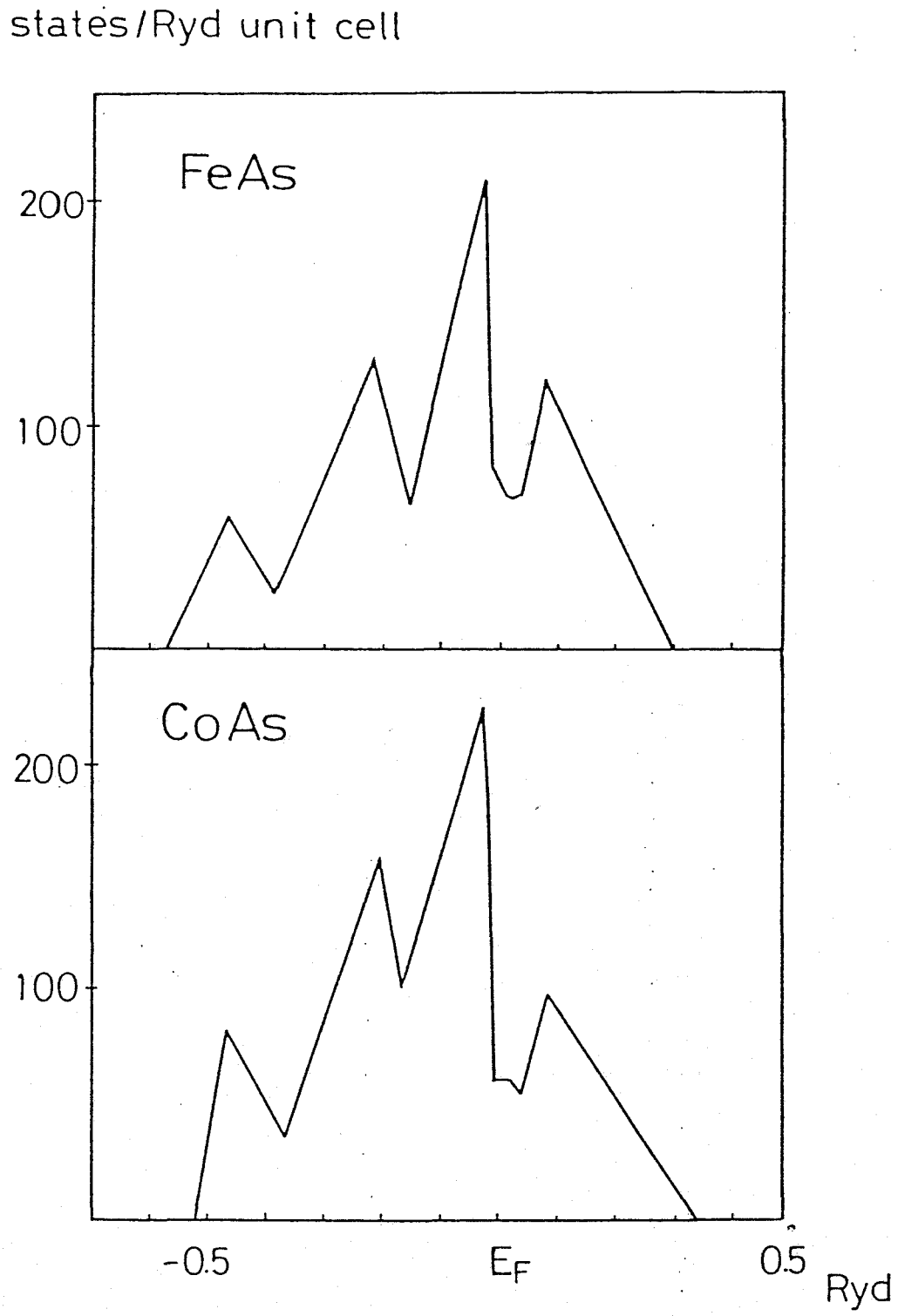

Fig.4-2(a) and (b). Model density of states of FeAs and CoAs.

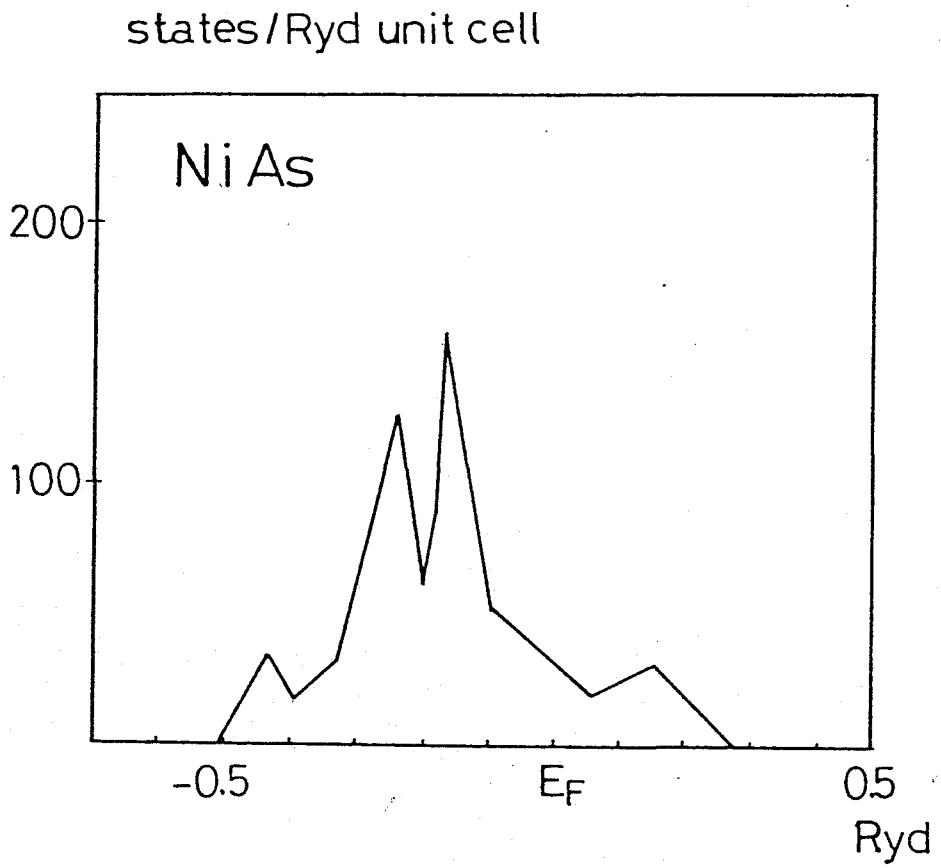

Fig.4-2(c). Model density of states of NiAs.

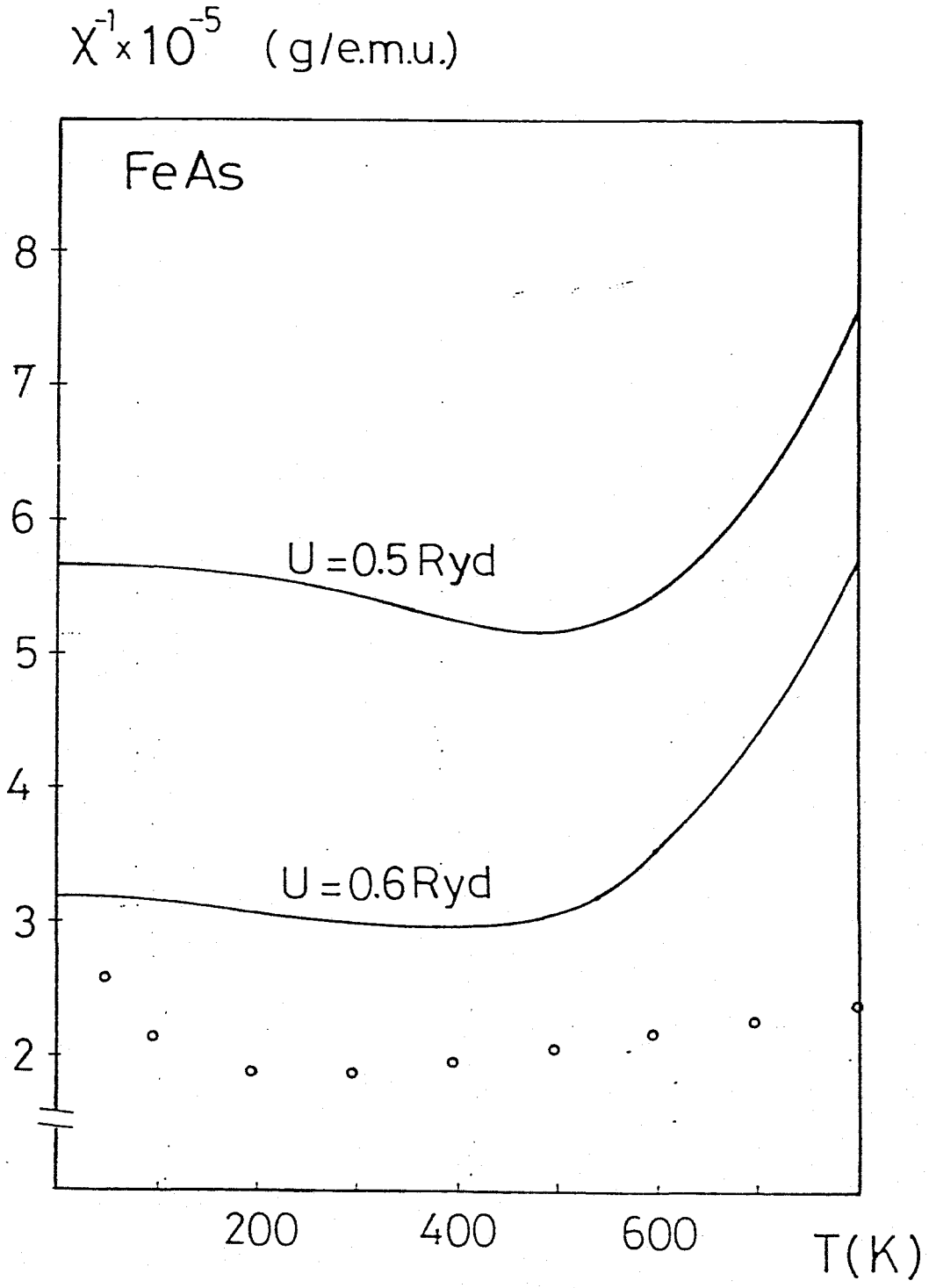

Fig.4-3(a). Calculated paramagnetic susceptibility of FeAs for U=0.5 and 0.6 Ryd (thick curves). The used parameters are $\langle\sigma\rangle$=0.4 and c=0.05. Open circles represent the observed results.

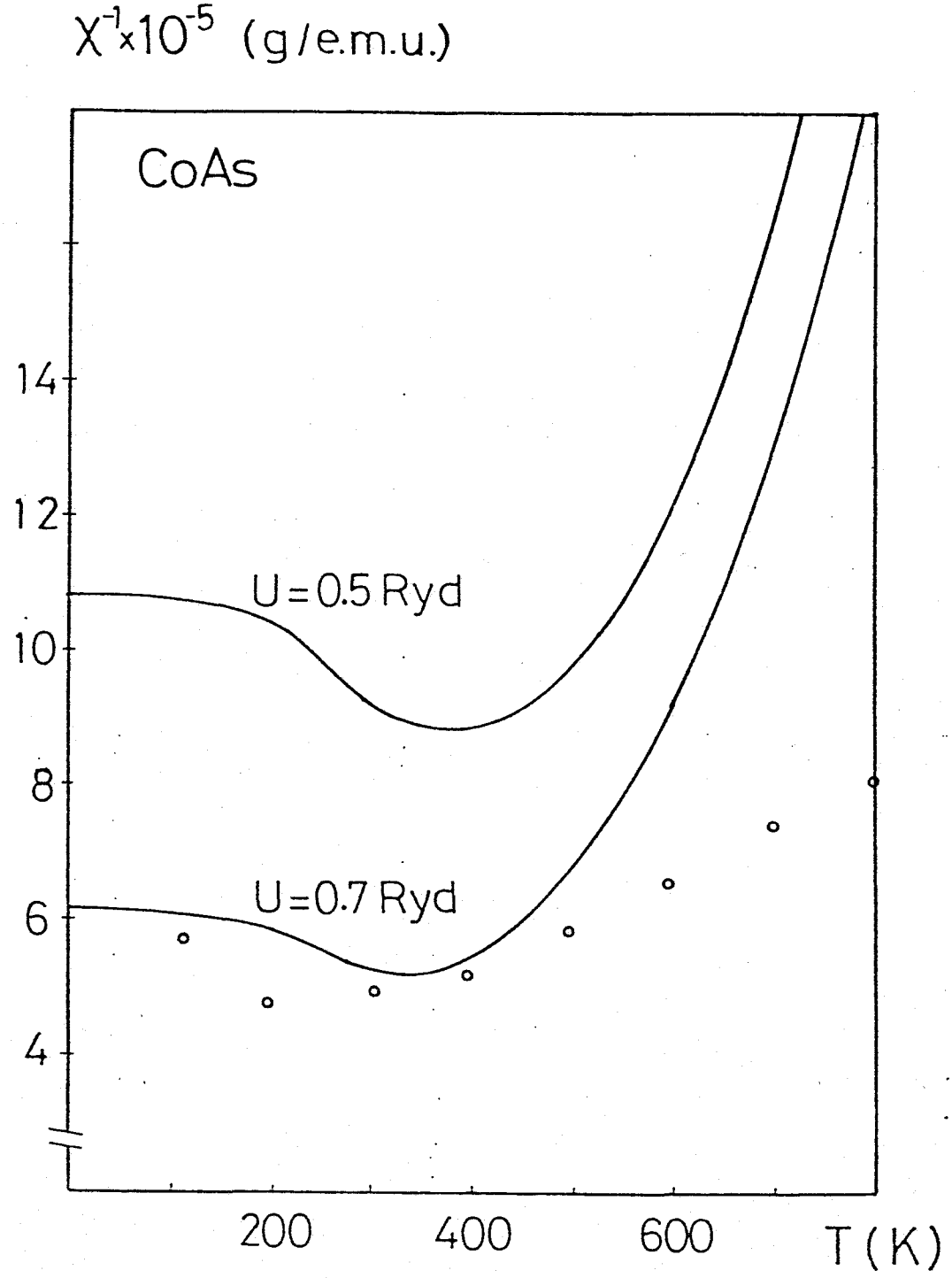

Fig.4-3(b). Calculated paramagnetic susceptibility of CoAs for U=0.5 and 0.7 Ryd (thick curves). The used parameters are $\langle\sigma\rangle$=0.4 and c=0.05. Open circles represent the observed results.

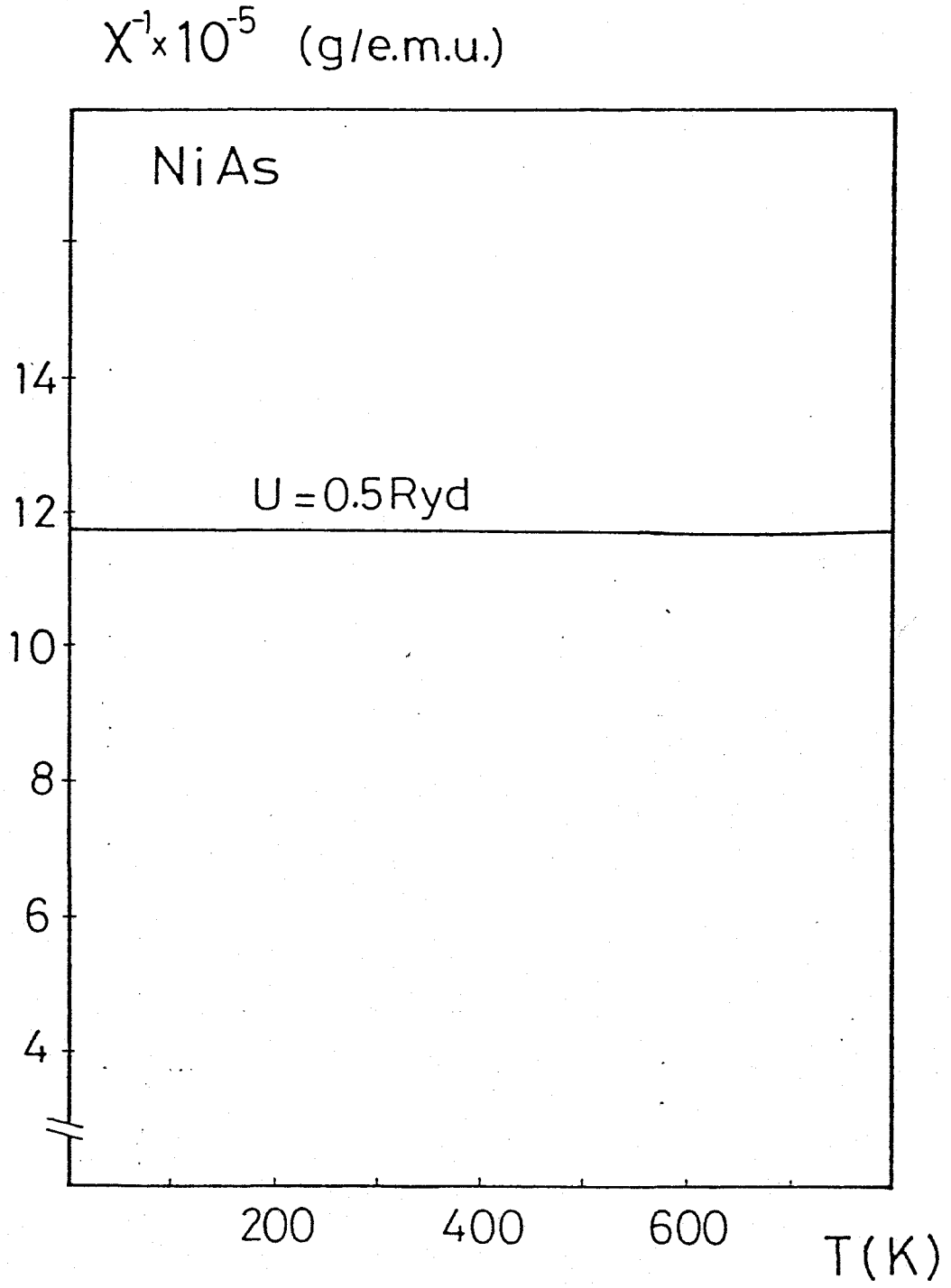

Fig.4-3(c). Calculated paramagnetic susceptibility of NiAs for U=0.5 Ryd. The used parameters are $\langle\sigma\rangle$=0.4 and c=0.05.

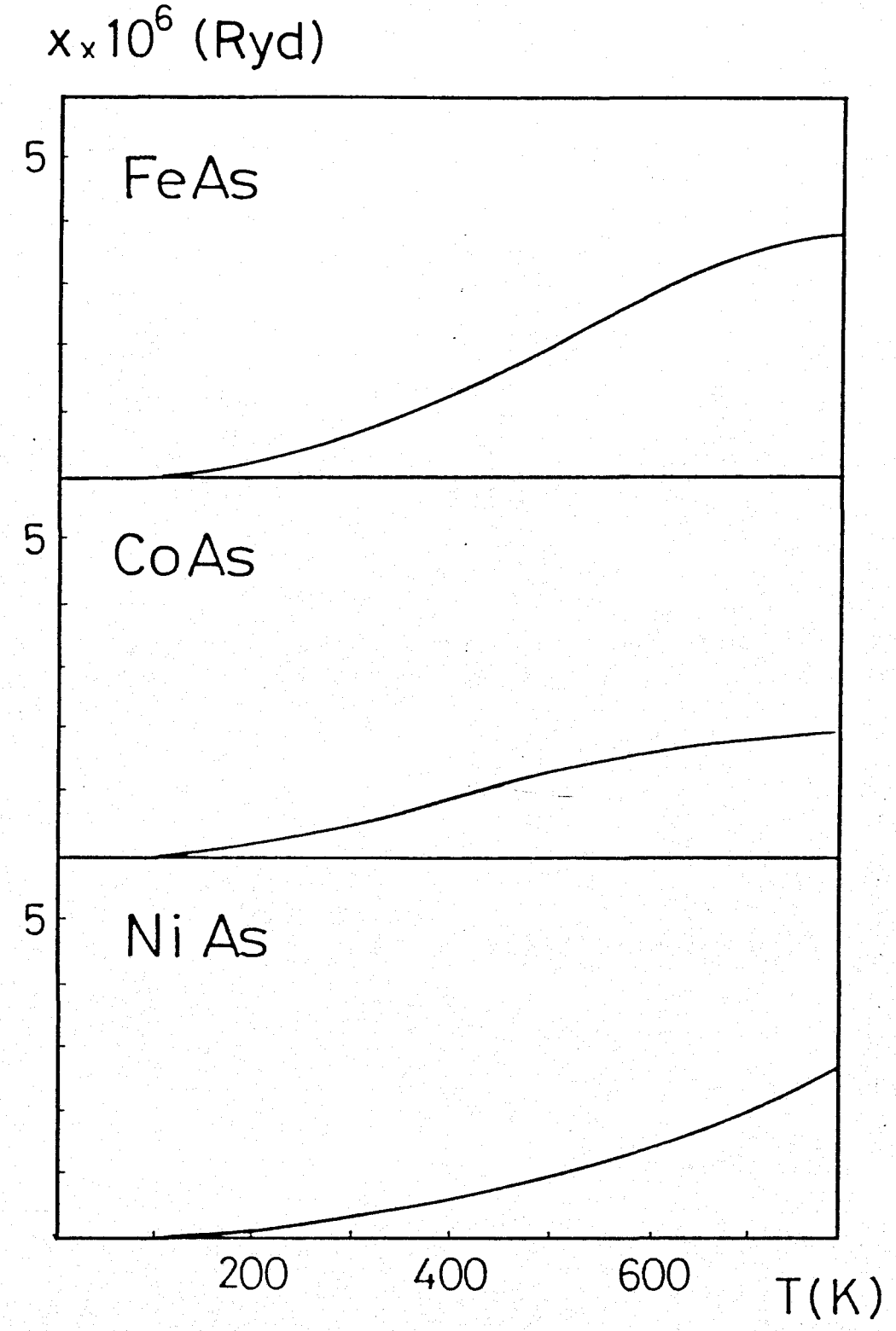

Fig.4-4. The average square amplitude of local field, x, for FeAs, CoAs and NiAs.

4.2 Double helical magnetic ordering of FeAs

4.2.1 Model Hamiltonian

The crystal structure of FeAs is of the MnP-type and four Fe atoms and four As atoms are contained in the unit cell. From the results of the band calculation, it has been found that the electronic states near the Fermi level, which play an important role in magnetism, arise mainly from Fe-d orbitals. If we pay attention to Fe atoms only, we can use a smaller unit cell as shown in Fig.4-5, in which two Fe atoms are contained. In this paper we consider a system having two atoms (a and b) in the unit cell and use a simplified tight-binding model in which a single orbital for each atom is assumed. The anisotropy energy is neglected. The Hamiltonian we consider is

$$\begin{aligned} H = & \sum_{ij\sigma} t_1 (a_{i\sigma}^{\dagger} b_{j\sigma} + b_{j\sigma}^{\dagger} a_{i\sigma}) + \sum_{ij\sigma} t_2 (a_{i\sigma}^{\dagger} b_{j\sigma} + b_{j\sigma}^{\dagger} a_{i\sigma}) \\ & + \sum_{ii'\sigma} t_3 a_{i\sigma}^{\dagger} a_{i'\sigma} + \sum_{jj'\sigma} t_3 b_{j\sigma}^{\dagger} b_{j'\sigma} \\ & + U \sum_{i} n_{i\uparrow} n_{i\downarrow} + U \sum_{j} n_{j\uparrow} n_{j\downarrow}, \end{aligned} \tag{4.11}$$

where $a_{i\sigma}^{\dagger}$ ($a_{i\sigma}$) and $b_{j\sigma}^{\dagger}$ ($b_{j\sigma}$) are the creation (annihilation) operators of the electron on the a-atom in the ith unit cell and that on the b-atom in the jth unit cell, respectively, and $n_{i\sigma}=a_{i\sigma}^{\dagger}a_{i\sigma}$ and $n_{j\sigma}=b_{j\sigma}^{\dagger}b_{j\sigma}$. t_1 and t_2 are the transfer integrals

between nearest and second nearest neighbor a-b atoms, respectively, and t_3 is the transfer integrals between nearest neighbor a-a and b-b atoms (see Fig.4-5). U is the intra-atomic Coulomb integral for each atom. We apply the Hartree-Fock self-consistent approximation to the single-orbital intra-atomic Coulomb interaction terms:

$$\hat{o}_1\hat{o}_2 = \langle\hat{o}_1\rangle\hat{o}_2 + \hat{o}_1\langle\hat{o}_2\rangle - \langle\hat{o}_1\rangle\langle\hat{o}_2\rangle , \tag{4.12}$$

where $\hat{o}_1$ and $\hat{o}_2$ denote operators such as $a^{\dagger}_{k\sigma}a_{k+q\sigma}$ etc. and $\langle\hat{o}_1\rangle$ and $\langle\hat{o}_2\rangle$ denote average values. By using the Fourier transformations given by

$$a_{i\sigma} = \frac{1}{\sqrt{N}}\sum_{k} a_{k\sigma}e^{-ik\cdot r_i} \tag{4.13}$$

and

$$b_{j\sigma} = \frac{1}{\sqrt{N}}\sum_{k} b_{k\sigma}e^{-ik\cdot(r_j+\tau)} ,$$

the Hamiltonian becomes

$$\begin{aligned} H = {} & \sum_{k\sigma}[T_1(k)a^{\dagger}_{k\sigma}b_{k\sigma} + T_1^{*}(k)b^{\dagger}_{k\sigma}a_{k\sigma} + T_3(k)(a^{\dagger}_{k\sigma}a_{k\sigma} + b^{\dagger}_{k\sigma}b_{k\sigma})] \\ & + U\sum_{kq\sigma}\sum [A_{q-\sigma}a^{\dagger}_{k+q\sigma}a_{k\sigma} + B_{q-\sigma}b^{\dagger}_{k+q\sigma}b_{k\sigma}] - NU\sum_{q}[A_{q\uparrow}A_{q\downarrow} + B_{q\uparrow}B_{q\downarrow}] \\ & - U\sum_{kq}[A^{+}_{q}a^{\dagger}_{k+q\downarrow}a_{k\uparrow} + B^{+}_{q}b^{\dagger}_{k+q\downarrow}b_{k\uparrow} + A^{-}_{-q}a^{\dagger}_{k\uparrow}a_{k+q\downarrow} + B^{-}_{-q}b^{\dagger}_{k\uparrow}b_{k+q\downarrow}] \\ & + NU\sum_{q}[|A^{+}_{q}|^2 + |B^{+}_{q}|^2], \end{aligned} \tag{4.14}$$

where

$$A_{q\sigma} = \frac{1}{N}\langle \sum_k a^{\dagger}_{k\sigma} a_{k+q\sigma} \rangle \quad , \quad B_{q\sigma} = \frac{1}{N}\langle \sum_k b^{\dagger}_{k\sigma} b_{k+q\sigma} \rangle$$

$$A^{+}_{q} = \frac{1}{N}\langle \sum_k a^{\dagger}_{k\uparrow} a_{k+q\downarrow} \rangle \quad , \quad B^{+}_{q} = \frac{1}{N}\langle \sum_k b^{\dagger}_{k\uparrow} b_{k+q\downarrow} \rangle , \qquad (4.15)$$

$$A^{-}_{-q} = \frac{1}{N}\langle \sum_k a^{\dagger}_{k\downarrow} a_{k-q\uparrow} \rangle = A^{+*}_{q} , \quad B^{-}_{-q} = \frac{1}{N}\langle \sum_k b^{\dagger}_{k\downarrow} b_{k-q\uparrow} \rangle = B^{+*}_{q}$$

and

$$T_1(k) = t_1 \sum_j e^{ik\cdot(r_i - r_j - \tau)} + t_2 \sum_j e^{ik\cdot(r_i - r_j - \tau)} \qquad (4.16)$$

$$T_3(k) = t_3 \sum_j e^{ik\cdot(r_i - r_j)} .$$

The summation in eq.(4.16) is taken for the neighboring pairs connected by each transfer integral. We denote the position vector of the a-atom in the ith unit cell as r_i and that of the b-atom in the jth unit cell as $r_j+\tau$.

In the paramagneic state, only q=0 terms among $A_{q\sigma}$ and $B_{q\sigma}$ are non-vanishing and $A_{0\uparrow}$ ($B_{0\uparrow}$) equals $A_{0\downarrow}$ ($B_{0\downarrow}$). Then, the Hamiltonian for the paramagnetic state is given by

$$H = \sum_{k\sigma} [T_1(k) a^{\dagger}_{k\sigma} b_{k\sigma} + T^{*}_1(k) b^{\dagger}_{k\sigma} a_{k\sigma} + (T_3(k)+UA_0) a^{\dagger}_{k\sigma} a_{k\sigma} + (T_3(k)+UB_0)\, b^{\dagger}_{k\sigma} b_{k\sigma}] - NU[A_0^2 + B_0^2] . \qquad (4.17)$$

Introducing new operators $\alpha_{k\sigma}$ and $\beta_{k\sigma}$ defined by

$$a_{k\sigma} = \left[\frac{T_1(k)}{2|T_1(k)|} \right]^{1/2} (\alpha_{k\sigma} - \beta_{k\sigma}), \tag{4.18a}$$

$$b_{k\sigma} = \left[\frac{T_1^*(k)}{2|T_1(k)|} \right]^{1/2} (\alpha_{k\sigma} + \beta_{k\sigma}), \tag{4.18b}$$

$$a_{k\sigma}^\dagger = \left[\frac{T_1^*(k)}{2|T_1(k)|} \right]^{1/2} (\alpha_{k\sigma}^\dagger - \beta_{k\sigma}^\dagger), \tag{4.18c}$$

$$b_{k\sigma}^\dagger = \left[\frac{T_1(k)}{2|T_1(k)|} \right]^{1/2} (\alpha_{k\sigma}^\dagger + \beta_{k\sigma}^\dagger), \tag{4.18d}$$

the Hamiltonian of eq. (4.17) is diagonalized as follows:

$$H = \sum_{k\sigma}\sum \left[E_k^\alpha \alpha_{k\sigma}^\dagger \alpha_{k\sigma} + E_k^\beta \beta_{k\sigma}^\dagger \beta_{k\sigma} \right] - NU \left[A_0^2 + B_0^2 \right]. \tag{4.19}$$

The eigenvalues E_k^α and E_k^β are given by

$$E_K^\alpha = |T_1(k)| + T_3(k) + UA_0, \tag{4.20a}$$

$$E_k^\beta = -|T_1(k)| + T_3(k) + UB_0, \tag{4.20b}$$

where α and β denote band suffices.

Using $\alpha_{k\sigma}$ and $\beta_{k\sigma}$, the Hamiltonian given by eq.(4.14) becomes

$$
\begin{aligned}
H \;=\; & \sum_{k\sigma}\sum \Big[\; E_k^{\alpha}\,\alpha_{k\sigma}^{\dagger}\alpha_{k\sigma} \;+\; E_k^{\beta}\,\beta_{k\sigma}^{\dagger}\beta_{k\sigma} \;\Big] \\
& + U \sum_{kq}\sum_{\sigma}{}' \Big[A_{q-\sigma}\gamma^{*}(k,q)(\alpha_{k+q\sigma}^{\dagger} - \beta_{k+q\sigma}^{\dagger})(\alpha_{k\sigma}-\beta_{k\sigma}) \\
& \qquad + B_{q-\sigma}\gamma(k,q)\;(\alpha_{k+q\sigma}^{\dagger} + \beta_{k+q\sigma}^{\dagger})(\alpha_{k\sigma}+\beta_{k\sigma})\;\Big] \\
& - U \sum_{kq} \Big[A_q^{+}\,\gamma^{*}(k,q)(\alpha_{k+q\downarrow}^{\dagger} - \beta_{k+q\downarrow}^{\dagger})(\alpha_{k\uparrow}-\beta_{k\uparrow}) \\
& \qquad + B_q^{+}\,\gamma(k,q)\;(\alpha_{k+q\downarrow}^{\dagger} + \beta_{k+q\downarrow}^{\dagger})(\alpha_{k\uparrow}+\beta_{k\uparrow}) \\
& \qquad + A_{-q}^{-}\,\gamma(k,q)(\alpha_{k\uparrow}^{\dagger} - \beta_{k\uparrow}^{\dagger})(\alpha_{k+q\downarrow}-\beta_{k+q\downarrow}) \\
& \qquad + B_{-q}^{-}\,\gamma^{*}(k,q)(\alpha_{k\uparrow}^{\dagger} + \beta_{k\uparrow}^{\dagger})(\alpha_{k+q\downarrow}+\beta_{k+q\downarrow})\Big] \\
& - NU \sum_{q}\Big[(A_{q\uparrow}A_{q\downarrow} + B_{q\uparrow}B_{q\downarrow}) - (|A_q^{+}|^2 + |B_q^{+}|^2)\Big]\;,
\end{aligned}
\tag{4.21}
$$

where

$$
\gamma(k,q) \;=\; \left(\frac{T_1^{*}(k)\;T_1(k+q)}{4\,|T_1(k)|\,|T_1(k+q)|} \right)^{1/2} . \tag{4.22}
$$

$\sum_{q}{}'$ in eq. (4.21) denotes that terms of q=0 are excluded in the summation.

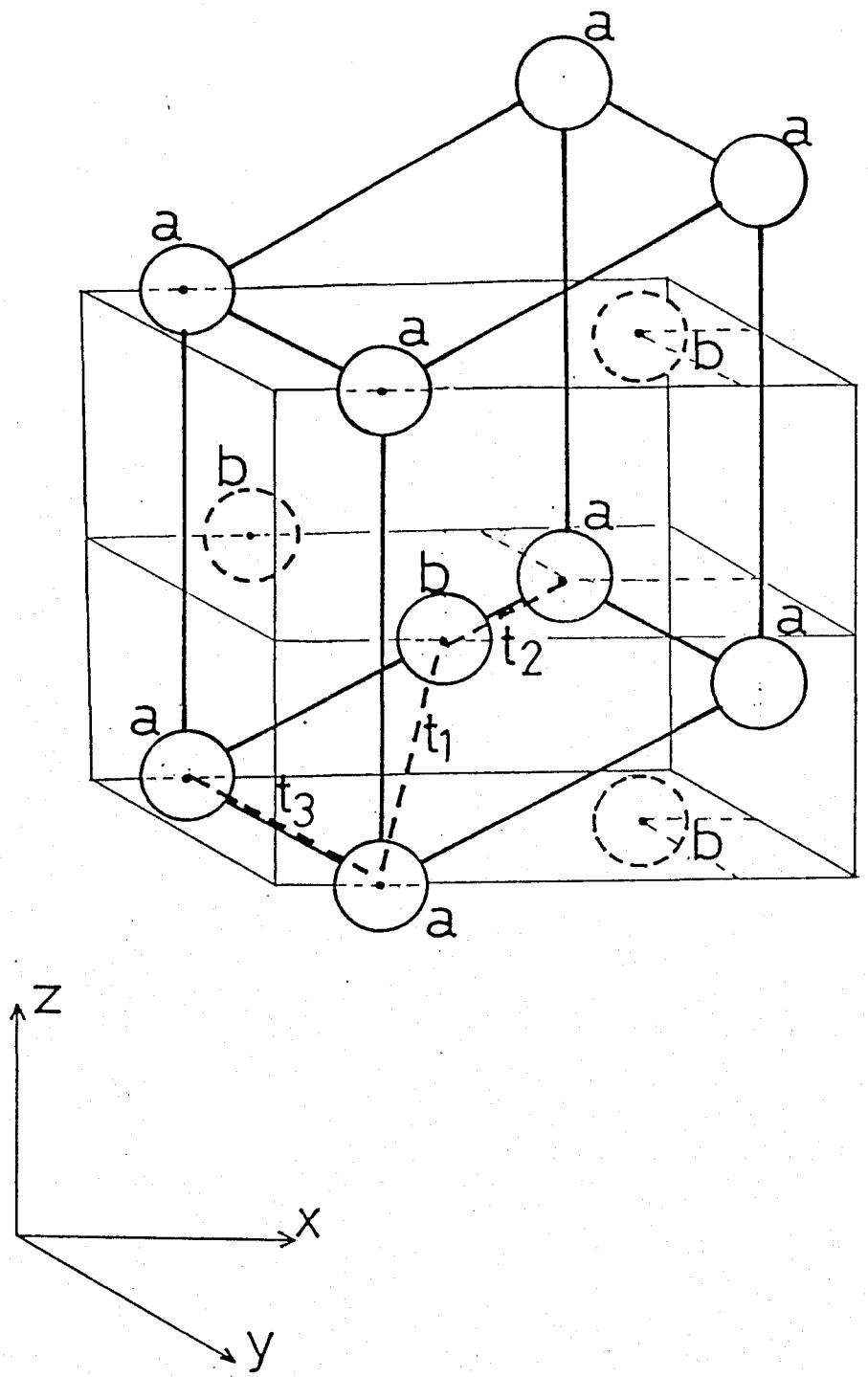

Fig.4-5. Unit cell of the lattice constructed by Fe atoms. Two sublattices are denoted as a and b, respectively, and transfer integrals are denoted as t_1, t_2 and t_3.

4.2.2 Instability of the paramagnetic phase

4.2.2(a) Formulation

First, we study the instability of the paramagnetic phase against the formation of a magnetic order whose spatial variation is described by the wave vector $\mathbf{q}$[34]. We consider the interaction between a magnetic moment and a magnetic field. In an itinerant system, z-component of spin density is written as

$$S_z(\mathbf{r})=\mu_B\sum_i[|\phi^a(\mathbf{r}-\mathbf{r}_i)|^2(a^\dagger_{i\uparrow}a_{i\uparrow}-a^\dagger_{i\downarrow}a_{i\downarrow}) + |\phi^b(\mathbf{r}-\mathbf{r}_i-\tau)|^2(b^\dagger_{i\uparrow}b_{i\uparrow}-b^\dagger_{i\downarrow}b_{i\downarrow})\ ] \tag{4.23}$$

ϕ^a and ϕ^b in eq.(4.23) represent Wannier functions on a- and b-atoms, respectively. After the Fourier transformation $S_z(\mathbf{r})$ is written as

$$S_z(\mathbf{r})=\mu_B\sum_{\mathbf{q}'}\sum_{\mathbf{G}}e^{i(\mathbf{q}'+\mathbf{G})\cdot\mathbf{r}}[I^a_{-\mathbf{q}'\mathbf{G}}s^a_z(-\mathbf{q}')+e^{-i\mathbf{G}\cdot\tau}\ I^b_{-\mathbf{q}'\mathbf{G}}s^b_z(-\mathbf{q}')] \tag{4.24}$$

where

$$s^a_z(-\mathbf{q})=\sum_{\mathbf{k}}(a^\dagger_{\mathbf{k}\uparrow}a_{\mathbf{k}-\mathbf{q}\uparrow}+a^\dagger_{\mathbf{k}\downarrow}a_{\mathbf{k}-\mathbf{q}\downarrow})\ , \tag{4.25a}$$

$$s^b_z(-\mathbf{q})=\sum_{\mathbf{k}}(b^\dagger_{\mathbf{k}\uparrow}b_{\mathbf{k}-\mathbf{q}\uparrow}+b^\dagger_{\mathbf{k}\downarrow}b_{\mathbf{k}-\mathbf{q}\downarrow})\ , \tag{4.25b}$$

$$I^a_{-q} = \frac{1}{V}\int |\phi^a(r')|^2 e^{i(q+G)\cdot r'} dr' \ , \qquad (4.25c)$$

$$I^b_{-q} = \frac{1}{V}\int |\phi^b(r')|^2 e^{i(q+G)\cdot r'} dr' \ , \qquad (4.25d)$$

q: a wave vector in the Brillouine zone,

G: a reciprocal lattice vector,

V: volume of the crystal .

When magnetic field $H^a(q)$ and $H^b(q)$ which are conjugate to $s^a_z(-q)$ and $s^b_z(-q)$, respectively, are applied to the system, the Zeeman interaction is written as

$$H' = \mu_B [I^a_{-q} s^a_z(-q) H^a(q) + I^b_{-q} s^b_z(-q) H^b(q)] \ , \qquad (4.26)$$

where $I^a_{-q} = I^a_{-q,0}$ etc. To obtain eq.(4.26) we neglected the terms except G=0 in eq.(4.24), considering that spatial variation of the Wannier functions in the unit cell is small.

Wave number dependent magnetic moments of A- and B-sublattices are defined as

$$M^a(q) = \mu_B I^a_q (A_{q\downarrow} - A_{q\uparrow}) \quad M^b(q) = \mu_B I^b_q (B_{q\downarrow} - B_{q\uparrow}), \qquad (4.27)$$

Within the framework of the linear response theory, we obtain the following relation[35]:

$$\begin{pmatrix} H^a(q) \\ H^b(q) \end{pmatrix} = \begin{pmatrix} \bar{\chi}^{aa}(q) & \bar{\chi}^{ab}(q) \\ \bar{\chi}^{ba}(q) & \bar{\chi}^{bb}(q) \end{pmatrix} \begin{pmatrix} M^a(q) \\ M^b(q) \end{pmatrix} \equiv \bar{\chi}(q) \begin{pmatrix} M^a(q) \\ M^b(q) \end{pmatrix} , \qquad (4.28)$$

by solving equations of motion of the magnetizations (see appendix C). $\bar{\chi}^{aa}(q)$ etc. in eq. (4.28) are calculated as

$$\bar{\chi}^{aa}(\mathbf{q}) = -\frac{1}{2\mu_B^2 |I_{\mathbf{q}}^a|^2} \frac{\Gamma_1(\mathbf{q}) + U[\Gamma_1(\mathbf{q})^2 - |\Gamma_2(\mathbf{q})|^2]}{\Gamma_1(\mathbf{q})^2 - |\Gamma_2(\mathbf{q})|^2} , \quad (4.29a)$$

$$\bar{\chi}^{ab}(\mathbf{q}) = \frac{1}{2\mu_B^2 I_{-\mathbf{q}}^a I_{\mathbf{q}}^b} \frac{\Gamma_2(\mathbf{q})^*}{\Gamma_1^2(\mathbf{q}) - |\Gamma_2(\mathbf{q})|^2} , \quad (4.29b)$$

$$\bar{\chi}^{bb}(\mathbf{q}) = -\frac{1}{2\mu_B^2 |I_{\mathbf{q}}^b|^2} \frac{\Gamma_1(\mathbf{q}) + U[\Gamma_1(\mathbf{q})^2 - |\Gamma_2(\mathbf{q})|^2]}{\Gamma_1(\mathbf{q})^2 - |\Gamma_2(\mathbf{q})|^2} , \quad (4.29c)$$

$$\bar{\chi}^{ba}(\mathbf{q}) = \frac{1}{2\mu_B^2 I_{\mathbf{q}}^a I_{-\mathbf{q}}^b} \frac{\Gamma_2(\mathbf{q})}{\Gamma_1^2(\mathbf{q}) - |\Gamma_2(\mathbf{q})|^2} = \bar{\chi}^{ab}(\mathbf{q})^* \quad (4.29d)$$

where

$$\Gamma_1(\mathbf{q}) = \frac{1}{4N} \sum_{\mathbf{k}} [\chi_0^{\alpha\alpha}(\mathbf{k},\mathbf{q}) + \chi_0^{\beta\beta}(\mathbf{k},\mathbf{q}) + \chi_0^{\alpha\beta}(\mathbf{k},\mathbf{q}) + \chi_0^{\beta\alpha}(\mathbf{k},\mathbf{q})], \quad (4.30a)$$

$$\Gamma_2(\mathbf{q}) = \frac{1}{4N} \sum_{\mathbf{k}} \frac{T_1^*(\mathbf{k}+\mathbf{q}) T_1(\mathbf{k})}{|T_1(\mathbf{k}+\mathbf{q})||T_1(\mathbf{k})|} [\chi_0^{\alpha\alpha}(\mathbf{k},\mathbf{q}) + \chi_0^{\beta\beta}(\mathbf{k},\mathbf{q}) - \chi_0^{\alpha\beta}(\mathbf{k},\mathbf{q}) - \chi_0^{\beta\alpha}(\mathbf{k},\mathbf{q})], \quad (4.30b)$$

$$\chi_0^{\mu\nu}(\mathbf{k},\mathbf{q}) = \frac{f(E_{\mathbf{k}}^{\mu}) - f(E_{\mathbf{k}+\mathbf{q}}^{\nu})}{E_{\mathbf{k}}^{\mu} - E_{\mathbf{k}+\mathbf{q}}^{\nu}} . \quad (\mu,\nu = \alpha,\beta) \quad (4.31)$$

We consider the case where a- and b-sites are occupied by the same kind atoms, therefore $I_{\mathbf{q}}^a = I_{\mathbf{q}}^b$ and $\bar{\chi}^{aa}(\mathbf{q}) = \bar{\chi}^{bb}(\mathbf{q})$. The instability condition for the paramagnetic phase is obtained by solving the following equation:

$$\det[\bar{\chi}(q)] = \bar{\chi}^{aa}(q)^2 - |\bar{\chi}^{ab}(q)|^2 = 0 \ . \qquad (4.32)$$

By inserting eqs.(4.29) and (4.30) into eq. (4.32), we obtain

$$1 + 2U\Gamma_1(q) + U^2[\Gamma_1^2(q) - |\Gamma_2(q)|^2] = 0 \ . \qquad (4.33)$$

From eq. (4.33), U is solved as

$$U = \begin{cases} -\dfrac{1}{\Gamma_1(q) + |\Gamma_2(q)|} & (4.34a) \\ -\dfrac{1}{\Gamma_1(q) - |\Gamma_2(q)|} \ . & (4.34b) \end{cases}$$

If the minimum value of U given by eq.(4.34) is obtained for $q=Q$, we may say that the magnetic ordering described by the wave vector Q is most likely to be realized. From the definition of $\Gamma_1(q)$ and $\Gamma_2(q)$ given by eq. (4.30), it is found that $\Gamma_1(q)$ is always negative and $|\Gamma_1(q)|>|\Gamma_2(q)|$. Therefore, U given by eq. (4.34b) takes a smaller value compared with that given by eq. (4.34a). Hereafter, we consider only eq. (4.34b) as an instability condition of the paramagnetic phase. We denote U given by eq. (4.34b) as U_c. If $H^a(q)=H^b(q)=0$, eq.(4.28) leads to the relation

$$\bar{\chi}^{aa}(q)M^a(q) + \bar{\chi}^{ab}(q)M^b(q) = 0 \ . \qquad (4.35)$$

For $q=Q$, eq.(4.35) becomes

$$\frac{M^b(Q)}{M^a(Q)} = -\frac{\bar{\chi}^{aa}(Q)}{\bar{\chi}^{ab}(Q)} \ . \qquad (4.36)$$

From eq. (4.32), $|\bar{\chi}^{aa}(Q)|$ equals $|\bar{\chi}^{ab}(Q)|$. Therefore, we have found that the absolute value of $M^a(Q)$ equals that of $M^b(Q)$. In real space, the magnetic moments on a- and b- sublattices are expressed as

$$M^a(\mathbf{r}) = M^a(Q)e^{-iQ\cdot r} \quad , \quad M^b(\mathbf{r}) = M^b(Q)e^{-iQ\cdot r} \quad . \tag{4.37}$$

The relative phase angle, ϕ_{12}, between the magnetic moments on a- and b- atoms in the ith unit cell is defined as

$$\frac{M^b(\mathbf{r}_i+\tau)}{M^a(\mathbf{r}_i)} = \frac{M^b(Q)}{M^a(Q)} e^{-iQ\cdot\tau} \equiv e^{i\phi_{12}} . \tag{4.38}$$

By eqs. (4.36) and (4.38), ϕ_{12} is determined as

$$e^{i\phi_{12}} = - \frac{\bar{\chi}^{aa}(Q)}{\bar{\chi}^{ab}(Q)} e^{-iQ\cdot\tau}$$

or

$$\phi_{12} = \pi + \arg\left[\frac{\bar{\chi}^{aa}(Q)}{\bar{\chi}^{ab}(Q)} \right] + \arg[e^{-iQ\cdot\tau}] \quad . \tag{4.39a}$$

From eq. (4.29), $\bar{\chi}^{aa}(Q)$ is a real quantity and a phase factor of $\bar{\chi}^{ab}(Q)$ arises from $\Gamma_2(Q)^*$, therefore ϕ_{12} is given by

$$\phi_{12} = \pi + \arg[\Gamma_2(Q)] + \arg[e^{-iQ\cdot\tau}] \tag{4.39b}$$

4.2.2(b) Results and discussion

In order to use the model Hamiltonian given by eq.(4.11) for the real substance FeAs, we have determined the transfer integrals t_1, t_2 and t_3 of the tight-binding band so as to reproduce the density of states of the electronic bands, which mainly consist of Fe-d orbitals, obtained in §2 by the self-consistent APW band calculation. Their values are as follows: t_1=-0.07 Ryd, $t_2/|t_1|$=-1.0 and $t_3/|t_1|$=-0.2. For comparison, we show in Fig.4-6(a) the density of states of the tight-binding model band calculated by using these values of the transfer integrals. As seen from the results of Fig.2-12(a) and Fig.4-6(a), a characteristic feature having two prominent peaks of the d-band density of states is well reproduced by the model band. Furthermore, the number of electrons, n, is also a parameter. We have determined n, namely the position of the Fermi level, so that the Fermi surface of the tight-binding model band becomes similar to that obtained by the APW band calculation as shown in Fig.4-6(b). The value of n is about 1.1.

By using the parameter values determined above, we have calculated $\Gamma_1(\mathbf{q})$ and $\Gamma_2(\mathbf{q})$ as functions of $\mathbf{q}$ along the symmetry lines. 8000 points in the 1st Brillouin zone are used for the summation over $\mathbf{k}$ in eq.(4.30). Then we have evaluated U_c given by eq.(4.34b) as a function of $\mathbf{q}$. The results are shown in Fig.4-7(a) and (b). The smallest U_c is obtained for $\mathbf{q}=0.4\times(2\pi/c)$. This value is very close to the observed helical

wave vector $q=0.375\times(2\pi/c)$. Next, by eq.(4.39b) we have calculated ϕ_{12} as a function of q. The result is shown in Fig.4-7(c). For $q=0.4\times(2\pi/c)$, ϕ_{12} is obtained as $\phi_{12}=158^{0}$. This value is in good agreement with the observed one, 140^{0}.

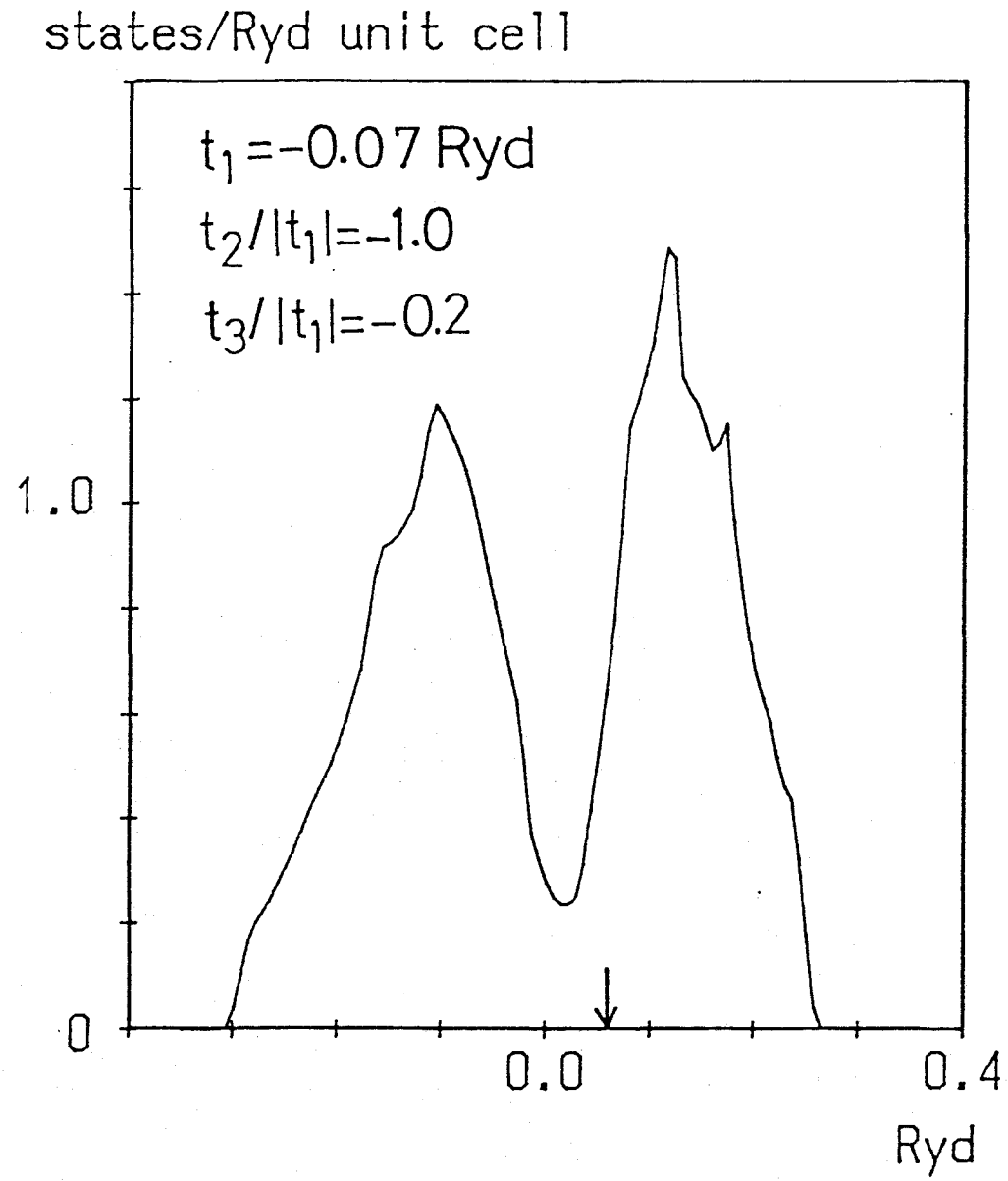

Fig.4-6(a). Density of states of the tight-binding model band. An arrow denotes the Fermi level for n=1.1.

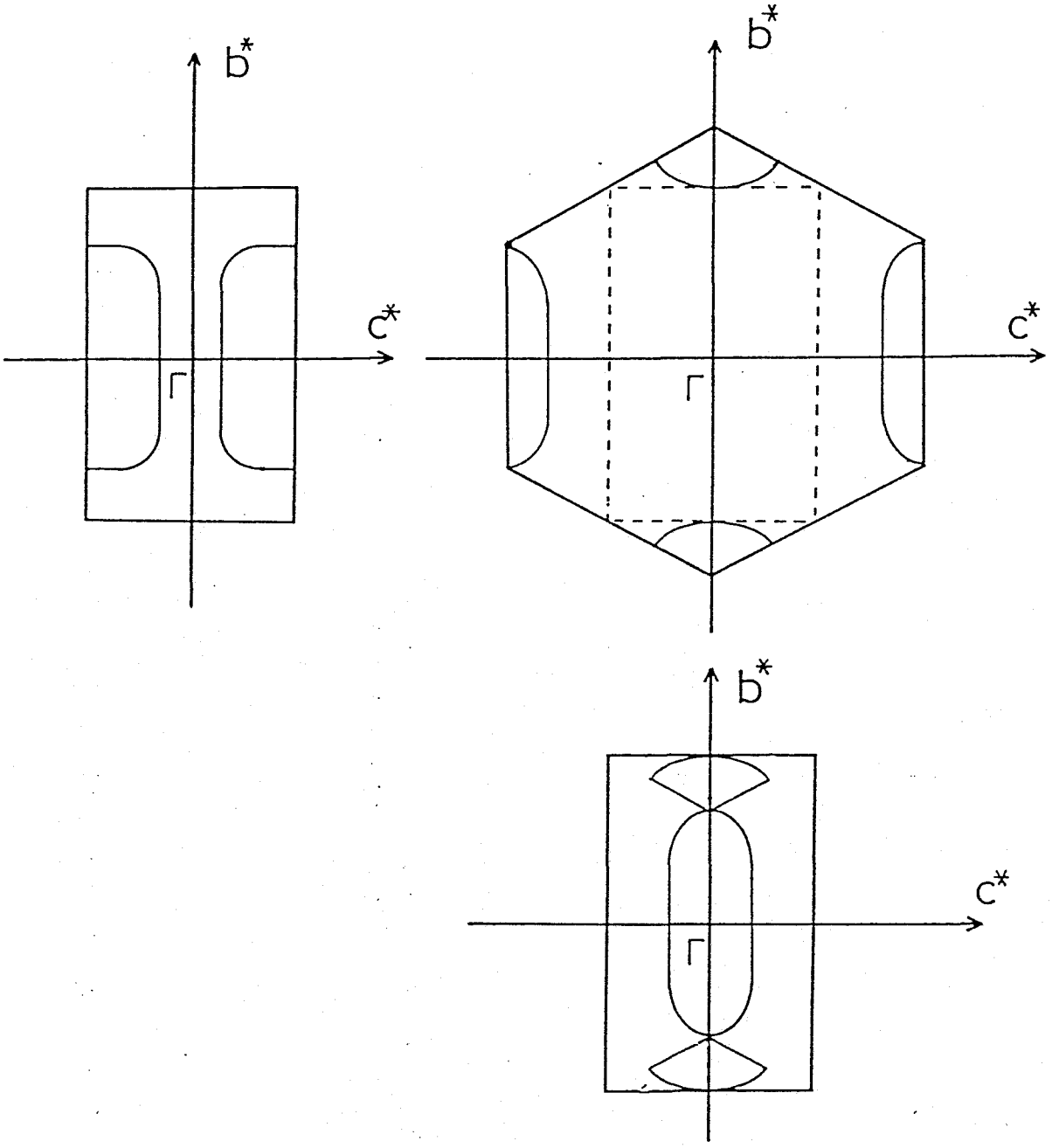

Fig.4-6(b). Cross section of Fermi surface of the model band (right) is similar to that of the Fermi surface of the APW band (left), when it is folded into the orthorhombic Brillouin zone.

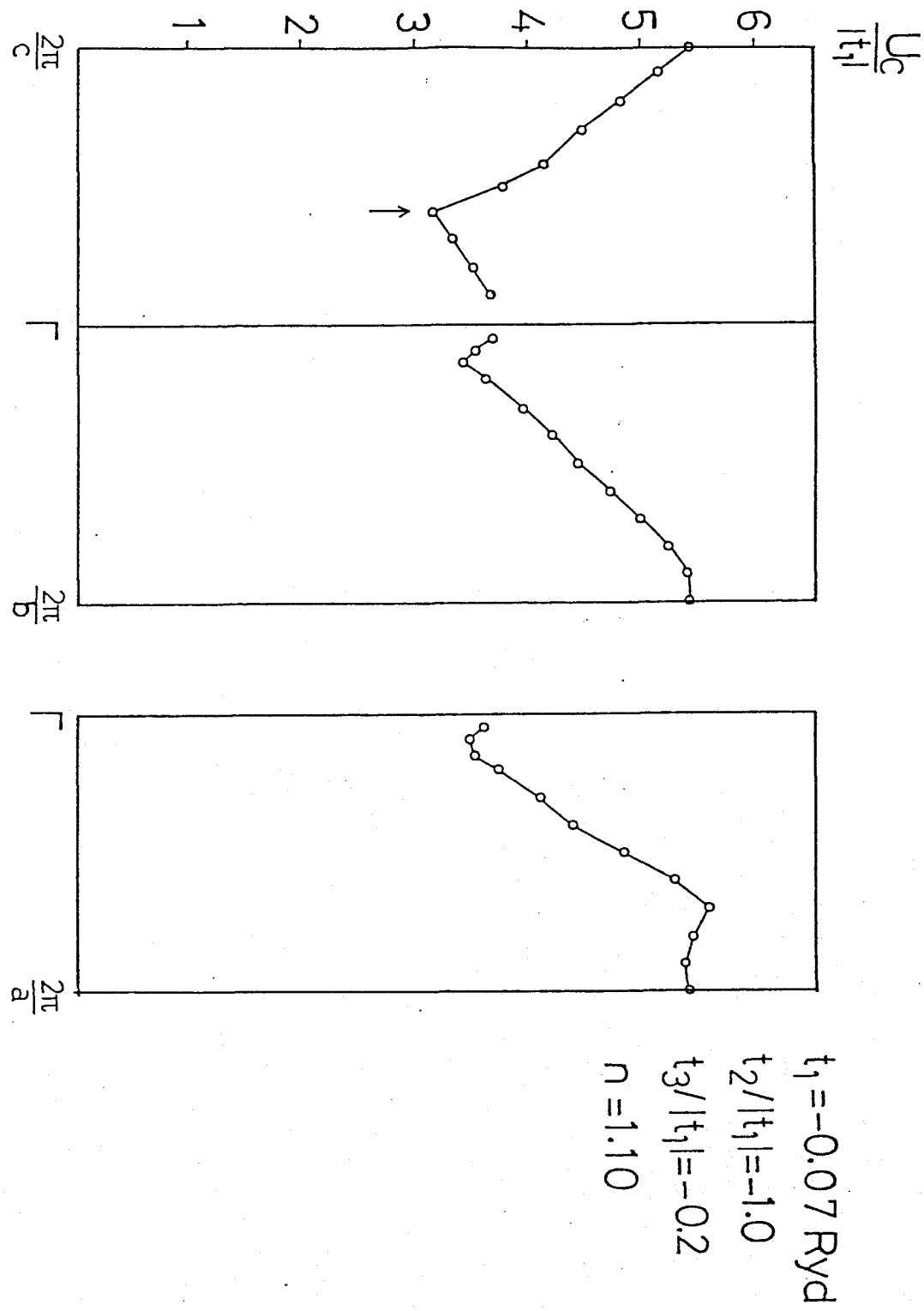

Fig.4-7(a). U_c (defined by eq.(4.34b)) as a function of wave vectors q. An arrow denotes the smallest value.

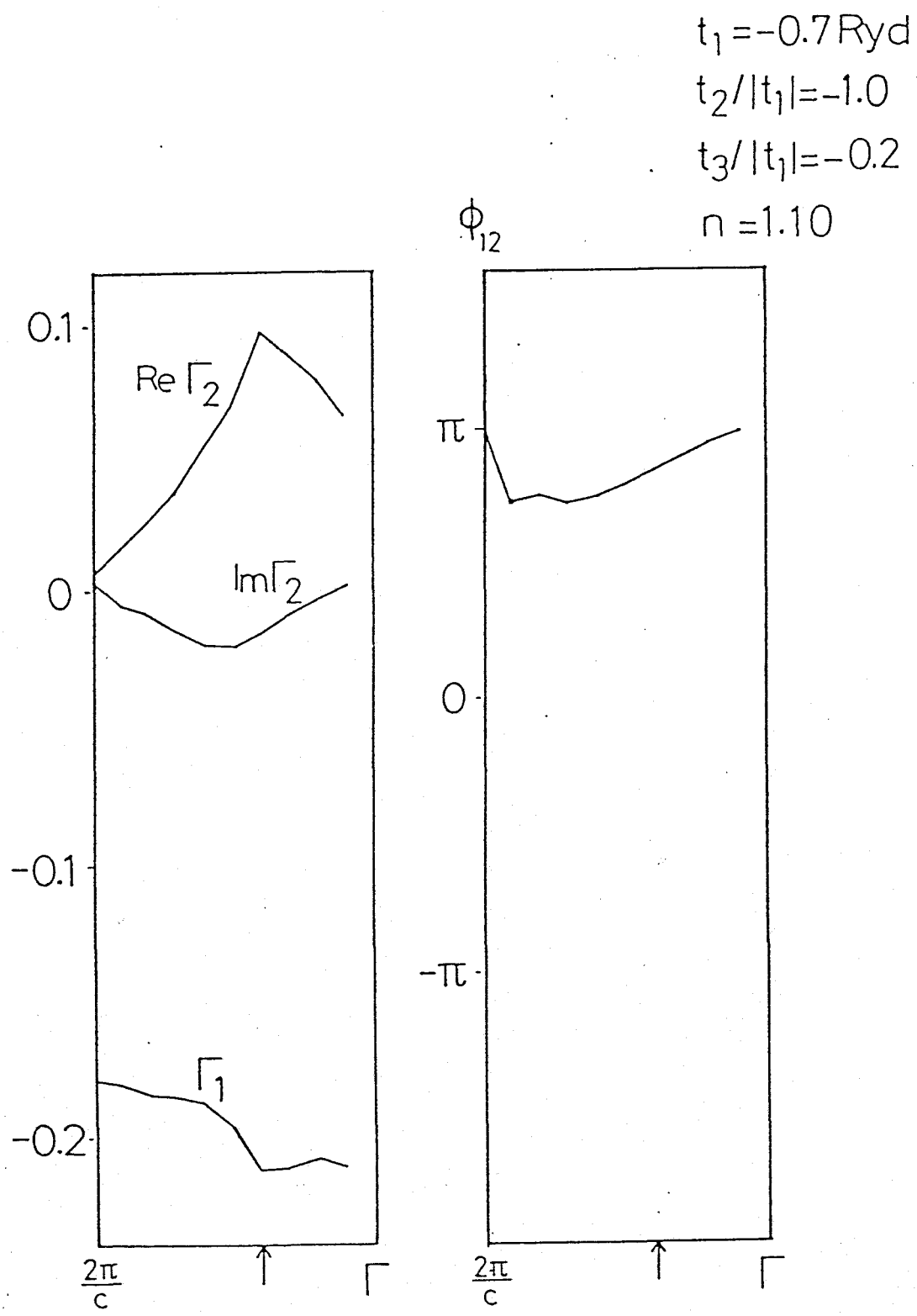

Fig.4-7(b). $\Gamma_1(q)$ and $\Gamma_2(q)$ as functions of q (left).

(c). ϕ_{12} (defined by eq.(4.39b)) as a function of q (right).

4.2.3 Helical SDW state

4.2.3(a) Formulation

In this section we assume that the helical SDW described by the wave vector Q is realized. In such case the Hamiltonian given by eq. (4.14) is rewritten, within the Hartree-Fock approximation for the Coulomb interaction term, as the following matrix form:

$$H = \sum_{\mathbf{k}} \Psi^{\dagger}(\mathbf{k},\mathbf{Q})\hat{H}(\mathbf{k},\mathbf{Q})\Psi(\mathbf{k},\mathbf{Q}) + \frac{NUn^2}{2} + NU(|A_{\mathbf{Q}}^{+}|^2 + |B_{\mathbf{Q}}^{+}|^2), \quad (4.40)$$

$$\hat{H}(\mathbf{k},\mathbf{Q}) = \begin{pmatrix} T_3(\mathbf{k}) & T_1(\mathbf{k}) & -UA_{-\mathbf{Q}}^{-} & 0 \\ T_1^{*}(\mathbf{k}) & T_3(\mathbf{k}) & 0 & -UB_{-\mathbf{Q}}^{-} \\ -UA_{\mathbf{Q}}^{+} & 0 & T_3(\mathbf{k}+\mathbf{Q}) & T_1(\mathbf{k}+\mathbf{Q}) \\ 0 & -UB_{\mathbf{Q}}^{+} & T_1^{*}(\mathbf{k}+\mathbf{Q}) & T_3(\mathbf{k}+\mathbf{Q}) \end{pmatrix}, \quad (4.41)$$

$$\Psi(\mathbf{k},\mathbf{Q}) = \begin{pmatrix} a_{\mathbf{k}\uparrow} \\ b_{\mathbf{k}\uparrow} \\ a_{\mathbf{k}+\mathbf{Q}\downarrow} \\ b_{\mathbf{k}+\mathbf{Q}\downarrow} \end{pmatrix}, \qquad \Psi^{\dagger}(\mathbf{k},\mathbf{Q}) = [\, a_{\mathbf{k}\uparrow}^{\dagger} \; b_{\mathbf{k}\uparrow}^{\dagger} \; a_{\mathbf{k}+\mathbf{Q}\downarrow}^{\dagger} \; b_{\mathbf{k}+\mathbf{Q}\downarrow}^{\dagger} \,], \quad (4.42)$$

where n denotes a number of elecrtons of each atom and is given by $n=A_{0\uparrow}+A_{0\downarrow}=B_{0\uparrow}+B_{0\downarrow}$. $A_{\mathbf{Q}}^{+}$, $B_{\mathbf{Q}}^{+}$, $A_{-\mathbf{Q}}^{-}$ and $B_{-\mathbf{Q}}^{-}$ in eq. (4.41) represent spin densities which are defined by eq. (4.15). With the use of unitary matrix U, whose elements are expressed as

$U_{\mu\nu}(\mu,\nu=1,2,3,4)$, $\hat{H}(\mathbf{k},\mathbf{Q})$ can be diagonalized as

$$\Psi^{\dagger}\hat{H}(\mathbf{k},\mathbf{Q})\Psi = \Psi^{\dagger}UU^{\dagger}\hat{H}(\mathbf{k},\mathbf{Q})UU^{\dagger}\Phi = \Phi^{\dagger}\begin{pmatrix} E_{\mathbf{k}1} & & & \\ & E_{\mathbf{k}2} & & \\ & & E_{\mathbf{k}3} & \\ & & & E_{\mathbf{k}4} \end{pmatrix}\Phi. \quad (4.43)$$

The eigen-function Φ is obtained as

$$\Phi \equiv U^{\dagger}\Psi = \begin{pmatrix} c_1 \\ c_2 \\ c_3 \\ c_4 \end{pmatrix}, \quad (4.44)$$

$$\Phi^{\dagger} \equiv \Psi^{\dagger}U = [\ c_1^{\dagger}\ c_2^{\dagger}\ c_3^{\dagger}\ c_4^{\dagger}\ ].$$

From eqs. (4.44) $a_{\mathbf{k}\uparrow}^{\dagger}$ etc. are expressed as

$$\begin{aligned}
a_{\mathbf{k}\uparrow}^{\dagger} &= \sum_{\mu=1}^{4} U_{1\mu}^{*}c_{\mu}^{\dagger}, \quad a_{\mathbf{k}\uparrow} = \sum_{\mu=1}^{4} U_{1\mu}c_{\mu}, \\
b_{\mathbf{k}\uparrow}^{\dagger} &= \sum_{\mu=1}^{4} U_{2\mu}^{*}c_{\mu}^{\dagger}, \quad a_{\mathbf{k}\uparrow} = \sum_{\mu=1}^{4} U_{2\mu}c_{\mu}, \\
a_{\mathbf{k}+\mathbf{Q}\downarrow}^{\dagger} &= \sum_{\mu=1}^{4} U_{3\mu}^{*}c_{\mu}^{\dagger}, \quad a_{\mathbf{k}+\mathbf{Q}\downarrow} = \sum_{\mu=1}^{4} U_{3\mu}c_{\mu}, \\
b_{\mathbf{k}+\mathbf{Q}\downarrow}^{\dagger} &= \sum_{\mu=1}^{4} U_{4\mu}^{*}c_{\mu}^{\dagger}, \quad b_{\mathbf{k}+\mathbf{Q}\downarrow} = \sum_{\mu=1}^{4} U_{4\mu}c_{\mu}.
\end{aligned} \quad (4.45)$$

With the use of eqs.(4.45), $A_{\mathbf{Q}}^{+}$, $B_{\mathbf{Q}}^{+}$, $A_{-\mathbf{Q}}^{-}$ and $B_{-\mathbf{Q}}^{-}$ can be written as

$$A_{\mathbf{Q}}^{+} = \frac{1}{N}\sum_{\mathbf{k}}\sum_{\mu,\nu=1}^{4} U_{1\mu}^{*}U_{3\nu}\langle c_{\mu}^{\dagger}c_{\nu}\rangle = \frac{1}{N}\sum_{\mathbf{k}\mu=1}^{4} U_{1\mu}^{*}U_{3\mu}f(E_{\mathbf{k}\mu}),$$

$$B_Q^+ = \frac{1}{N}\sum_k \sum_{\mu,\nu=1}^{4} U_{2\mu}^* U_{4\nu} \langle c_\mu^\dagger c_\nu \rangle = \frac{1}{N}\sum_{k\mu=1}^{4} U_{2\mu}^* U_{4\mu} f(E_{k\mu}),$$

$$A_{-Q}^- = \frac{1}{N}\sum_k \sum_{\mu,\nu=1}^{4} U_{1\mu} U_{3\nu}^* \langle c_\mu^\dagger c_\nu \rangle = \frac{1}{N}\sum_{k\mu=1}^{4} U_{1\mu} U_{3\mu}^* f(E_{k\mu}), \qquad (4.46)$$

$$B_{-Q}^- = \frac{1}{N}\sum_{k\mu,\nu=1}^{4} U_{2\mu} U_{4\nu}^* \langle c_\mu^\dagger c_\nu \rangle = \frac{1}{N}\sum_{k\mu=1}^{4} U_{2\mu} U_{4\mu}^* f(E_{k\mu}),$$

where $f(E_{k\mu})$ denotes the Fermi distribution function. From these eqs.(4.46), we can determine A_Q^+, B_Q^+, A_{-Q}^- and B_{-Q}^- self-consistently as functions of the temperature.

In order to obtain the most stable helical SDW state, we calculate the total electronic energy of the SDW system as a function of Q. This energy is expressed as

$$E_{SDW} = \sum_{k\mu=1}^{4} E_{k\mu} f(E_{k\mu}) + \frac{NUn^2}{2} + NU(|A_Q^+|^2 + |B_Q^+|^2). \qquad (4.47)$$

The second and the third terms of the right hand side of eq. (4.47) denote a correction of interaction energy contained in one electron energy, $E_{k\mu}$. On the other hand the total electronic energy of paramagnetic phase is obtained from eq.(4.19) as

$$E_{para} = \sum_{k\sigma} [E_k^\alpha f(E_k^\alpha) + E_k^\beta f(E_k^\beta)] - \frac{NUn^2}{2}. \qquad (4.48)$$

If we set $A_Q^+ = B_Q^+ = A_{-Q}^- = B_{-Q}^- = 0$ in eq.(4.47), E_{SDW} becomes equal to E_{para}. A_Q^+ and B_Q^+ determined self-consistently represent the Fourier components of the spin densities which are modulated by the wave vector Q on the A- and B- sublattices, respectively. Phase angle ϕ_{12} between moments of a- and b-atoms in the same

unit cell is obtained by the following relation:

$$\frac{\langle s_b^+ \rangle}{\langle s_a^+ \rangle} = \frac{B_Q^+}{A_Q^+} e^{-iQ\cdot\tau} = e^{i\phi_{12}}. \qquad (4.49)$$

4.2.3(b) Results and discussion

We have calculated E_{SDW} given by eq.(4.47) for zero temperature. For the parameters t_1, t_2, t_3 and n, the same values as used in §4.2.2 have been adopted. E_{SDW} calculated as a function of U for various Q is shown in Fig.4-8(a). For each Q, if $U < U_c$, where U_c has the same value with that given by eq. (4.34b) , E_{SDW} becomes equal to E_{para} because A_Q^+, B_Q^+ etc. do not have self-consistent solutions of finite values, except zero. In Fig.4-8(b) we show E_{SDW} calculated as a function of Q for $U/|t_1| = 6$ and 8, respectively. From the results shown in Fig.4-8(a) and (b), it has been found that the lowest value of E_{SDW} is obtained for $Q=0.4\times(2\pi/c)$. This fact means that the most stable helical SDW state is realized for $Q=0.4\times(2\pi/c)$. This conclusion is consistent with the result obtained from the paramagnetic instability studied in §4.2.2. Next, ϕ_{12} given by eq. (4.49) is calculated as a function of Q and the result is shown in Fig.4-8(c). The Q-dependence of ϕ_{12} is similar to that shown in Fig.4-7(b). For $Q=0.4\times(2\pi/c)$, ϕ_{12} becomes about 153^0.

$|A_Q^+|$, which is determined self-consistently, is plotted in Fig.4-8(d) as a function of U for various Q. If we take

$U/|t_1|=4.5$, the amplitude of SDW, $|A_Q^+|$, becomes about 0.25 for $Q=0.4\times(2\pi/c)$. This value corresponds to the observed moment 0.5 μ_B/Fe, since the magnetic moment per an atom equals $2|A_Q|$.

Other MnP-type compounds FeP[36], CrAs[37] and MnP[38] show also double helical magnetic ordering with propagation vector along the c-axis. All these magnetic ordering would be explained on the basis of similar argument to that described in §4.2.

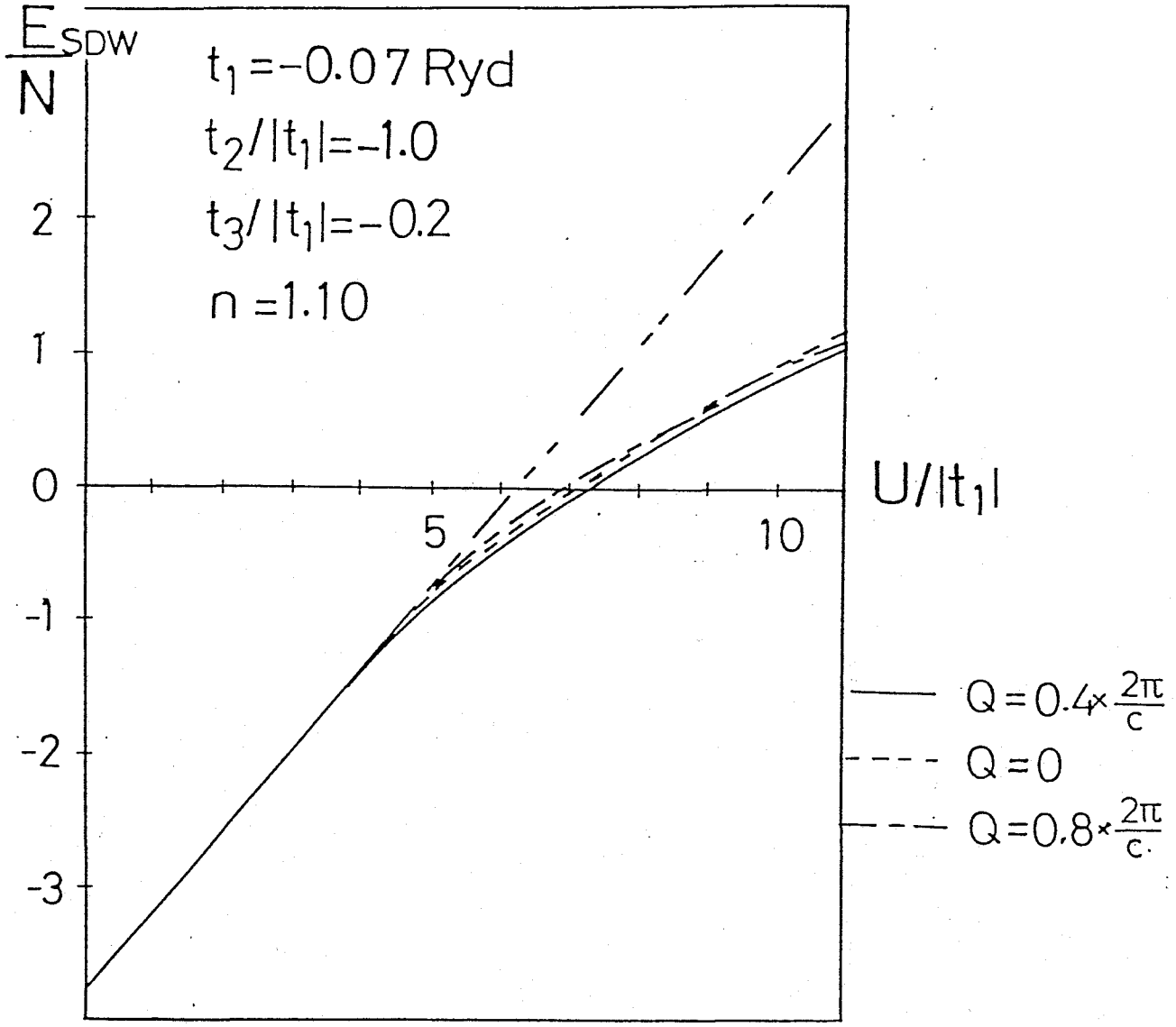

Fig.4-8(a). E_{SDW} as functions of U for some values of wave vectors Q. The double-dot-dashed line (——·——) denotes E_{para}.

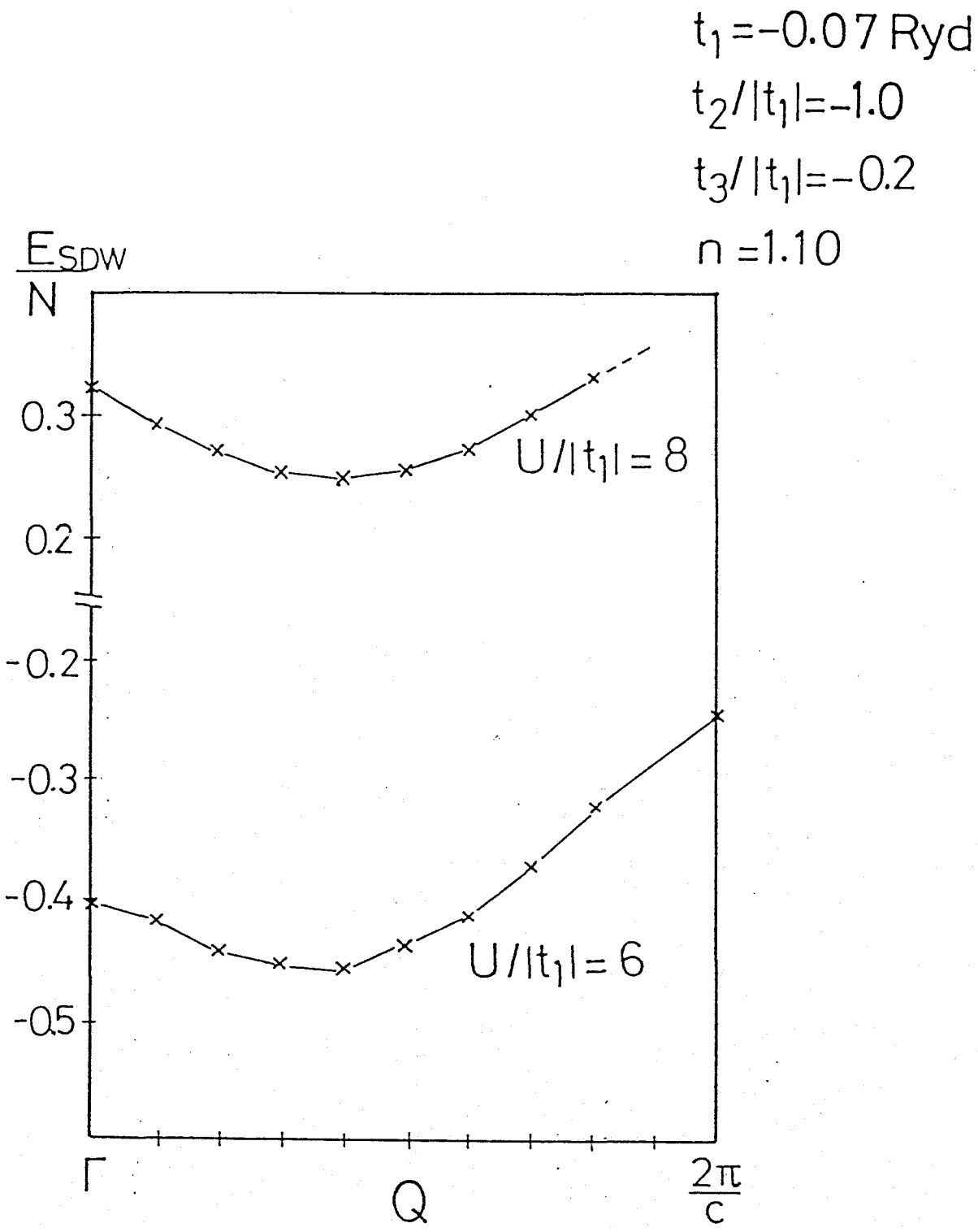

Fig.4-8(b). E_{SDW} for $U/|t_1|$ = 6 and 8 as functions of Q.

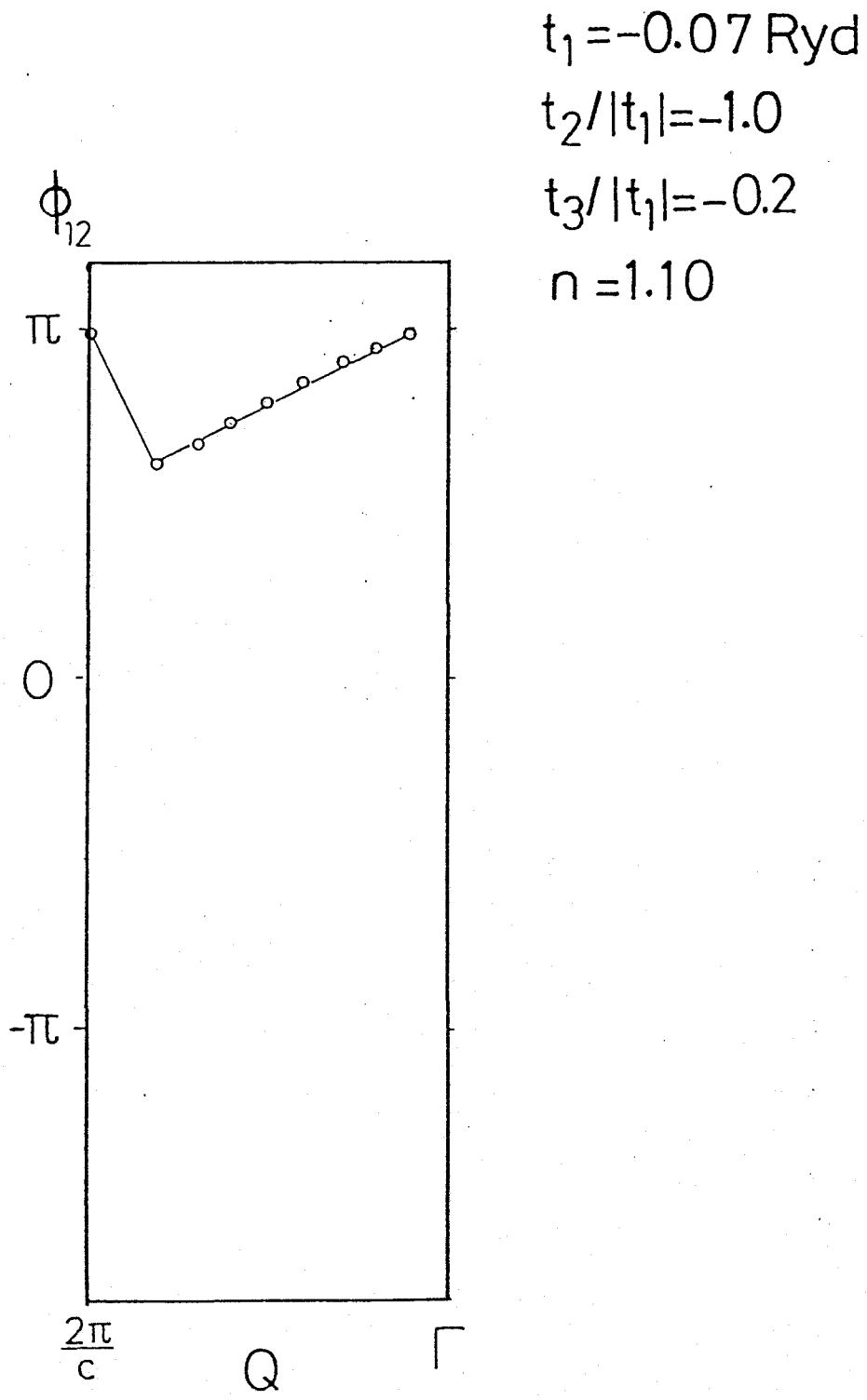

Fig.4-8(c). ϕ_{12} (defined by eq.(4.49)) as a function of Q.

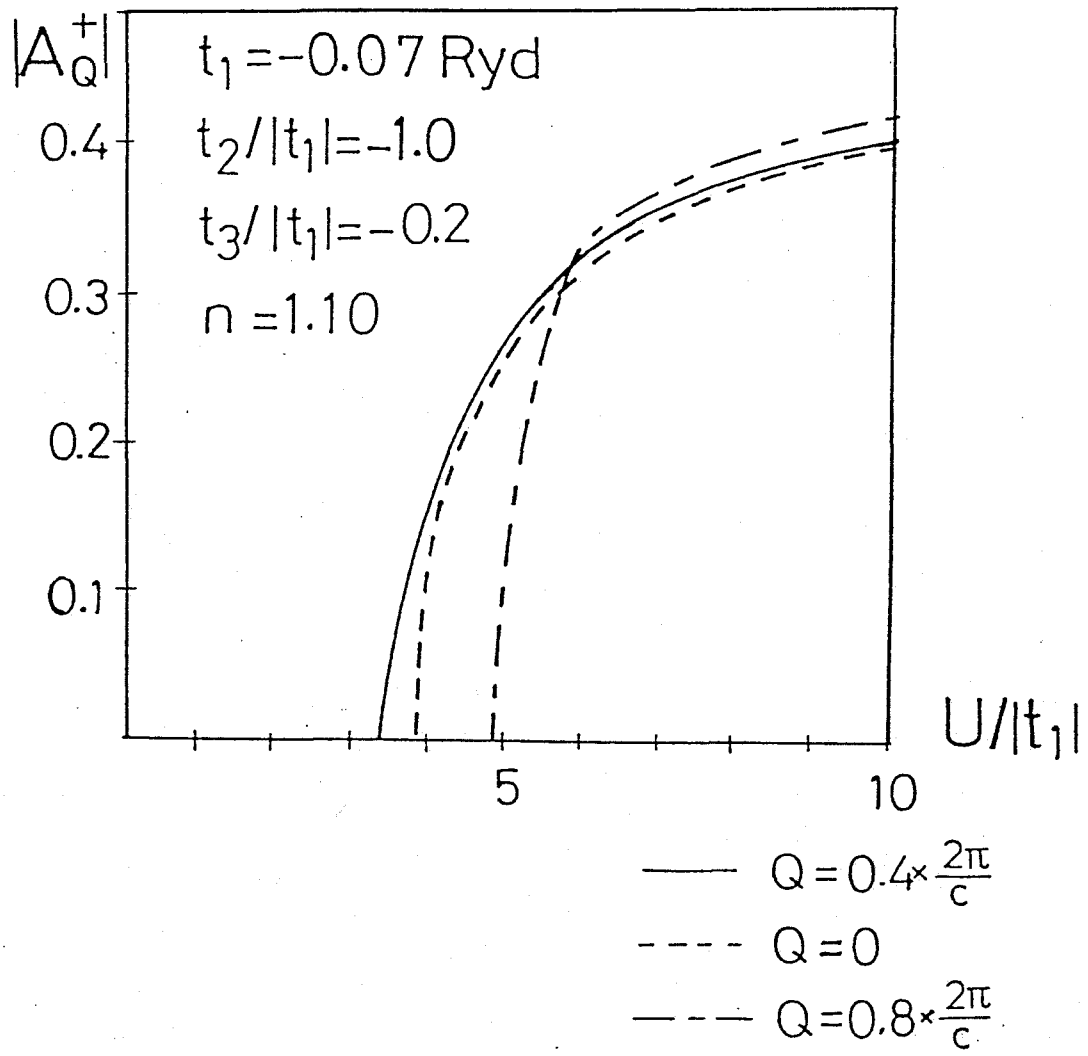

Fig.4-8(d). $|A_Q^+|$ for some values of Q as functions of $U/|t_1|$.

References

1) K.Selte and A.Kjekshus, Acta Chem. Scand.27 (1973) 3195

2) T.Suzuki and H.Ido, J. Phys. Soc. Jpn. 51 (1982) 3149

3) K.Selte, A.Kjekshus, G.Valde and A.F.Andresen, Acta Chem. Scand.A30 (1976) 468

4) K.Selte, A.Kjekshus and A.F.Andresen, Acta Chem. Scand. 26 (1972) 3101

5) F.Hulliger, Structure and Bonding(Berlin) 4 (1968) 83

6) A.Kjekshus and K.P.Walseth, Acta Chem. Scand.23(1969)2621

7) R.Podloucky, J. Phys. F14 (1984) L145

8) K.Motizuki, K.Katoh and A.Yanase, J. Phys. C19 (1986) 495

9) K.Katoh and K.Motizuki, J. Phys. Soc. Jpn. 56 (1987) 655

10) W.Reimers, E.Hellner, W.Treutmann and G.Heger, J. Phys. C15 (1982) 3597

11) K.Yamaguchi, H.Watanabe, H.Yamamoto and Y.Yamaguchi, J. Phys. Soc. Jpn. 31 (1971) 1042

12) H.Boller and A.Kallel, Solid State Comm. 9 (1971) 1699

13) K.Selte, A.Kjekshus and A.F.Andresen, Acta Chem.Scand. A28 (1974) 61

14) K.Selte, A.Kjekshus, G.Valde and A.F.Andresen, Acta Chem.Scand. A30 (1976) 8

15) K.Selte and A.Kjekshus, Acta Chem. Scand. 25 (1971) 3277

16) I.Delphin, K.Selte, A.Kjekshus and A.F.Andresen, Acta Chem. Scand. A32 (1978) 179

17) T.L.Loucks, Augmented Plane Wave Metod (Benjamin, New York, 1967)

18) P.S.Lyman and C.T.Prewitt, Acta Cryst. B40 (1984) 14

19) D.D.Koeling and B.N.Harmon,J. Phys. C10 (1977) 3107

20) O.Gunnarsson and B.I.Lundqvist, Phys.Rev. B13 (1976) 4274

21) O.Jepsen and O.K.Anderson, Solid State Comm. 9 (1971)1763

22) G.Lehmann and M.Taut, Phys.stat.sol.(b)54 (1972) 469

23) R.W.Godby, G.A.Benesh, R.Haydock and V.Heine, Phys.Rev.B32 (1985) 655

24) N.Suzuki, T.Yamasaki and K.Motizuki, J. Phys.C21(1988)6133

25) V.Jaccarino, G.K.Wertheim, J.H.Wernick, L.R.Walker and S.Arajs, Phys. Rev.160 (1967) 476

26) Y.Takahashi and T.Moriya, J. Phys. Soc. Jpn. 46 (1979)1451

27) K.Tajima, Y.Endoh, J.E.Fischer and G.Shirane, Phys. Rev. B38 (1988) 6954

28) O.Nakanishi, A.Yanase and A.Hasegawa, J. Magn. Magn. Mater. 15-18 (1980) 879

29) K.Motizuki, J. Magn. Magn. Mater. 70 (1987) 1

30) T.Moriya and Y.Takahashi, J. Phys. Soc. Jpn. 45 (1978) 397

31) W.E.Evenson, J.R.Schrieffer and S.Q.Wang, J. Appl. Phys. 41 (1970) 1199

32) T.Moriya, Spin Fluctuations in Itinerant Electron Magnetism (Springer, Verlin, 1985) pp.157-193

33) T.Moriya, J. Phys. Soc. Jpn. 51 (1982) 420

34) D.Penn, Phys. Rev. 142 (1966) 350

35) H.Ohnishi,K.Katoh and K.Motizuki, J.Magn. Magn. Mater. 31-34 (1983) 55

36) G.P.Felcher, F.A.Smith, D.Bellavance and A.Wold, Phys. Rev.B3 (1971) 3046

37) H.Watanabe, N.Kazama, Y.Yamaguchi and M.Ohashi, J. Appl. Phys. 40 (1969) 1128

38) G.P.Felcher, J.Appl. Phys. 37 (1966) 1056

Appendix A Lattice dynamics of a NiAs-type compound

We have calculated phonon frequencies of NiAs-type CoAs within the rigid ion model and the harmonic approximation assuming short range forces between some neighboring atoms. Long range Coulomb interaction between distant atoms is neglected as it is considered to be small because of screening effect of conduction electrons.

Accompanied with displacements of atoms, crystal potential is expanded within the 2nd order of the displacements as

$$V = V_0 + \sum_{\ell\nu\alpha} \left.\frac{\partial V}{\partial u^{\alpha}_{\ell\nu}}\right|_0 u^{\alpha}_{\ell\nu} + \frac{1}{2}\sum_{\ell\nu\alpha}\sum_{\ell'\nu'\beta} \left.\frac{\partial^2 V}{\partial u^{\alpha}_{\ell\nu}\partial u^{\beta}_{\ell'\nu'}}\right|_0 u^{\alpha}_{\ell\nu} u^{\beta}_{\ell'\nu'} , \tag{A.1}$$

where $u^{\alpha}_{\ell\nu}$ denotes the displacement in the α-direction of the νth atom in the ℓth unit cell. Derivatives in eq.(A.1) mean the values at the equilibrium points and the 1st derivatives at the equilibrium points are zero. The Lagrangian of the system is written as

$$= \sum_{\ell\nu\alpha} \frac{M_\nu}{2} \dot{u}^{\alpha 2}_{\ell\nu} - V_0 - \frac{1}{2}\sum_{\ell\nu\alpha}\sum_{\ell'\nu'\beta} \phi^{\alpha\beta}_{\ell\nu\ell'\nu'} u^{\alpha}_{\ell\nu} u^{\beta}_{\ell'\nu'} , \tag{A.2}$$

where M_ν is mass of the νth atom and we have defined as

$$\phi^{\alpha\beta}_{\ell\nu\ell'\nu'} = \left.\frac{\partial^2 V}{\partial u^{\alpha}_{\ell\nu}\partial u^{\beta}_{\ell'\nu'}}\right|_0 . \tag{A.3}$$

By using eq.(A.2) the equation of motion is obtained as

$$M_\nu \ddot{u}^\alpha_{\ell\nu} = -\sum_{\ell'\nu'\beta} \phi^{\alpha\beta}_{\ell\nu\ell'\nu'} u^\beta_{\ell'\nu'}. \qquad (A.4)$$

The equation of motion given by eq.(A.4) can be solved by using the Fourier transformation. We express the displacement of an atom as

$$u^\alpha_{\ell\nu} = = \frac{1}{\sqrt{NM_\nu}} \sum_{q\lambda} Q_{q\lambda}\, \varepsilon^\alpha_{q\lambda}(\nu) e^{-i(q\cdot R_\ell - \omega_q t)} \qquad (A.5)$$

where $Q_{q\lambda}$ is the normal coordinate of a phonon with wave vector q and mode λ, $\varepsilon^\alpha_{q\lambda}(\nu)$ is a polarization vector and ω_q denotes a phonon frequency. Substituting eq.(A.5) into eq.(A.4), we obtain

$$\omega_q^2 \varepsilon^\alpha_{q\lambda}(\nu) = \sum_{\ell'\nu'\beta} \frac{\phi^{\alpha\beta}_{\ell\nu\ell'\nu'}}{\sqrt{M_\nu M_{\nu'}}} \varepsilon^\beta_{q\lambda}(\nu') e^{iq\cdot(R_\ell - R_{\ell'})}. \qquad (A.6)$$

Here we define a dynamical matrix as

$$D^{\alpha\beta}_q(\nu,\nu') = \sum_{\ell'\nu'\beta} \frac{\phi^{\alpha\beta}_{\ell\nu\ell'\nu'}}{\sqrt{M_\nu M_{\nu'}}} e^{iq\cdot(R_\ell - R_{\ell'})}. \qquad (A.7)$$

Using eqs.(A.6) and (A.7), phonon frequencies and polarization vectors are obtained as eigen-values and eigen-vectors of the dynamical matrix.

The parameter $\phi^{\alpha\beta}_{\ell\nu\ell'\nu'}$ is a force in the α-direction acting on the νth atom in the ℓth unit cell due to a displacement in the β-direction of the ν'th atom in the ℓ'th unit cell. We have treated these forces between atom a and atom b as follows:

We assume that $\phi^{\alpha\beta}_{ab}$ depends only on relative distance between

two atoms $r=|r_a-r_b|$. In this approximation $\phi_{ab}^{\alpha\beta}$ is written as

$$\phi_{ab}^{\alpha\beta} = -[(\delta_{\alpha\beta} - \frac{r_\alpha r_\beta}{r^2})\phi_{ab}^{t} + r_\alpha r_\beta \phi_{ab}^{\ell}] \ , \qquad (A.8)$$

where r_α denotes α-component of the vector r_a-r_b and

$$\phi_{ab}^{t} = \frac{1}{r}\frac{dV}{dr} \ , \quad \phi_{ab}^{\ell} = \frac{1}{r^2}\frac{d^2V}{dr^2} \qquad (A.9)$$

We take x'-axis parallel to r_a-r_b, and take y'- and z'-axes perpendicular to the x'-axis. The force which acts on atom b , F_b^α (α=x',y',z') , due to displacement of atom a , u_a^α, can be expressed as

$$\begin{pmatrix} F_b^{x'} \\ F_b^{y'} \\ F_b^{z'} \end{pmatrix} = \begin{pmatrix} -\phi_{ab}^{\ell} & 0 & 0 \\ 0 & -\phi_{ab}^{t} & 0 \\ 0 & 0 & -\phi_{ab}^{t} \end{pmatrix} \begin{pmatrix} u_a^{x'} \\ u_a^{y'} \\ u_a^{z'} \end{pmatrix} \ , \qquad (A.10)$$

where suffices ℓ and t denote longitudinal and transverse, respectively. We have taken into account four kinds of force constants between neighboring atoms (shown in Fig.A-1) as follows:

ϕ_{13} : the nearest neighboring Co-As,

ϕ_{11} : Co-Co neighboring in the c-plane,

ϕ_{33} : As-As neighboring in the c-plane,

ϕ_{12} : Co-Co neghboring along the c-axis ,

The values of force constants used in the calculation are as follows:

$$\phi_{11}^{\ell} = 2.0 \ , \quad \phi_{11}^{t} = 0.20 \ ,$$
$$\phi_{12}^{\ell} = 4.0 \ , \quad \phi_{12}^{t} = 0.40 \ ,$$

$$\phi^{\ell}_{33} = 2.0 \quad , \quad \phi^{t}_{33} = 0.20 \quad ,$$
$$\phi^{\ell}_{13} = 12.0 \quad , \quad \phi^{t}_{13} = 1.20 \quad . \qquad 10^4 \text{ dyn/cm}$$

The transverse components of the force constants are assumed to be 1/10 of the longitudinal components.

Calculated phonon dispersion curves along the symmetry lines and density of states are shown in Fig.A-2 and A-3, respectively. The Density of states is calculated using phonon frequencies at 60 points in 1/24 Brillouin zone. As shown in Fig.A-3 the phonon density of states is divided into two parts: 0- 290 cm^{-1} and 290 - 400 cm^{-1}. Although the oscillation of Co and that of As hybridize each other, the lower energy part mainly consists of the oscillation of As and the upper energy part mainly consists of that of Co. Phonon frequencies of the M_4^- mode, by which the MnP-type distortion is described, are 166.3, 291.1 and 394.7 cm^{-1}. We expect that these M_4^- phonon frequencies will be soft due to the electron-lattice interaction.

In order to fit the calculated phonon frequencies to experimental result, we show here an analytical expression of the dynamical matrix at the Γ point. The dynamical matrix at the Γ point is written as

$$
\begin{array}{c}
\begin{array}{cccccccccccc}
x_1 & y_1 & z_1 & x_2 & y_2 & z_2 & x_3 & y_3 & z_3 & x_4 & y_4 & z_4
\end{array} \\
\left(\begin{array}{cccccccccccc}
a & 0 & 0 & \alpha & 0 & 0 & \gamma & 0 & 0 & \gamma & 0 & 0 \\
0 & a & 0 & 0 & \alpha & 0 & 0 & \gamma & 0 & 0 & \gamma & 0 \\
0 & 0 & b & 0 & 0 & \beta & 0 & 0 & \delta & 0 & 0 & \delta \\
\alpha & 0 & 0 & a & 0 & 0 & \gamma & 0 & 0 & \gamma & 0 & 0 \\
0 & \alpha & 0 & 0 & a & 0 & 0 & \gamma & 0 & 0 & \gamma & 0 \\
0 & 0 & \beta & 0 & 0 & b & 0 & 0 & \delta & 0 & 0 & \delta \\
\gamma & 0 & 0 & \gamma & 0 & 0 & c & 0 & 0 & 0 & 0 & 0 \\
0 & \gamma & 0 & 0 & \gamma & 0 & 0 & c & 0 & 0 & 0 & 0 \\
0 & 0 & \delta & 0 & 0 & \delta & 0 & 0 & d & 0 & 0 & 0 \\
\gamma & 0 & 0 & \gamma & 0 & 0 & 0 & 0 & 0 & c & 0 & 0 \\
0 & \gamma & 0 & 0 & \gamma & 0 & 0 & 0 & 0 & 0 & c & 0 \\
0 & 0 & \delta & 0 & 0 & \delta & 0 & 0 & 0 & 0 & 0 & d
\end{array}\right),
\end{array}
\tag{A.11}
$$

where x_1 denotes a displacement in the x-direction of atom 1 (1, 2: Co and 3, 4: As) and so on.

$$
a = \frac{1}{M_1}[2\phi_{12}^t + 3\{\phi_{13}^\ell \cos^2\theta + \phi_{13}^t(1+\sin^2\theta)\}] ,
$$

$$
b = \frac{2}{M_1}[\phi_{12}^\ell + 3\phi_{13}^\ell \sin^2\theta + 3\phi_{13}^t \cos^2\theta)] ,
$$

$$
c = \frac{3}{M_2}[\phi_{13}^\ell \cos^2\theta + \phi_{13}^t(1+\sin^2\theta)] ,
$$

$$
d = \frac{6}{M_2}[\phi_{13}^\ell \sin^2\theta + 3\phi_{13}^t \cos^2\theta)\}] ,
$$

$$
\alpha = -\frac{2\phi_{12}^t}{\sqrt{M_1 M_2}} , \qquad \beta = -\frac{2\phi_{12}^\ell}{\sqrt{M_1 M_2}} ,
$$

$$
\gamma = -\frac{3}{2\sqrt{M_1 M_2}}[\phi_{13}^\ell \cos^2\theta + \phi_{13}^t(1+\sin^2\theta)\}] ,
\tag{A.12}
$$

$$\delta = -\frac{3}{\sqrt{M_1 M_2}}\left[\phi_{13}^{\ell}\sin^2\theta + \phi_{13}^{t}\cos^2\theta)\}\right] ,$$

M_1 and M_2 denote mass of a Co atom and an As atom, and

$$\theta = \tan^{-1}\left[\frac{\sqrt{3}c}{4a}\right] \quad (a,c: \text{lattice constants}).$$

By using the unitary transformation to the normal mode shown in Table A-1, the dynamical matrix given by eq.(A.11) is written as

$$\begin{array}{c} \Gamma_2^- \quad \Gamma_4^- \; \Gamma_3^+ \quad \Gamma_6^- \quad \Gamma_6^- \quad \Gamma_5^+ \; \Gamma_5^+ \; \Gamma_5^- \; \Gamma_5^- \\ \left(\begin{array}{cccccccccc} b+\beta & 2\delta & & & & & & & & \\ 2\delta & d & & & & & & & & \\ & & b-\beta & & & & & & & \\ & & & d & & & & & & \\ & & & & a+\alpha & 2\gamma & & & & \\ & & & & 2\gamma & c & & & & \\ & & & & & & a+\alpha & 2\gamma & & \\ & & & & & & 2\gamma & c & & \\ & & & & & & & & c & \\ & & & & & & & & & c \\ & & & & & & & & & & a-\alpha \\ & & & & & & & & & & & a-\alpha \end{array}\right) , \end{array} \qquad (A.13)$$

Using eqs.(A.12) and (A.13) the phonon frequencies at the Γ point are given by

$$\begin{aligned} \omega^2(\Gamma_2^-) &= 0, \; b+d+\beta , \\ \omega^2(\Gamma_4^-) &= b-\beta , \\ \omega^2(\Gamma_3^+) &= d , \\ \omega^2(\Gamma_6^-) &= 0, \; a+c+\alpha , \\ \omega^2(\Gamma_5^+) &= c , \\ \omega^2(\Gamma_5^-) &= a-\alpha . \end{aligned} \qquad (A.14)$$

Table A-1 Phonon normal modes at high symmetry points

$\Gamma = 2\Gamma_2^- + \Gamma_4^- + \Gamma_3^+ + \Gamma_5^+ + 2\Gamma_6^- + \Gamma_5^-$

$\Gamma_2^- : c_1(z_1+z_2) + c_2(z_3+z_4)$

$\Gamma_4^- : (z_1-z_2)/\sqrt{2}$

$\Gamma_3^+ : (z_3-z_4)/\sqrt{2}$

$\Gamma_5^+ : c_1(x_3-x_4)+c_2(y_3-y_4)$

$\Gamma_6^- : c_1(x_1+x_2)+c_2(x_3+x_4)\ ,\ c_1(y_1+y_2)+c_2(y_3+y_4)$

$\Gamma_5^- : c_1(x_1-x_2)+c_2(y_1-y_2)$

$M = M_1^+ + M_1^- + M_4^+ + M_3^+ + 3M_4^- + 3M_2^- + 2M_3^-$

$M_1^+ : (x_3+x_4)/\sqrt{2}$

$M_1^- : (y_1-y_2)/\sqrt{2}$

$M_4^+ : (y_3+y_4)/\sqrt{2}$

$M_3^+ : (z_3+z_4)/\sqrt{2}$

$M_4^- : c_1(x_1-x_2) + c_2(z_1+z_2) + c_3(z_3-z_4)$

$M_2^- : c_1(x_1+x_2) + c_2(z_1-z_2) + c_3(x_3-x_4)$

$M_3^- : c_1(y_1+y_2) + c_2(y_3-y_4)$

$K = K_1 + 2K_3 + K_4 + 4K_5 + 4K_6$

$K_1 : (x_3+iy_3)/2 - \omega^2(x_4-iy_4)/2$

$K_3 : c_1(z_1-z_2) + c_2[(x_3+iy_3)+\omega^2(x_4-iy_4)]$

$K_4 : (z_1+z_2)/\sqrt{2}$

$K_5 : c_1(x_1+x_2) + c_2(y_1+y_2) + c_3(x_3-iy_3) + c_4(x_4-iy_4)$

$K_6 : c_1(x_1-x_2) + c_2(y_1-y_2) + c_3z_3 + c_4z_4$

$\omega = e^{2\pi i/3}$

$$A = 2A_1 + 4A_3$$

$$A_1 : c_1(z_1+z_2) + c_2(z_3+z_4)$$

$$c_1(z_1-z_2) + c_2(z_3-z_4)$$

$$A_2 : c_1(x_1+x_2) + c_2(x_3+x_4)$$

$$c_1(y_1+y_2) + c_2(y_3+x_4)$$

$$c_1(x_1-x_2) + c_2(x_3-x_4)$$

$$c_1(y_1-y_2) + c_2(y_3-y_4)$$

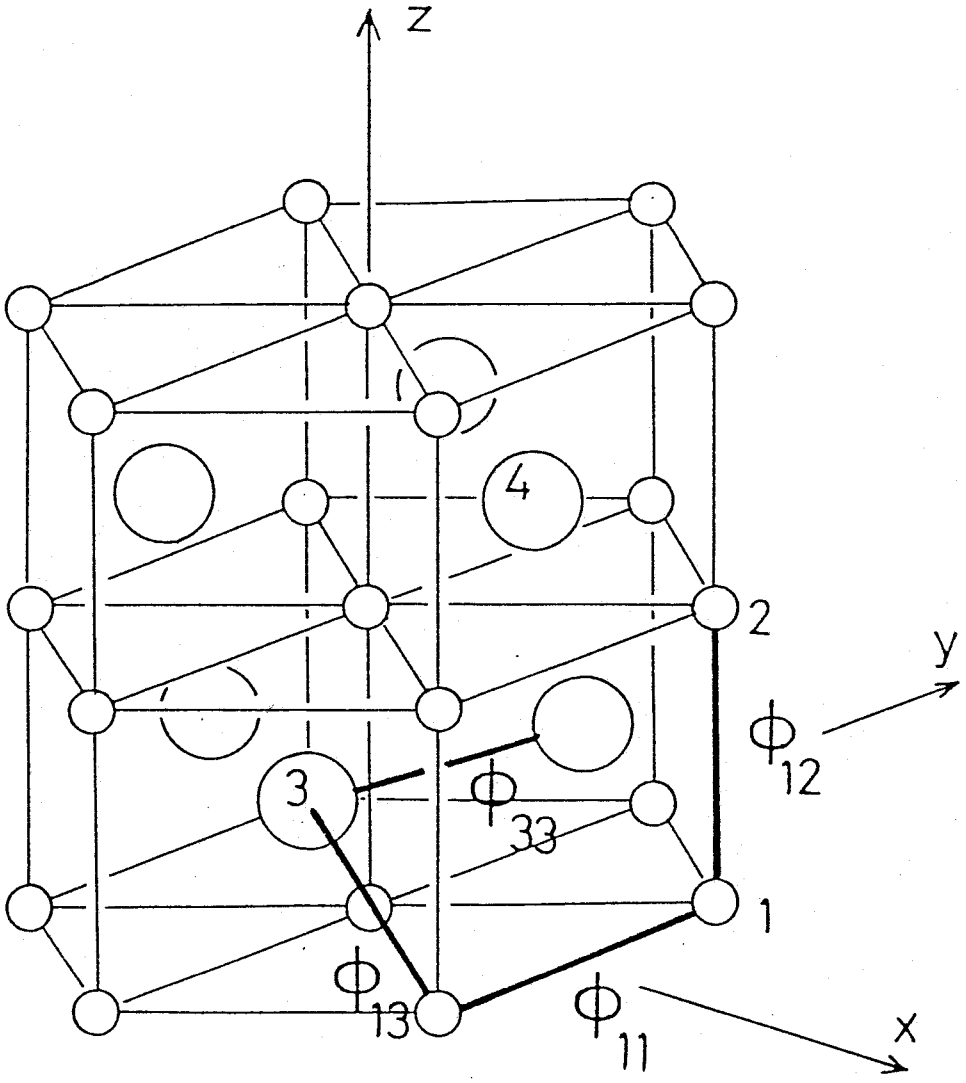

Fig.A-1. Neighboring pairs of atoms and the short range forces.

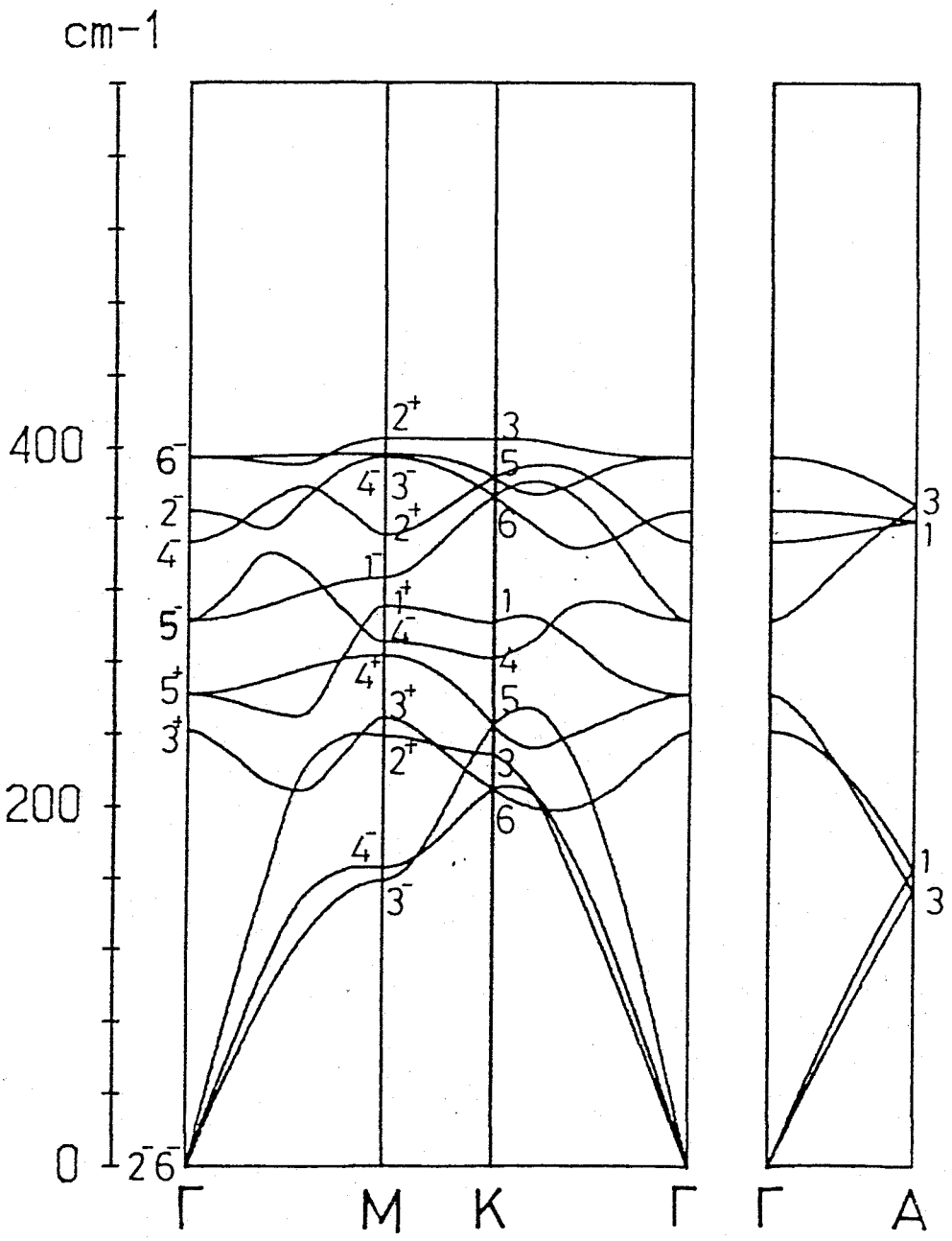

Fig.A-2. Phonon dispersion curves of CoAs (NiAs-type).

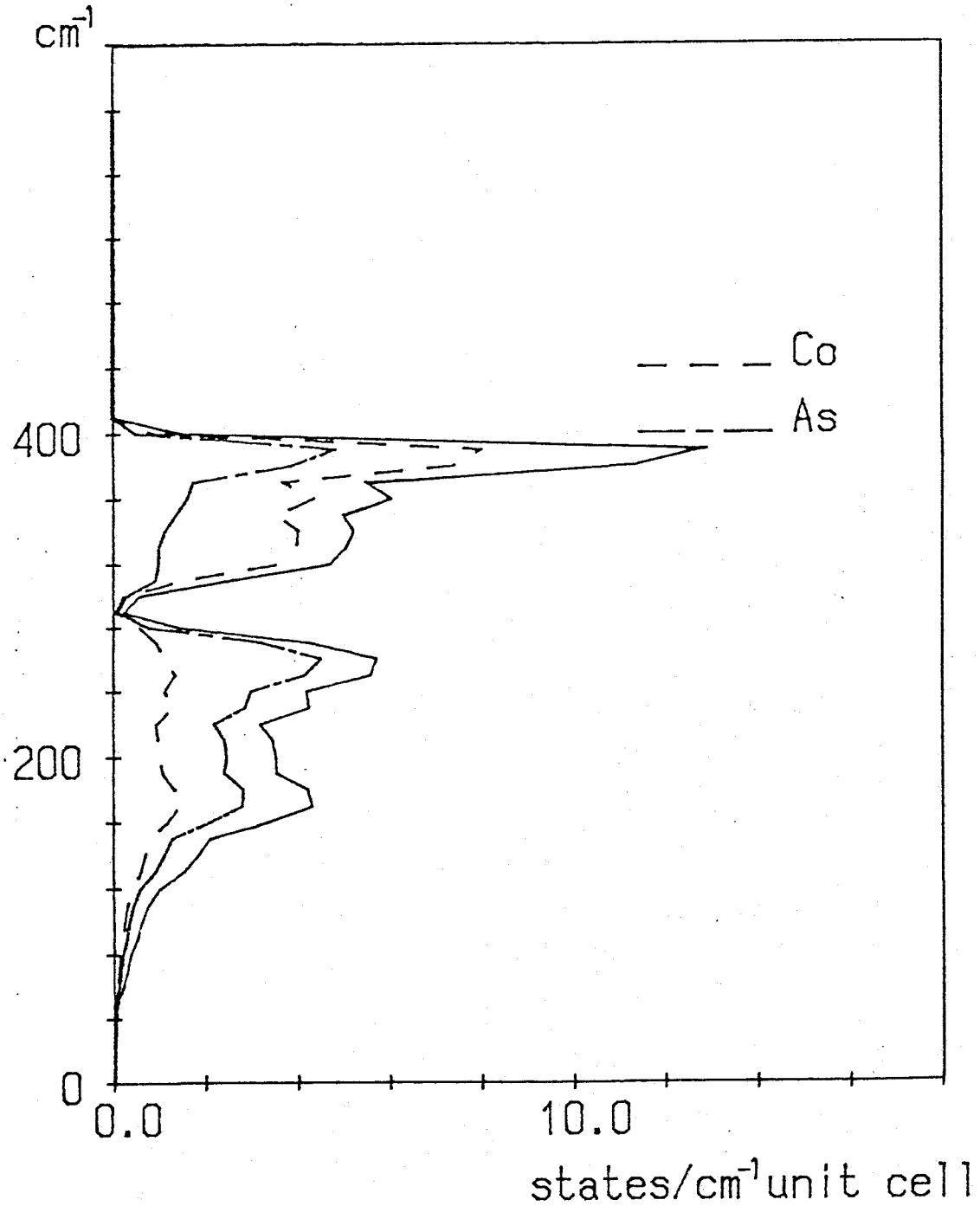

Fig.A-3. Phonon density of states of CoAs (NiAs-type).

Appendix B Derivation of the self-consistent equations for the paramagnetic susceptibility

We summarize a derivation of the self-consistent equations given by eqs.(4.7) to obtain the paramagnetic susceptibility. By using the Stratonovich-Hubbard transformation, the many-body problem can be transformed into an one-body problem under randomly fluctuating fields. $e^{-\beta\Delta F}$ given by eq.(4.5c) is written as

$$e^{-\beta\Delta F} = \int \prod_j \delta\xi_j \int \prod_j \delta\eta_j \exp\{-\frac{\pi}{\beta}\sum_j \int_0^\beta d\tau [(\xi_j(\tau)-h_0/\bar{c})^2+\eta_j(\tau)^2]-\beta\psi[\xi,\eta]\}, \tag{B.1a}$$

where

$$e^{-\beta\psi[\xi,\eta]} = <T_\tau \exp\{(\pi UT)^{1/2}\sum_j \int d\tau [\xi_j(\tau)(n_{j\uparrow}(\tau)-n_{j\downarrow}(\tau)) + i\eta_j(\tau)(n_{j\uparrow}(\tau)+n_{j\downarrow}(\tau))]\}> , \tag{B.1b}$$

$\bar{c} = (4\pi UT)^{1/2}$ and $h_0=(0,0,h_0)$.

$\xi_j(\tau)$ and $\eta_j(\tau)$ are time varying fields acting on the spin and the charge densities of the jth site, respectively. Using eq. (4.4) and (B.1), magnetization in the direction of h_0 is obtained as

$$M = \frac{1}{\beta}\frac{\partial \ell ogZ}{\partial h_0} = (\frac{N\pi T}{U})^{1/2}[\xi^z_{00} - (\frac{N}{4\pi UT})^{1/2}h_0], \tag{B.2}$$

where N is number of atoms. ξ_{qm} is the Fourier component of

$\xi_j(\tau)$ defined by

$$\xi_{qm}=\frac{1}{\sqrt{N}\beta}\sum_j\int_0^\beta d\tau\ e^{i(q\cdot r_j+\omega_m\tau)}\xi_j(\tau) \qquad (B.3)$$

$\omega_m=2\pi mT$ (m: integer).

Using eq.(B.2) the paramagnetic susceptibility, χ, is obtained as

$$\chi = \frac{\partial M}{\partial h_0} =(N\pi T/U)^{1/2}\frac{\partial \xi_{00}^z}{\partial h_0} - \frac{N}{2U} \qquad (B.4)$$

Since ξ_{00} is a macroscopic quantity, we can replace ξ_{00} by the value at the saddle point as follows:

$$2\pi T(\xi_{00}^z - \frac{\sqrt{N}h_0}{\bar{c}}) + <\frac{\partial\psi}{\partial\xi_{00}^z}>= 0. \qquad (B.5)$$

Taking the derivative of eq.(B.5) with respect ξ_{00}^z, we obtain

$$\frac{\partial h_0}{\partial \xi_{00}^z} = (4\pi UT/N)^{1/2}(1+\frac{1}{2\pi T}\frac{\partial}{\partial\xi_{00}^z}<\frac{\partial\psi}{\partial\xi_{00}^z}>). \qquad (B.6)$$

Substituting eq.(B.6) into eq.(B.4), χ is obtained in the form as

$$\chi = \frac{1}{2I}\frac{1}{1+\frac{1}{2\pi T}\frac{\partial}{\partial\xi_{00}^z}<\frac{\partial\psi}{\partial\xi_{00}^z}>} - \frac{1}{2I}, \qquad (B.7)$$

where $I=U/N$.

A model functional for $\psi[\xi,\eta]$, which describes the spin-fluctuations in both an itinerant system and a localized-spin system, is introduced. We set $h_0=0$ and replace η_j by the value at the saddle point. The model functional is as follows :

$$\psi[\xi] = -2\pi UT \sum_{qm} X_{qm}(\xi_{qm}\cdot\xi_{-q-m}) + \pi NL(x)$$

$$= -2\pi UT \sum_{ij} X_{ij}(\xi_i\cdot\xi_j) + \pi NL(x) \quad , \tag{B.8}$$

$$x = \frac{T}{N}\sum_{qm} \xi_{qm}\cdot\xi_{-q-m} \tag{B.9a}$$

$$\pi NL(x) = -T \sum_{\sigma=\pm 1}\int_{-\infty}^{\infty} d\varepsilon\ \rho(\varepsilon)\log[1+e^{-\beta(\varepsilon-\sigma B)}], \tag{B.9b}$$

$$B=(\pi Ux)^{1/2} \quad ,$$

$$X_{ii}=0 \text{ or } \sum_{q} X_{qm}=0 \quad , \tag{B.9c}$$

where $\rho(\varepsilon)$ denotes the density of states. The first and the second terms of the model functional given by eq.(B.8) represent non-local and local parts, respectively. x is the average square amplitude of the local field and it is related to the average square amplitude of the local spin density as follows :

$$\langle s_j^2\rangle = \frac{\pi}{U}(x - \frac{3T}{2\pi}) \tag{B.10}$$

Substituting eq.(B.8) into eq.(B.1a) we obtain

$$e^{-\beta\Delta F} = \int \prod_q d\xi_q \exp[-\pi\{\sum_{qm} \xi_{qm}\cdot\xi_{-q-m} - 2U\sum_{qm} X_{qm}(\xi_{qm}\cdot\xi_{-q-m}) + N\beta L(x)\}]$$

$$\times \int dx\,\delta(\sum_{qm} \xi_{qm}\cdot\xi_{-q-m} - \beta Nx)$$

$$= \int \prod_q d\xi_q \exp[-\pi\{\sum_{qm} \xi_{qm}\cdot\xi_{-q-m} - 2U\sum_{qm} X_{qm}(\xi_{qm}\cdot\xi_{-q-m}) + N\beta L(x)\}]$$

$$\times iU\int dx\int d\lambda\ \exp\{-2\pi U\lambda(\sum_{qm}\xi_{qm}\cdot\xi_{qm}-\beta Nx)$$

$$=iU\int dx\int d\lambda\ \exp\{-\pi[N\beta x+N\beta L(x)-2UN\beta x]\} \qquad (B.11)$$

$$\times\int\prod_{q}d\xi_{qm}\ \exp\{-2\pi U\sum_{qm}(\lambda-X_{qm})\xi_{qm}\cdot\xi_{-q-m}\}.$$

Integration over ξ_{qm} can be performed analytically as

$$e^{-\beta\Delta F}=iU\int dx\int d\lambda\exp\{-N\pi\beta[(1-2U\lambda)x+L(x)]-\frac{3}{2}\sum_{qm}\log[2U(\lambda-X_{qm})]\}. \qquad (B.12)$$

In the evaluation of the integral over x and λ by the saddle point method, we obtain following two relations :

$$(1-2U\lambda)+\frac{\partial L(x)}{\partial x}=0\ . \qquad (B.13)$$

$$2\pi UN\beta x=\sum_{qm}\frac{3}{2(\lambda-X_{qm})}\ . \qquad (B.14)$$

We have neglected x-dependence of X_{qm}. Using eqs.(B.13) and (B.14), x is written as

$$x=\frac{3T}{2\pi N}\sum_{qm}\frac{1}{1-2U(X_{qm}-\frac{1}{2U}\frac{\partial L}{\partial x})}=\frac{3T}{2\pi N}\sum_{qm}\frac{1}{1-2I\bar{X}_{qm}}\ . \qquad (B.15)$$

For the last term of eq.(B.15), we have defined as

$$\bar{X}_{qm}=NX_{qm}-\frac{1}{2I}\frac{\partial L}{\partial x}\ . \qquad (B.16)$$

Using eq.(B.8) and (B.16), we obtain the following relation :

$$\frac{\partial}{\partial \xi^z_{00}} \left\langle \frac{\partial \psi}{\partial \xi^z_{00}} \right\rangle = -4\pi TU\left(X_{00} + \frac{\partial L}{\partial x}\right) = -4\pi TI\ \bar{\chi}_{00}. \tag{B.17}$$

Substituting eq.(B.17) into eq.(B.7), we get the expression of the paramagnetic susceptibility given by

$$\chi = \frac{\bar{\chi}_{00}}{1-2I\bar{\chi}_{00}} . \tag{B.18}$$

Taking sum with respect q in eq.(B.16) and using the relation given by eq.(B.9c), we obtain

$$\frac{1}{N}\sum_q \bar{\chi}_{qm} = -\frac{1}{2I}\frac{\partial L}{\partial x} \quad \text{or} \quad NX_{qm} = \bar{\chi}_{qm} - \frac{1}{N}\sum_q \bar{\chi}_{qm} . \tag{B.19}$$

Solving eqs.(B.15), (B.16), (B.18) and (B.19) self-consistently, we can calculate the paramagnetic susceptibility.

Appendix C Derivation of $\bar{\chi}(q\omega)$

We derive eq.(4.29), the expression of the wave number and frequency dependent inverse magneic susceptibility of a system with a number of atoms in unit cell. We consider only one orbital for each atom. We start from following Hubbard Hamiltonian :

$$H = \sum_{\mu}\sum_{ij\sigma} t_{\mu}(a^{\dagger}_{i\mu\sigma}a_{j\mu\sigma}+a^{\dagger}_{j\mu\sigma}a_{i\mu\sigma}) + \sum_{\mu\nu ij\sigma}\hat{t}_{\mu\nu}(a^{\dagger}_{i\mu\sigma}a_{j\nu\sigma}+ a^{\dagger}_{j\nu\sigma}a_{i\mu\sigma})$$

$$+ \sum_{\mu}\sum_{i}\sum_{\sigma} V_{\mu}a^{\dagger}_{i\mu\sigma}a_{i\mu\sigma} + \sum_{\mu}\sum_{i} U_{\mu}n^{\mu}_{i\uparrow}n^{\mu}_{i\downarrow} , \qquad (C.1)$$

where $a_{i\mu\sigma}(a^{\dagger}_{i\mu\sigma})$ is an annihilation (creation) operator with spin σ at the μth atom in the ith unit cell, $n^{\mu}_{j\sigma}$ is the number operator, t_{μ} and $\hat{t}_{\mu\nu}$ denote transfer integrals of intra-sublattice and inter-sublattice, respectively, V_{μ} is an atomic-site energy of μth atom and U_{μ} is an intra-atomic Coulomb integral of μth atom. Using the Fourier transformation and the Hartree-Fock approximation eq.(C.1) is written as

$$H = \sum_{\mu}\sum_{\mathbf{k}\sigma} T_{\mu}(\mathbf{k})a^{\dagger}_{\mu\mathbf{k}\sigma}a_{\mu\mathbf{k}\sigma} + \sum_{\mu\nu}[\hat{T}_{\mu\nu}(\mathbf{k})a^{\dagger}_{\mu\mathbf{k}\sigma}a_{\nu\mathbf{k}\sigma}+ \hat{T}^{*}_{\mu\nu}(\mathbf{k})a^{\dagger}_{\nu\mathbf{k}\sigma}a_{\mu\mathbf{k}\sigma}]$$

$$+\sum_{\mu}\sum_{\mathbf{k}\mathbf{q}'}\sum_{\sigma} U_{\mu}A^{\mu}_{\mathbf{q}'-\sigma}a^{\dagger}_{\mu\mathbf{k}+\mathbf{q}'\sigma}a_{\mu\mathbf{k}\sigma} - N\sum_{\mu}\sum_{\mathbf{q}'} U_{\mu}A^{\mu}_{\mathbf{q}'\uparrow}A^{\mu}_{\mathbf{q}'\downarrow} , \qquad (C.2)$$

where

$$T_{\mu}(\mathbf{k}) = \sum_{j}[t_{\mu}e^{i\mathbf{k}\cdot(\mathbf{r}_j-\mathbf{r}_i)}] + V_{\mu} , \qquad (C.3a)$$

$$\hat{T}_{\mu\nu}(k)=\sum_j \hat{t}_{\mu\nu} e^{ik\cdot(r_j-r_i)-ik\cdot(\tau_\nu-\tau_\mu)} , \qquad (C.3b)$$

$$A^{\mu}_{q\sigma} = \frac{1}{N}\langle \sum_k a^{\dagger}_{\mu k\sigma} a_{\mu k+q\sigma}\rangle . \qquad (C.3c)$$

In a paramagnetic phase only terms of q'=0 in eq.(C.2) are non-vanishing and the Hamiltonian becomes

$$H_{para}=\sum_\mu \sum_{k\sigma} T_\mu(k) a^{\dagger}_{\mu k\sigma} a_{\mu k\sigma} + \sum_{\mu\nu} [\hat{T}_{\mu\nu}(k) a^{\dagger}_{\mu k\sigma} a_{\nu k\sigma} + \hat{T}^{*}_{\mu\nu}(k) a^{\dagger}_{\nu k\sigma} a_{\mu k\sigma}]$$

$$+\sum_\mu \sum_k \sum_\sigma U_\mu A^{\mu}_{O-\sigma} a^{\dagger}_{\mu k\sigma} a_{\mu k\sigma} - N\sum_\mu U_\mu A^{\mu}_{O\uparrow} A^{\mu}_{O\downarrow} , \qquad (C.4)$$

When the magnetic field $H^{\mu}(q\omega)$ is applied on the μth atom in the unit cell, the Hamiltonian of the Zeeman interaction is written as

$$H' = \sum_\mu \sum_k (a^{\dagger}_{\mu k\uparrow} a_{\mu k-q\uparrow} - a^{\dagger}_{\mu k\downarrow} a_{\mu k-q\downarrow}) \mu_B I^{\mu}_{-q} H^{\mu}(q\omega) , \qquad (C.5)$$

It is convenient to transform the Hamiltonian given by eqs. (C.2) and (C.5) with a unitary matrix $U_k(\mu,n)$ by which H_{para} is diagonalized. We express an operator $a_{\mu k\sigma}$ as a linear combination of new operators $\alpha_{nk\sigma}$ as

$$a_{\mu k\sigma} = \sum_n U_k(\mu,n)\alpha_{nk\sigma} , \qquad (C.6)$$

where n is the band suffix. Using eq.(C.6), eqs.(C.2) and (C.5) are written as

$$H = \sum_n \sum_{k\sigma} E^{n}_{k} \alpha^{\dagger}_{nk\sigma}\alpha_{nk\sigma} \qquad (C.7a)$$

$$+\sum_\mu \sum_{k\sigma} U_\mu A^{\mu}_{q-\sigma} [\sum_{nn'} U^{*}_{k+q}(\mu,n) U_k(\mu,n')] \alpha^{\dagger}_{nk+q\sigma}\alpha_{n'k\sigma} - N\sum_\mu U_\mu A^{\mu}_{q\uparrow} A^{\mu}_{-q\downarrow} ,$$

$$H' = \sum_{\mu k} \Big[\sum_{nn'} U^{*}_{k}(\mu,n) U_{k-q}(\mu,n') \Big] (\alpha^{\dagger}_{nk\uparrow} \alpha_{n'k-q\uparrow} - \alpha^{\dagger}_{nk\downarrow} \alpha_{n'k-q\downarrow}) \mu_B I^{\mu}_{-q} H^{\mu}(q\omega), \tag{C.7b}$$

where E^{n}_{k} is the eigen value of H_{para}. In eq.(C.7a) we have kept only terms of q'=q non-vanishing. Using eq.(C.6) we obtain

$$\langle a^{\dagger}_{\mu k\sigma} a_{\mu k+q\sigma} \rangle = \sum_{nn'} [U^{*}_{k}(\mu,n) U_{k+q}(\mu,n')] \langle \alpha^{\dagger}_{nk\sigma} \alpha_{n'k+q\sigma} \rangle , \tag{C.8}$$

The equation of motion for $\langle \alpha^{\dagger}_{nk\sigma} \alpha_{n'k+q\sigma} \rangle$ is obtained as

$$\begin{aligned} i \frac{\partial}{\partial t} \langle \alpha^{\dagger}_{nk\sigma} \alpha_{n'k+q\sigma} \rangle &= \langle [\alpha^{\dagger}_{nk\sigma} \alpha_{n'k+q\sigma} , H + H'] \rangle \\ &= (E^{n'}_{k+q} - E^{n}_{k}) \langle \alpha^{\dagger}_{nk\sigma} \alpha_{n'k+q\sigma} \rangle \\ &\quad + \sum_{\mu} [U_{\mu} A^{\mu}_{q-\sigma} + \sigma \mu_B I^{\mu}_{-q} H^{\mu}(q\omega)] U^{*}_{k+q}(\mu,n') U_{k}(\mu,n) \\ &\quad \times \langle \alpha^{\dagger}_{nk\sigma} \alpha_{nk\sigma} - \alpha^{\dagger}_{n'k+q\sigma} \alpha_{n'k+q\sigma} \rangle . \end{aligned} \tag{C.9}$$

We consider that $H^{\mu}(q\omega)$ (and also $\langle \alpha^{\dagger}_{nk\sigma} \alpha_{n'k+q\sigma} \rangle$) depends on time as $e^{-i\omega t}$. Eq.(C.9) is written as

$$\langle \alpha^{\dagger}_{nk\sigma} \alpha_{n'k+q\sigma} \rangle = \chi_0^{nn'}(kq\omega) \Big[\sum_{\mu'} U^{*}_{k+q}(\mu',n') U_{k}(\mu',n) \{ U_{\mu'} A_{q-\sigma} + \sigma \mu_B I^{\mu'}_{-q} H^{\mu'}(q\omega) \} \Big], \tag{C.10}$$

where

$$\chi_0^{nn'}(kq\omega) = \frac{f(E^{n}_{k}) - f(E^{n'}_{k+q})}{E^{n}_{k} - E^{n'}_{k+q} - \omega} . \tag{C.11}$$

Substituting eq.(C.10) into eq.(C.8) we obtain

$$\langle a^{\dagger}_{\mu k\sigma} a_{\mu' k+q\sigma} \rangle = \sum_{nn'\mu'} U^{*}_{k}(\mu,n) U_{k+q}(\mu,n') U^{*}_{k+q}(\mu',n') U_{k}(\mu',n)$$
$$\times \chi_0^{nn'}(kq\omega)[\, U_{\mu'}, A^{\mu'}_{q-\sigma} + \sigma\mu_B I^{\mu'}_{-q} H^{\mu'}(q\omega)]. \tag{C.12}$$

We define here

$$\Gamma^{\mu\mu'}(kq\omega) = \sum_{nn'} U^{*}_{k}(\mu,n) U_{k+q}(\mu,n') U^{*}_{k+q}(\mu',n') U_{k}(\mu',n) \chi_0^{nn'}(kq\omega), \tag{C.13a}$$

$$\Gamma^{\mu\mu'}(q\omega) = \sum_{k} \Gamma^{\mu\mu'}(kq\omega) \ . \tag{C.13b}$$

Using eqs.(C.12) and (C.13), eq.(C.3c) is written as

$$A^{\mu}_{q\uparrow} = \sum_{\mu'} \Gamma^{\mu\mu'}(q\omega)[\, U_{\mu'}, A^{\mu'}_{q\downarrow} + \mu_B I^{\mu'}_{-q} H^{\mu'}(q\omega)], \tag{C.14a}$$

$$A^{\mu}_{q\downarrow} = \sum_{\mu'} \Gamma^{\mu\mu'}(q\omega)[\, U_{\mu'}, A^{\mu'}_{q\uparrow} - \mu_B I^{\mu'}_{-q} H^{\mu'}(q\omega)]. \tag{C.14b}$$

The wave number and frequency dependent magnetization on the μth atom is defined as

$$M^{\mu}(q\omega) = \mu_B I^{\mu}_{q} (A^{\mu}_{q\downarrow} - A^{\mu}_{q\uparrow}). \tag{C.15}$$

Using eqs.(C.14) and (C.15) we can express the relation between magnetic fields and magnetizations induced by the magnetic fields as

$$-\sum_{\mu'} [\frac{I^{\mu}_{q}}{I^{\mu}_{q}} U_{\mu'}, \Gamma^{\mu\mu'}(q\omega) + \delta_{\mu\mu'},] M^{\mu'}(q\omega) = 2\sum_{\mu'} \mu_B^2 I^{\mu}_{q} I^{\mu'}_{-q} \Gamma^{\mu\mu'}(q\omega) H^{\mu'}(q\omega). \tag{C.16}$$

From now on we consider the case of §4.4.2 when unit cell contains two same kind atoms. We express (μ,μ') as (a,b) and

(n,n') as (α,β) and we set $U_a=U_b=U$ and $I_q^a=I_q^b=I_q$. In this case eq.(C.16) is written as

$$-\begin{pmatrix} 1+U\Gamma_1 & U\Gamma_2^* \\ U\Gamma_2 & 1+U\Gamma_1 \end{pmatrix}\begin{pmatrix} M^a(q\omega) \\ M^b(q\omega) \end{pmatrix} = 2|I_q|^2\mu_B^2\begin{pmatrix} \Gamma_1 & \Gamma_2^* \\ \Gamma_2 & \Gamma_1 \end{pmatrix}\begin{pmatrix} H^a(q\omega) \\ H^b(q\omega) \end{pmatrix}. \quad (C.17)$$

We expressed as $\Gamma_1=\Gamma^{aa}(q\omega)=\Gamma^{bb}(q\omega)$ and $\Gamma_2=\Gamma^{ba}(q\omega)=\Gamma^{ab*}(q\omega)$ in eq.(C.17). Using eq.(C.17), the inverse susceptibility $\bar{\chi}(q\omega)$ is written as

$$\begin{pmatrix} H^a(q\omega) \\ H^b(q\omega) \end{pmatrix} = -\frac{1}{2\mu_B^2|I_q|^2}\begin{pmatrix} \Gamma_1 & \Gamma_2^* \\ \Gamma_2 & \Gamma_1 \end{pmatrix}^{-1}\begin{pmatrix} 1+U\Gamma_1 & U\Gamma_2^* \\ U\Gamma_1 & 1+U\Gamma_1 \end{pmatrix}\begin{pmatrix} M^a(q\omega) \\ M^b(q\omega) \end{pmatrix}$$

$$= -\frac{1}{2\mu_B^2|I_q|^2}\begin{pmatrix} \dfrac{\Gamma_1+U[\Gamma_1^2-|\Gamma_2|^2]}{\Delta} & \dfrac{\Gamma_2^*}{\Delta} \\ \dfrac{\Gamma_2}{\Delta} & \dfrac{\Gamma_1+U[\Gamma_1^2-|\Gamma_2|^2]}{\Delta} \end{pmatrix}\begin{pmatrix} M^a(q\omega) \\ M^b(q\omega) \end{pmatrix}$$

$$= \begin{pmatrix} \bar{\chi}^{aa} & \bar{\chi}^{ab} \\ \bar{\chi}^{ba} & \bar{\chi}^{bb} \end{pmatrix}\begin{pmatrix} M^a(q\omega) \\ M^b(q\omega) \end{pmatrix}$$

$$\equiv \bar{\chi}(q\omega)\begin{pmatrix} M^a(q\omega) \\ M^b(q\omega) \end{pmatrix}, \quad (C.18)$$

where

$$\Delta = \Gamma_1^2 - |\Gamma_2|^2 . \quad (C.19)$$

In the case of §4.2.2, as shown in eq. (4.18) the unitary matrix U_k is

$$U_k = \frac{1}{[2|T_1(k)|]^{1/2}} \begin{pmatrix} T_1(k)^{1/2} & -T_1(k)^{1/2} \\ T_1(k)^{*1/2} & T_1(k)^{*1/2} \end{pmatrix} . \qquad (C.20)$$

Substituting eq.(C.20) into eq.(C.13), we obtain the expression of Γ_1 and Γ_2 as

$$\Gamma_1(q\omega) = \sum_k \frac{1}{4} [\, \chi_0^{\alpha\alpha}(kq\omega) + \chi_0^{\beta\beta}(kq\omega) + \chi_0^{\alpha\beta}(kq\omega) + \chi_0^{\beta\alpha}(kq\omega)] \,, \qquad (C.21)$$

$$\Gamma_2(q\omega) = \sum_k \frac{T_1(k+q)^* T_1(k)}{4|T_1(k+q)||T_1(k)|} [\chi_0^{\alpha\alpha}(kq\omega) + \chi_0^{\beta\beta}(kq\omega) - \chi_0^{\alpha\beta}(kq\omega) - \chi_0^{\beta\alpha}(kq\omega)],$$

Appendix D Various types of ferro- and antiferro-magnetic ordering

By using the instability theory discussed in §4.2.2, we discuss on the special cases of Q, in which Q is given by 0 or G/2 (G is one of the reciprocal lattice vectors). As shown in eq.(4.39), to determine ϕ_{12} we must calculate the phase angle of $\Gamma_2(Q)$. $\Gamma_2(Q)$ is expressed as

$$\Gamma_2(Q) = \sum_{k} T_1^*(k+Q)\ T_1(k) \times \xi(k,Q), \tag{D.1}$$

where ξ is defined as

$$\xi(k,Q)= \frac{\chi^{\alpha\alpha}(k,Q)+\chi^{\beta\beta}(k,Q)-\chi^{\alpha\beta}(k,Q)-\chi^{\beta\alpha}(k,Q)}{4N|T_1(k+Q)||T_1(k)|}. \tag{D.2}$$

Here we study, as an example, a two dimensional lattice which consists of two kinds of square lattices as shown in Fig.D-1. Two atoms, 1 and 2, are included in the unit cell. The position of the atom 1 is (0,0) and that of the atom 2 is $\tau=(\tau_a, b/2)$, where τ_a is not a/2. Since, each atom is not in the position having the inversion symmetry, we consider two kinds of transfer integrals t_1 and t_2 between the atom 1 and the atom 2 as shown in Fig.D-1. In this case, $T_1(k)$ defined by eq.(4.16) is written as

$$T_1(k) = 2\ e^{-ik\cdot(\tau-b/2)}\cos(k\cdot b/2)[t_1+t_2e^{ik\cdot a}], \tag{D.3}$$

where a and b are lattice vectors. Thus we can write as

$$T_1^*(k+Q)\ T_1(k) = 4e^{iQ\cdot(\tau-b/2)}\ \cos(k\cdot b/2)\cos[(k+Q)\cdot b/2]$$

$$x\ [t_1^2 + t_2^2\ e^{-iQ\cdot a} + t_1 t_2(e^{ik\cdot a} + e^{-i(k+Q)\cdot a})]. \quad (D.4)$$

From eqs.(D.2) and (D.3), $\Gamma_2(Q)$ can be written as

$$\Gamma_2(Q) = e^{iQ\cdot(\tau-b/2)}A(Q), \quad (D.5)$$

where $A(Q)$ is

$$A(Q) = \sum_k \cos(k\cdot b/2)\cos[(k+Q)\cdot b/2]$$
$$x[t_1^2 + t_2^2\ e^{-iQ\cdot a} + t_1 t_2(e^{ik\cdot a} + e^{-i(k+Q)\cdot a})]\xi(k,Q)\ . \quad (D.6)$$

Inserting eq. (D.5) into eq. (4.39b), ϕ_{12} is written as

$$\phi_{12} = \arg[e^{-iQ\cdot b/2}A(Q)] + \pi\ . \quad (D.7)$$

We consider the following cases:

(i) $Q = 0$ (ferro)

From eq.(D.6) it is found that $A(0)$ is real and ϕ_{12} is given by

$$\phi_{12} = \begin{cases} 0 & (A(0) < 0) \\ \pi & (A(0) > 0). \end{cases} \quad (D.8)$$

(ii) $Q = (0, \pi/b)$ (antiferro along the b-axis)

From eq.(D.6) it is found that $A(Q)$ is real. ϕ_{12} is given by

$$\phi_{12} = \begin{cases} -\pi/2 & (A(Q)<0) \\ \pi/2 & (A(Q)>0). \end{cases} \quad (D.9)$$

(iii) $Q = (\pi/a, 0)$ (antiferro along the a-axis)

In this case A(Q) is written as

$$A(Q) = \sum_{k} \cos^2(k\cdot\tau/2)[t_1^2 - t_2^2 + 2i\, t_1 t_2 \sin(k\cdot a)]\xi(k,Q). \quad (D.10)$$

The imaginary part of A(Q) is zero because $\xi(k,Q)$ is an even function of k and $\sin(k\cdot a)$ is an odd function of k. ϕ_{12} becomes

$$\phi_{12} = \begin{cases} 0 & (A(Q)<0) \\ \pi & (A(Q)>0). \end{cases} \quad (D.11)$$

(iv) $Q=(\pi/a,\pi/b)$ (antiferro along both the a- and b-axes)

In this case A(Q) is expressed as

$$A(Q) = -1/2 \sum_{k} \sin(k\cdot b)[t_1^2 - t_2^2 + 2i\, t_1 t_2 \sin(k\cdot a)]\xi(k,Q). \quad (D.12)$$

In the summation over k of eq.(D.10), terms $k=(k_a,k_b)$ and $k=(-k_a,k_b)$ cancel out each other. Therefore, A(Q) becomes a real number and ϕ_{12} is given by

$$\phi_{12} = \begin{cases} -\pi/2 & (A(Q)<0) \\ \pi/2 & (A(Q)>0). \end{cases} \quad (D.13)$$

The magnetic structures corresponding to the cases (i),(ii),(iii) and (iv) are shown in Fig.D-2(a),(b),(c) and (d), respectively. Thus in the case of Q=0 or 1/2 G (G is a reciprocal lattice vector), complex ferro or antiferromagnetic ordering is expected.

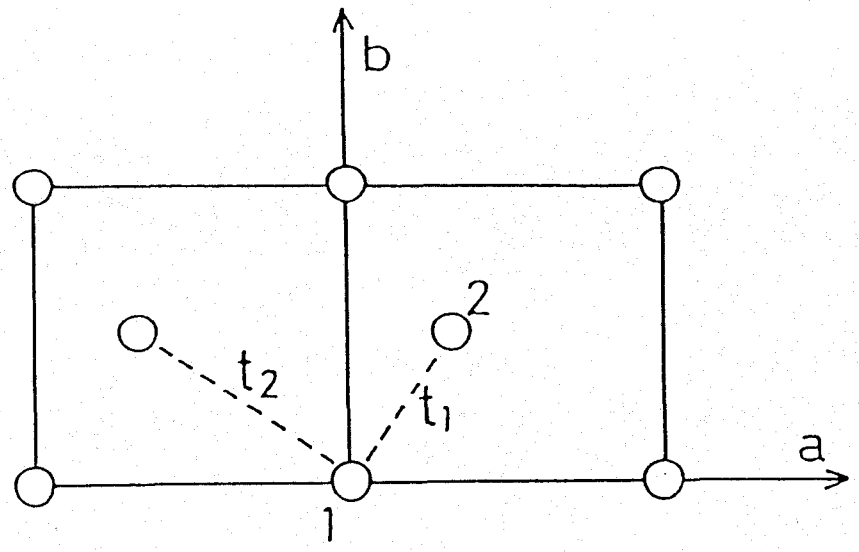

Fig.D-1. A two dimensional lattice with two sublattices.

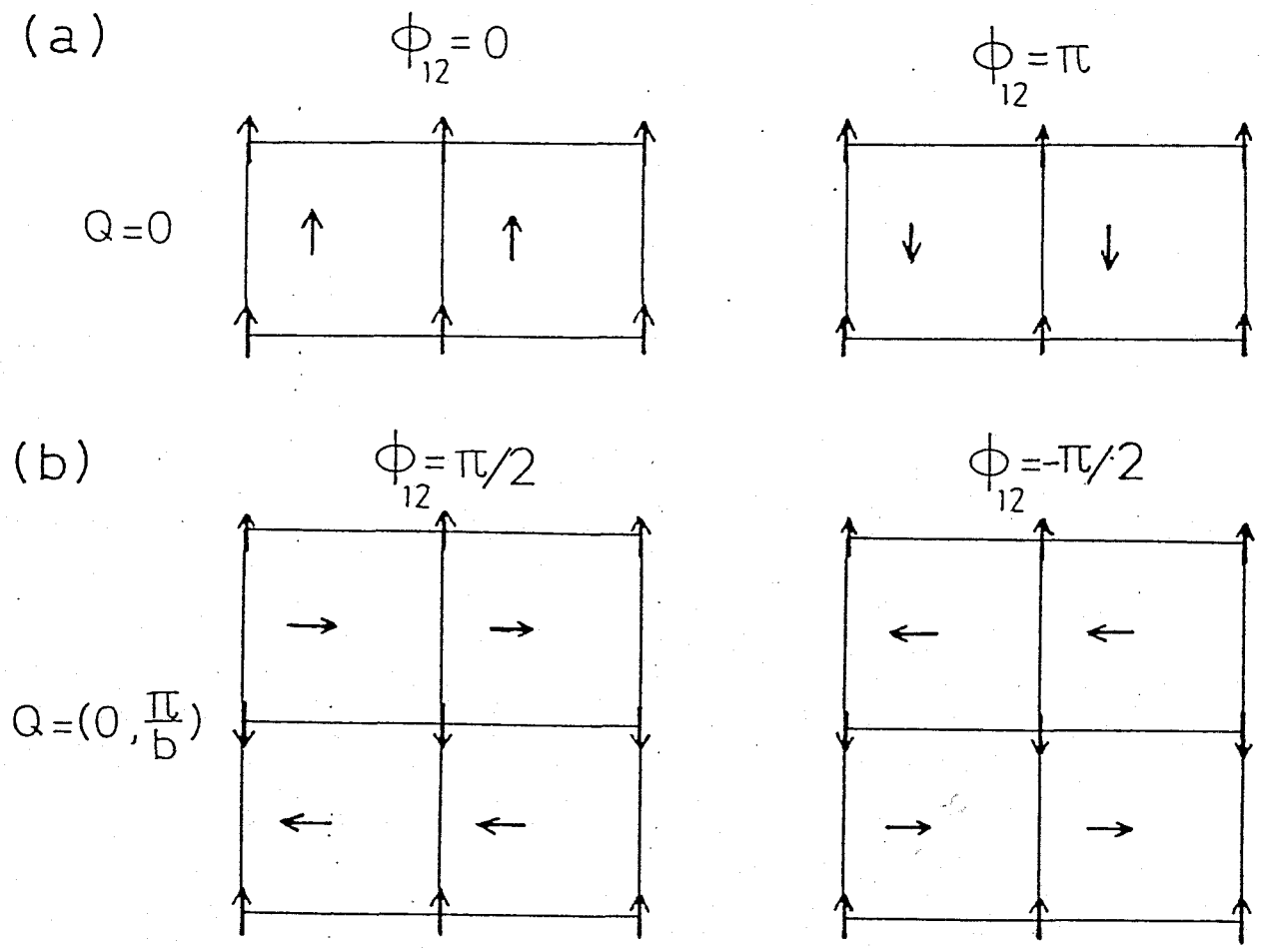

Fig.D-2. Various types of ferro- (a) and antiferro- (b) magnetic ordering.

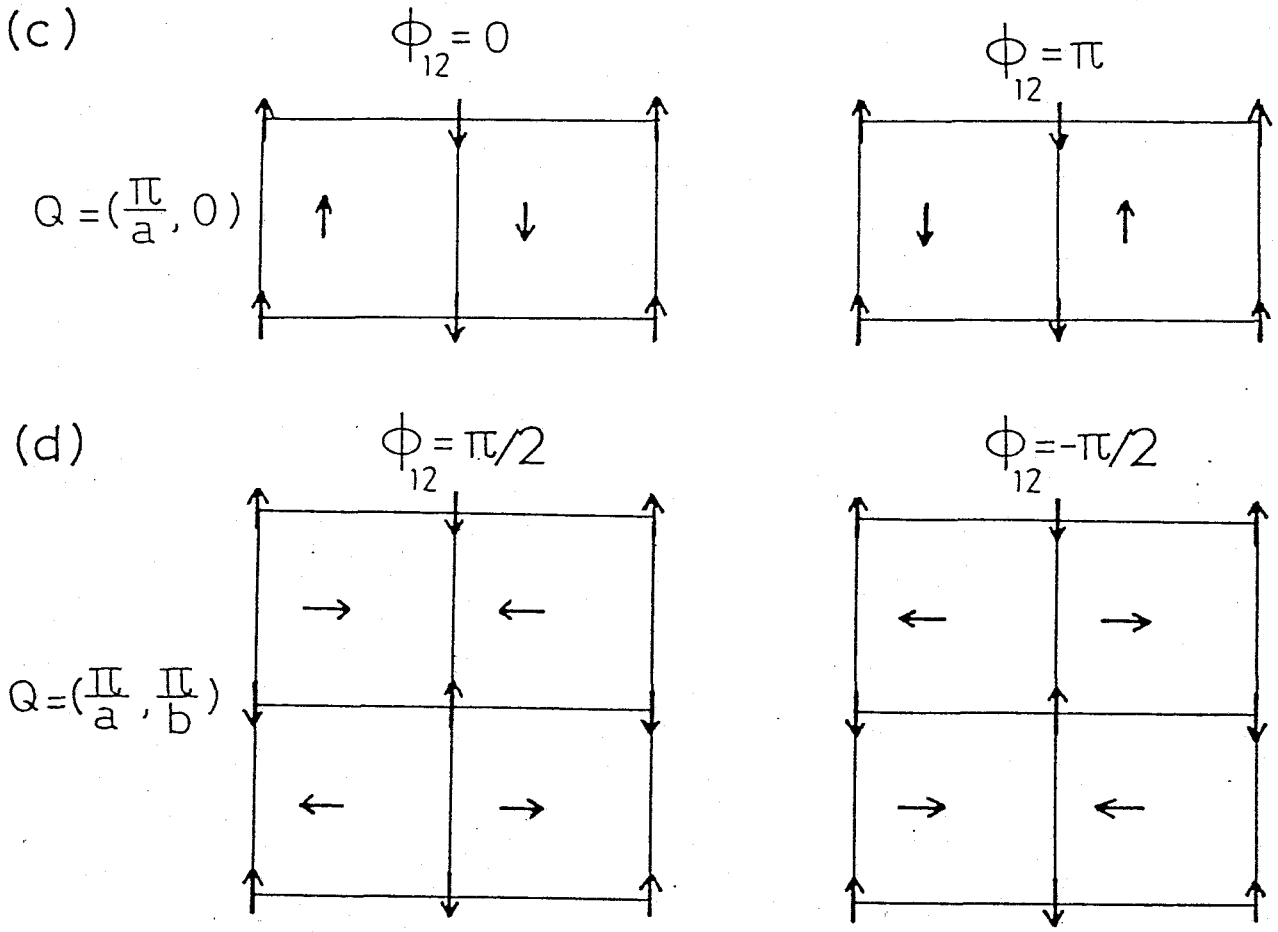

Fig.D-2. Various types of antiferomagnetic ordering.

List of Publications

1. M. Morifuji and K. Motizuki
Electronic Band Structures of FeAs,CoAs and NiAs.
J. Magn. Magn. Mat. 70 (1987) 70

2. M. Morifuji and K. Motizuki
Electronic Band Structure and Structural Transformation from NiAs-Type to MnP-Type of CoAs and NiAs.
J. Phys. Soc. Jpn. 57 (1988) 3411

3. K. Motizuki and M. Morifuji
Structural Phase Transition and Magnetism of NiAs-Type Transition Metal Pnictides.
Journal de Physique 49 (1988) C8 189